



September 10, 2018

Docket No. 52-048

U.S. Nuclear Regulatory Commission
ATTN: Document Control Desk
One White Flint North
11555 Rockville Pike
Rockville, MD 20852-2738

SUBJECT: NuScale Power, LLC Response to NRC Request for Additional Information No. 437 (eRAI No. 9465) on the NuScale Design Certification Application

REFERENCES: 1. U.S. Nuclear Regulatory Commission, "Request for Additional Information No. 437 (eRAI No. 9465)," dated April 26, 2018
2. NuScale Topical Report, "Evaluation Methodology for Stability Analysis of the NuScale Power Module," TR-0516-49417, Revision 0, dated July 2016

The purpose of this letter is to provide the NuScale Power, LLC (NuScale) response to the referenced NRC Request for Additional Information (RAI).

The Enclosures to this letter contain NuScale's response to the following RAI Question from NRC eRAI No. 9465:

- 15.09-1

Enclosure 1 is the proprietary version of the NuScale Response to NRC RAI No. 437 (eRAI No. 9465). NuScale requests that the proprietary version be withheld from public disclosure in accordance with the requirements of 10 CFR § 2.390. The enclosed affidavit (Enclosure 3) supports this request. Enclosure 2 is the nonproprietary version of the NuScale response.

This letter and the enclosed responses make no new regulatory commitments and no revisions to any existing regulatory commitments.

If you have any questions on this response, please contact Paul Infanger at 541-452-7351 or at pinfanger@nuscalepower.com.

Sincerely,

Zackary W. Rad
Director, Regulatory Affairs
NuScale Power, LLC

Distribution: Gregory Cranston, NRC, OWFN-8G9A
Samuel Lee, NRC, OWFN-8G9A
Rani Franovich, NRC, OWFN-8G9A



Enclosure 1: NuScale Response to NRC Request for Additional Information eRAI No. 9465, proprietary

Enclosure 2: NuScale Response to NRC Request for Additional Information eRAI No. 9465, nonproprietary

Enclosure 3: Affidavit of Zackary W. Rad, AF-0918-61723



Enclosure 1:

NuScale Response to NRC Request for Additional Information eRAI No. 9465, proprietary



Enclosure 2:

NuScale Response to NRC Request for Additional Information eRAI No. 9465, nonproprietary

Response to Request for Additional Information Docket: PROJ0769

eRAI No.: 9465

Date of RAI Issue: 04/26/2018

NRC Question No.: 15.09-1

Title 10 of the *Code of Federal Regulations* (10 CFR) Part 52, section 47 and section 79 require a final safety analysis report (FSAR) to analyze the design and performance of the structures, systems, and components (SSCs). Safety evaluations, performed to support the FSAR, require reactor physics parameters to determine reactor core performance under normal operations, including anticipated operational occurrences, and accident conditions. The description shall be sufficient to permit understanding of the system designs and their relationship to the safety evaluations. Title 10 of the Code of the Federal Regulations (CFR), Part 50, Appendix A, General Design Criterion (GDC) 10 – Reactor Design, states that the reactor core and associated coolant, control, and protection systems shall be designed with appropriate margin to assure that specified acceptable fuel design limits (SAFDLs) are not exceeded during any condition of normal operation, including the effects of anticipated operational occurrences (AOOs). GDC 12-Suppression of Reactor Power Oscillations requires that power oscillations which can result in conditions exceeding specified acceptable fuel design limits are not possible or can be detected and suppressed. Design-Specific Review Standard (DSRS) 15.9 provides review procedures and acceptance criteria for evaluating the safety analysis report (SAR) analysis and assessment of potential thermal-hydraulic instability concerns.

In FSAR Tier 2 section 15.9, "Stability," the applicant provides a description of thermal-hydraulic instabilities, conditions under which they might occur, and proposed methodology for complying with the above regulatory requirements. Rather than present and describe key events analyzed, initial conditions, biases, and results directly in the FSAR; FSAR Tier 2, Section 15.9 frequently cites the topical report (TR), "Evaluation Methodology for Stability Analysis of the NuScale Power Module," TR-0516-49417-P, which is incorporated by reference in Chapter 15.9 of DCD, for such information. For example, sections 15.9.2, 15.9.3.1, 15.9.3.2, 15.9.3.2, 15.9.3.5, and 15.9.3.7 of the FSAR reference conditions, bias values and results presented in the stability TR, describing the methodology, in place of presenting this information directly in the FSAR. In principal, incorporating-by-reference, limiting events, parameter values, and results into the final safety analysis report from the topical report is possible. However, several statements and disclaimers exist in the current stability TR that indicate information in the TR is for "illustrative purposes only" and that NuScale is not requesting approval for feature and parameters [values] used in the TR. These statements do not necessarily impact the applicant's request for approval



of its stability methodology. However to comply with the above regulatory requirements, these disclaimers should be removed from the TR, if the applicant intends to incorporate events, conditions, results provided from the TR to address FSAR acceptance criteria. Additionally, events, conditions, parameter values, and results cited in the TR may require revision to both the TR and the FSAR.

Also, information marked proprietary and ECI in the stability TR is inconsistent with markings of corresponding information presented in FSAR Tier 2 section 15.9. For example, none of the figures in section 15.9 of the FSAR are marked proprietary or ECI, but the same figures are designated as proprietary and ECI in the stability TR. Similarly, a significant amount of the information concerning event sequences, condition, and results provided in the stability TR is designated as proprietary and ECI. While equivalent, and often identical, information described in FSAR, Tier 2 subsections of section 15.9 is not designated proprietary and non-ECI. Examples include portions of sections 8.2 and 9.1 and 9.2 from the stability TR that are marked proprietary and ECI, while the equivalent information is not designated proprietary or ECI in section 15.9 of the FSAR. Any proposed revisions to the FSAR should ensure that sufficient stability related information is available for compliance with 15.47 and 15.79.

In order to make an affirmative finding with regard to the above regulatory requirements important to safety, the NRC staff requests that NuScale:

- 1) Clarify if NuScale intends to incorporate, by reference, stability events, initial conditions, and/or results from the stability TR into section 15.9 of the Tier 2 FSAR.

If the applicant intends to incorporate this information from the stability methodology TR into the FSAR, then the TR should be revised such that the following statements, in addition to other similar statements, be eliminated from stability TR:

- The Abstract of the TR states that NuScale is requesting approval of the computational methods described in the TR for demonstrating the stability of performance of the NPM and approval of the regional exclusion approach based on maintaining subcooling in the riser for protecting the onset of instabilities in the NPM. This topical report is not intended to provide final design values or evaluation of Stability. Rather, "example values for the various evaluations are provided for illustrative purposes"
- The executive summary states, "The methodology in this report utilizes design features and parameters as assumptions. NuScale is not requesting approval for these features and parameters as part of this review of this report."
- In section 8.2, "Stability Analysis for Operational Events" of the stability TRm the applicant states: "While not intended to be the final event evaluation, results are present to demonstrate the proper behavior of the code.... "Formal application of the stability methodology is expected to address and disposition plausible events associates with the licensing biases of NPM,"



- Section 10.4 of the stability TR, Stability analysis application says "demonstration examples of the scope of analysis in this report to support the applicability of the analytical methods of the PIM code."
- Section 10.4 of the stability TR, "Final analysis will be provided separately in the final design."

2) Reconcile proprietary and ECI designations of the stability TR with the non-proprietary and non-ECI designations for the identical or equivalent information provided in section 15.9 of the FSAR.

NuScale Response:

1) NuScale does not intend to incorporate, by reference, stability events, initial conditions, or example results presented in "Evaluation Methodology for Stability Analysis of the NuScale Power Module" TR-0516-49417 into FSAR Section 15.9. Rather, FSAR Section 15.9 will be updated appropriately in the Design Certification Application, Revision 2, to show stability events, initial conditions, and results.

2) Proprietary redaction markings in "Evaluation Methodology for Stability Analysis of the NuScale Power Module" TR-0516-49417 have been updated, as shown in the attached markup, to be consistent with equivalent information provided in FSAR Section 15.9.

Impact on Topical Report:

Topical Report TR-0516-49417, Evaluation Methodology for Stability Analysis of the NuScale Power Module, has been revised as described in the response above and as shown in the markup provided in this response.

Licensing Topical Report

Evaluation Methodology for Stability Analysis of the NuScale Power Module

~~July 2016~~

Draft Revision ~~10~~

Docket: PROJ0769

NuScale Power, LLC

1100 NE Circle Blvd., Suite 200

Corvallis, Oregon 97330

www.nuscalepower.com

© Copyright 2018 by NuScale Power, LLC

3.3.3 Reactor Core

The core configuration for the NPM consists of 37 fuel assemblies, 16 of which include control rod assemblies. The fuel assembly is a standard 17x17 PWR fuel assembly with 24 guide tube locations for control rod fingers and a central instrument tube. The assembly is nominally half the height of standard plant fuel and several spacer grids provide support. The fuel is UO_2 with Gd_2O_3 as a burnable absorber homogeneously mixed within the fuel for select rod locations. The U^{235} enrichment is below 4.95 percent.

3.4 Chemical and Volume Control System

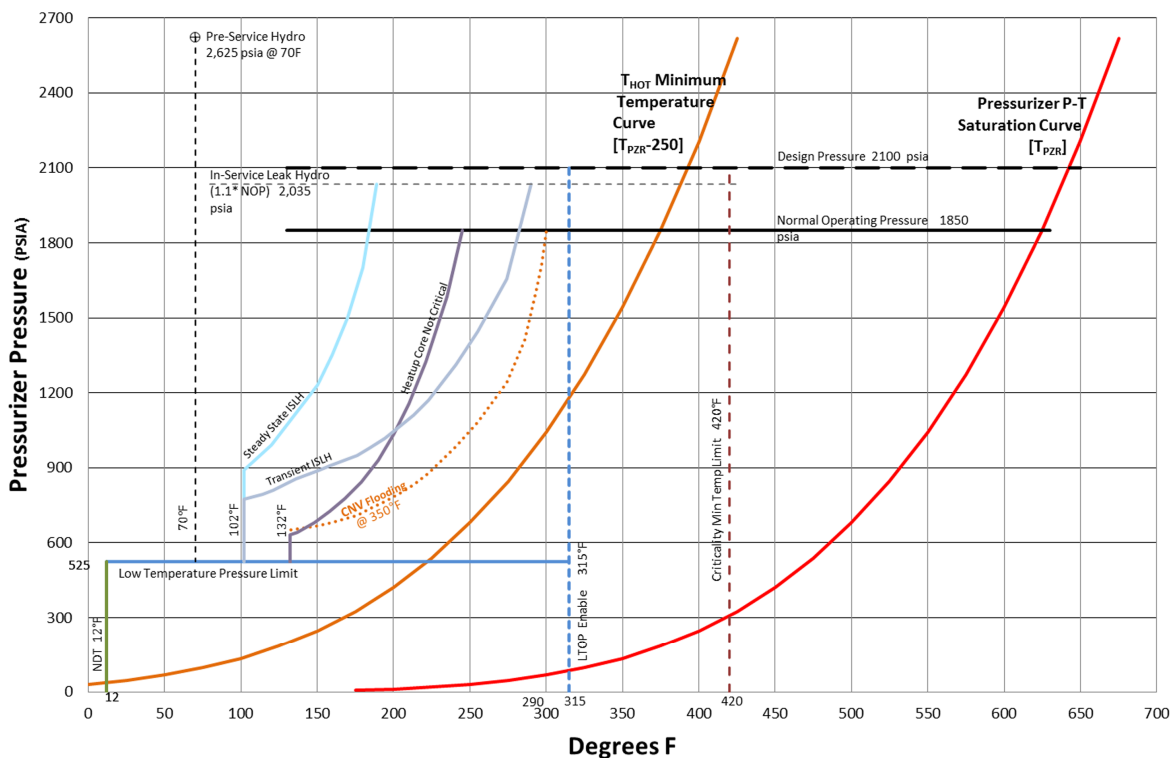
The CVCS is not required to function during or after an accident. During normal operation, the CVCS recirculates a portion of the primary coolant through demineralizers and filters to maintain primary coolant cleanliness and chemistry. A portion of the recirculated coolant supplies pressurizer spray for controlling reactor pressure. Injection of additional water controls primary system coolant inventory when primary coolant levels are low, during letdown of primary coolant to the liquid radioactive waste system, or when coolant inventory is high. Additionally, during the module start-up process, the CVCS adds heat to the primary coolant via the module heatup heat exchanger (also referred to as the startup heater) to establish natural circulation flow in the primary coolant system.

3.5 Startup and Shutdown

Figure 3-2 illustrates an example of the module startup path on a pressure-temperature plane. During startup, the operating domain pressure and temperature are increasing under CVCS heating and conditions are confined to a ~~ff~~-subcooled region so that no boiling occurs. Subsequently, reactivity insertion brings the core power gradually to the rated value while the system temperature increases while keeping a margin to core exit subcooling.

In the shutdown path, the trajectory on the pressure-temperature plane remains in the subcooled region so that no boiling in the riser is possible. ~~ff~~^{2(a),(c)}

ff



}}2(a),(c),ECI

Figure 3-2. Example Pressure-Temperature Operating Domain

3.6 Primary and Secondary Operating Conditions

Primary and secondary steady-state operating conditions are determined by engineering evaluations for a wide range of operating power levels. The evaluations address a number of design considerations, including control strategy (constant core inlet, average, or outlet temperature as a function of power) and SG operating conditions considering the desired steam temperature. Predictions are made for the NPM best-estimate primary coolant flow rates as functions of reactor power level. As described in Section 10.0, the application methodology addresses revisions to the best-estimate primary flow rate and addresses the effects of design minimum and maximum flow rate.

The steady-state operating conditions incorporate the effects of ambient heat losses and heat loss through non-regenerative heat exchange in the CVCS. {{

}}2(a),(c),ECI The heat loss in the CVCS non-regenerative heat exchanger is

assumed to be {{ }}^{2(a),(c)} These heat losses are not critical, except as they reduce the total heat transferred to the secondary system.

Representative primary initial conditions at rated power are as follows:

ff

- core power: 160 MW
- core inlet flow rate: 1304.9 lbm/s
- core inlet fluid temperature: 498.0 degrees-F
- primary system pressure: 1850 psia

Representative secondary initial conditions at rated power are as follows:

- feedwater flow rate: 149.0 lbm/s
- feedwater inlet temperature: 300.0 degrees-F
- steam pressure 500.0 psia

Table 3-1 lists representative values for primary system flow and core inlet temperature. Core inlet temperature at 15 percent power and higher is chosen to maintain an approximately constant core average temperature at all the power levels. Core inlet temperature below this value is based on linearly increasing temperature starting from the critical moderator temperature of 420 degrees-F. ~~ff~~^{2(a),(e)}

Table 3-1. Primary Steady-State Conditions

ff

%	MWt	Flow (lbm/s)	Core Inlet Temp (°F)
1	1.6	218.9	427.3
5	8	440.9	456.3
10	16	566.7	492.6
15	24	656.4	528.9
19.99	31.98	728.5	526.2
20	32	728.5	526.2
25	40	789.8	523.8
30	48	843.7	521.6
35	56	892.2	519.5
40	64	936.4	517.5
45	72	977.2	515.5
50	80	1015.2	513.7
55	88	1050.8	511.9
60	96	1084.5	510.2
65	104	1116.4	508.6
70	112	1146.8	506.9
75	120	1175.8	505.4
80	128	1203.6	503.8
85	136	1230.3	502.3
90	144	1256.0	500.8
95	152	1280.9	499.4
100	160	1304.9	498.0
102	163.2	1314.3	497.4

ff2(a),(e),ECI

Representative secondary system steady conditions at off-rated power are chosen consistent with expected plant operations, including transition of secondary conditions at ff-32 MW (20 percent) power from 50 degrees-F to 200 degrees-F feedwater temperature as the turbine comes on-line and feedwater heating begins. Feedwater flow conditions are chosen to give a steam temperature that is about 15 degrees-F lower than the core exit temperate in the primary system once the turbine is online. ff2(a),(e),ECI These conditions consider the effects of heat losses described earlier.

- low low primary system flow

Any of the above signals that exceed their specified limits are expected to result in a reactor trip.

Setpoints used in the analytical demonstration of the MPS performance for protecting the plant consider effects of uncertainties and delay times. Demonstrating these analytical setpoints is a main function of nuclear safety analysis activities and depends on a wide range of design input, including physical sensor design and placement, electrical system design, time for breakers to open couplings to release the control rods, and time for the control rods to physically enter the core.

Typical sensor response times used in determining analytical limits are ~~1~~ approximately 1 to 10 seconds and Table 3-2 lists representative values. Typical electrical signal processing times are 1.0 second and the typical trip breaker plus control rod delatch time is also 1.0 second. ~~1~~^{2(a),(e)}

Table 3-2. Assumed Safety Sensor Response Times

~~1~~

Sensor	Response Time, sec.
Temperature	7.0
Pressure	1.0
Power range flux	1.0
Source range flux	10.0
Level	2.0
Flow	5.0

~~1~~^{2(a),(e)}

While other MPS actuations may occur earlier than the times cited in Table 3-2, the demonstration analysis described in this report utilizes the hot leg temperature instrument combined with sensed pressure to provide an MPS trip that actuates when ~~1~~ less than 5 degrees-F subcooling is detected in the riser region above the core. ~~1~~^{2(a),(e),ECI}
The analyses use a total reactor trip delay time of 10 seconds from the time of physically exceeding the setpoint to start of control rod insertion. As described in Section 10.0, the application methodology addresses MPS settings and delays found in plant technical specifications and other sources.

4.0 Phenomenological Description of NuScale Power Module Stability

4.1 Introduction

As described in Section 3.0, the NPM is an integral PWR. The SG is integrated within the RPV and the primary coolant flow is driven by natural circulation, which is an important aspect of its passive design philosophy. The density difference between the relatively high temperature flow exiting the core and the lower temperature flow returning through the downcomer annulus where the SG is the heat sink creates the natural circulation driving head. This configuration presents ~~ff~~ several flow circuits where thermal-hydraulic instabilities are demonstrably excluded during the design stage with regard to causing reactor power oscillations. This section describes these flow circuits and the associated feedback and delay mechanisms to cover the phenomenological aspect of the stability behavior, and to put in perspective the subsequent mathematical and numerical studies that demonstrate NPM stability.

The first flow circuit is the main circulation loop of the core coolant flow, which is subcooled as required for PWR operation. However, in the absence of a recirculation pump, the natural circulation head is dependent on the power level and flow rate, which is a feedback mechanism that may potentially lead to unstable flow oscillations.

The second possible flow path for a potential instability is the closed path between two fuel assemblies or regions in the core also known as the parallel channel mode. In this mode, density waves in one region of the core oscillate out of phase with the flow in another region. This condition would maintain the core pressure drop boundary condition and the power and flow in each fuel assembly may oscillate if the necessary conditions for density wave instability exist.

The third possible flow instability is in the secondary side of the SG where subcooled liquid water is pumped into the helical tubes, boiling occurs, and superheated steam exits at the other end. Density waves, which are common in parallel boiling channels, have been identified as a potential instability mode within the SG tubes and studied experimentally. ~~112(a),(c),ECI~~

Various feedback mechanisms are included, and special consideration is given to the possible coupling of the SG dynamics and the flow stability in the primary loop. Feedback coupling between the thermal-hydraulic phenomena and the neutron kinetics is important where coolant and fuel rod temperatures provide reactivity feedback, and the core power response affects the coolant temperature and the density head that drives the flow and influences its stability. Pure neutronic stability, without thermal-hydraulic feedback coupling, is addressed separately in dedicated neutronic analyses in the design certification.

4.2 Background and Past Reactor Stability Studies

Open literature contains extensive studies of the stability of nuclear systems, which is only a subset of the larger body of work when industrial activities in this area by reactor and fuel vendors are included. The primary focus of historical stability work has been for

BWRs, where complex interactions of coolant density waves and nuclear reactivity may lead to flow and power oscillations -- a condition that must be excluded for normal operation and licensing of the reactor.

Reference 12.1.3 by Lahey and Drew provides an early survey of the literature on stability analysis and experimental data related to light water reactors. This extensive review covers a wide range of data and analytical methods and instability types in two-phase flow. The classification of physical instability mechanisms in Reference 12.1.3 is an expanded version of the one given in the review article by Bouré *et al.* (Reference 12.1.4). Lahey and Drew enlarged Bouré *et al.* classification by including nonlinear phenomena where supercritical Hopf bifurcation leads to finite amplitude limit cycle oscillations and subcritical bifurcation leads to the possibility of divergent oscillations if the initial perturbation is sufficiently large even when the initial state is linearly stable. Professor Hennig and his associates cover the topic of nonlinear oscillations for BWR conditions in several works (e.g., Reference 12.1.5). Lahey and Drew also included neutron reactivity coupled thermal-hydraulic instabilities, for which a later, more detailed monograph on the specific instability mode of nuclear-coupled density waves is given in Reference 12.1.6. A comprehensive review of BWR stability given in Reference 12.1.7 is another example of the stability work in the nuclear industry. The works cited are examples from a large body of literature that focuses on boiling flows, and does not mention single-phase flow instabilities. Nevertheless, the review provides a useful reference on the methodology of instability mode classification and a guide on how to approach stability analysis problems in the NPM design, in which natural circulation under single-phase flow conditions is the normal operation mode and substantial voiding is outside the range of intended operation.

The flow stability in PWRs has also been addressed in literature. A recent example in Reference 12.1.8 for a large forced-circulation PWR, identified and summarily dispositioned certain instability modes. Tong and Weisman (Reference 12.1.9) covered the topic of stability as part of their monograph book on PWR thermal analysis. As part of their stability discussion, they provided a classification of possible instabilities. A comprehensive review of natural circulation flow phenomena, including stability, of light water cooled nuclear plants sponsored by the IAEA with contributions from many leading experts in the field is found in Reference 12.1.10. Stability of natural circulation flow of two-phase and single-phase systems is covered with regards to phenomena, models, and experiments in test loops. Of the most interest are Annex 7 through 10. The IAEA report also provides tabulated classification of instability modes. Instability classification can be also found in the recent review article by Prasad *et al.* (Reference 12.1.11).

The methodology presented in this report is based on ~~the~~ contrasting a comprehensive classification of flow instabilities in single- and two-phase flow with the particular flow paths in the NPM in order to narrow down the relevant instability modes while excluding others that do not apply. ~~the~~ Once the potential instability modes are identified, the phenomena governing the various feedback mechanisms are recognized for inclusion in the governing equations of mathematical and numerical models.

⌘ Natural circulation is a special case in which the flow is driven by buoyancy and the flow path is closed. To conform to Eq. 4-1, it is possible to divide the natural circulation loop in two and consider the downcomer as a pump. An equivalent formulation simply considers ΔP as the integral of all pressure drop components along the closed loop, which includes the density head in the riser side and the downcomer side with opposite signs. The function $\Delta P(\dot{m})$ describes the steady-state flow characteristics because there are no inertia effects.

A steady-state solution gives the mass flow rate that corresponds to $\Delta P = 0$. When $\Delta P(\dot{m})$ is monotonic, that is the pressure drop increases with mass flow rate, there is only a single valid solution of the mass flow rate corresponding to $\Delta P = 0$. Multiple steady-state solutions are possible only when there is an inflection in the flow characteristic function and the slope is negative at one of the possible mass flow rate solutions. This condition is the fundamental cause of this instability; there are multiple possible solutions for mass flow rate with the same pressure residual.

In the special case in which the two-phase pressure drop is large and dominant, and the two-phase pressure drop multiplier is large, as in a natural circulation loop with long riser with small hydraulic diameter, an increase in the mass flow rate, which results in a decrease in the flow quality downstream of the heated section (core) would result in a net decrease in pressure drop. In this case, the slope of the function $\Delta P(\dot{m})$ with respect to the mass flow rate would be negative and that operating point becomes unstable. ⌘^{2(a),(c),ECI}

Evaluation: This mode is applicable in principle and a disposition is given below.

There is no possibility for negative slope of the $\Delta P(\dot{m})$ curve in the case of single-phase natural circulation and it can be demonstrated that in a substantially unconstricted flow path like the primary circuit in the NPM that this condition is also absent even under two-phase conditions. Figure 4-1 plots the flow characteristic function $\Delta P(\dot{m})$ for several power levels in which the pressure drop components are calculated for best-estimate models of the NPM using PIM. ⌘ Notice that the friction and form losses are calculated where flow pattern transitions may occur and at low flow, the flow may be turbulent in one part and laminar in another part of the flow circuit depending on the flow area and hydraulic diameter around the loop. ⌘^{2(a),(c),ECI} It is demonstrated that there is no negative slope at any power at the steady-state balanced loop operating points where $\Delta P = 0$. Moreover, negative slope is not found on the curve. Therefore, the flow excursion mode is not possible in the NPM.

Conclusion: Since there is no possibility for negative slope of the $\Delta P(\dot{m})$ curve in the case of single-phase natural circulation, the flow excursion mode cannot cause instabilities within the NPM. No further consideration of this instability mode is required within the stability analysis methodology.

4.3.1.3 Instability Mode: Flow Pattern Transition (Relaxation) Instability

Description: Flow regime transitions could in principle influence the pressure drop and create inflections of the pressure drop versus flow rate that might result in instability under certain conditions. Flow regime transitions include laminar-to-turbulent transitions and bubbly-to-annular flow transitions.

Evaluation: ~~ff~~The laminar-to-turbulent transition has already been included in the Ledinegg instability evaluation and found to be unconditionally stable. ~~jj^{2(a),(e)}~~Bubbly-to-annular flow regime transitions occur at high steam qualities and are outside the operational range of the NPM, which is single-phase flow with minimal, if any, local subcooled boiling. As shown later, other instability modes become excited at lower steam quality in the NPM riser and, therefore, the boiling regime transitions are bounded by these other phenomena.

Conclusion: The effects of flow regime transition are incorporated in the Ledinegg instability evaluation in Section 4.3.1.1 and that mode cannot cause instabilities within the NPM. Therefore, no further consideration of this instability mode is required within the stability analysis methodology.

4.3.1.4 Instability Mode: Flashing Instability

Description: For heaters located under a tall, adiabatic riser where the hot liquid entering the riser experiences a gradual decrease in static pressure as it travels up the riser, the reduction in pressure results in evaporation (flashing), which increases the driving head. The flow increase lowers the temperature of the liquid entering the riser and the flashing is suppressed, which reduces the driving head and lowers the flow to the effect that heater exit temperature increases and the cycle is repeated.

Evaluation: This instability mode is observed only in low-pressure systems with pressures lower than NPM operating pressure, but may be encountered during the startup of a natural circulation BWR. Therefore, this mode is not applicable to the NPM as a primary instability mechanism.

Conclusion: Although not applicable as a primary instability mechanism in the NPM due to the high operating pressure of the primary system, ~~ff~~flashing may exacerbate other instability mechanisms and the phenomena of vapor generation due to pressure changes. The effect is therefore included in the stability analysis methodology. ~~jj^{2(a),(e)}~~

4.3.1.5 Instability Mode: Geysering

Description: The description of the mechanism for geysering in the literature varies, in which the common features are periodic, or chaotic, oscillations due to cyclical vapor generation in a tall riser. The main difference between geysering and flashing instabilities is that in geysering the vapor is generated first in the heater section. Part of the geysering mechanism is the thermodynamic metastable liquid states in which liquid can become superheated (liquid temperature higher than saturation) due to low flow and lack of nucleation sites, and the equilibration occurs suddenly, generating large volumes of

vapor. In addition, the generation of a vapor slug may be attributed to subcooled boiling in the heater section.

Evaluation: Geysering instability is possible only in low-pressure systems with pressures lower than NPM operating pressure, and therefore, is not an applicable primary instability mode in NPM.

Conclusion: Although not an applicable primary instability mechanism in the NPM due to the high operating pressure of the primary system, {{

}}^{2(a),(c)}

4.3.2 Dynamic Instabilities

The NPM is a dynamical system that can be modeled using a set of state variables. These state variables include the parameters that define the flow field, such as liquid and vapor mass flow rates and temperatures, core thermal power, and heat flux. Depending on the model order, these variables can be defined at a number of locations in the NPM. The dynamical system is defined by a set of ordinary differential equations where the time derivative of each state variable is given as a generally nonlinear function of the state variable and any constraints, such as boundary conditions and external controls. The functions that determine the time derivatives of the state variables are obtained from the laws governing the physical phenomena, such as the applicable conservation laws and the equations governing fission reaction rates. In the case of a steady state corresponding to given external control, the time derivatives of the state variables vanish and the resulting system of equations can be solved for the set of the state variables (a point in the phase space). A point in the phase space corresponding to steady state is a fixed point. {{The steady-state solution may not be necessarily unique, where more than one fixed point is obtained; in that case, transitions among these points is possible. The instability of a fixed point when multiple steady-state solutions are possible has been discussed in Section 4.3.1.1 (Ledinegg static flow excursion). }}^{2(a),(e)}

The stability of a dynamical system refers to its behavior in the neighborhood of fixed points. A perturbation of one or more of the state variables at a fixed point introduces nonzero time derivatives and initiates a transient response. The system is stable if the system returns to the fixed point, either monotonically or while undergoing oscillations of decreasing magnitude. Linear stability is defined by the system returning to its fixed point following a small perturbation. Conversely, a linearly unstable system diverges exponentially from its initial fixed point either monotonically or by undergoing oscillations about the fixed point with exponentially growing amplitude. Monotonic divergence is not possible as it can occur only due to positive feedback mechanisms that are excluded by design; for example reactivity coefficients must be negative. Even in certain operating conditions where the boron concentration is high and moderator temperature reactivity coefficient is positive, the overall reactivity coefficient is negative when accounting for Doppler reactivity. Conversely, negative feedback mechanisms may lead to oscillatory behavior that can diverge if the feedback is delayed and sufficiently strong. A diverging

oscillation is the type that is possible in principle and has to be prevented for normal operation.

Nonlinear stability analysis refers to the system behavior in response to a large perturbation that can be induced externally or that results from the growth of a small perturbation of a linearly unstable fixed point. Nonlinear effects can limit the divergence of an oscillation (supercritical Hopf bifurcation, Reference 12.1.5) and the system settles into a stable limit cycle oscillation. It is also possible in principle for a subcritical Hopf bifurcation, that the nonlinear effects accelerate the growth of oscillation magnitude as the oscillation magnitude grows (Reference 12.1.12). For the latter case, a stable fixed point can become unstable given an initial perturbation of sufficiently large magnitude.

{{

}}^{2(a),(c)}-EC+

{{

}}^{2(a),(c)}

In the following sections, specific dynamic instabilities are discussed and evaluated according to their respective relevance to the NPM. These sections also provide the phenomenological background for understanding the prevalent instability modes and defining the requirements for the nonlinear time-domain tool to embody the NPM dynamical system.

4.3.2.1 Instability Mode: Pressure Drop Oscillations

Description: Pressure drop oscillations are the dynamic extension of Ledinegg static instability. For both instabilities, pressure drop versus flow rate is a multi-valued function. In the Ledinegg case, a flow excursion occurs once, bringing the flow from an unstable operating point to one or another stable point, depending on the direction of the perturbation. In the pressure drop oscillation, the transition from one flow state to the other is accompanied by a storage mechanism, such as compressing a volume of vapor, which causes a delayed rebound and cyclical transitions ensue.

Evaluation: The necessary condition of a multi-valued pressure drop versus flow rate has been evaluated for the NPM as part of the Ledinegg analysis and found to be unconditionally stable.

Conclusion: The effects of pressure drop oscillations are incorporated in the Ledinegg instability evaluation in Section 4.3.1.1 and that mode cannot cause instabilities within the NPM. Therefore, no further consideration of this instability mode is required within the stability analysis methodology.

4.3.2.2 Instability Mode: Acoustic Oscillations

Description: The mechanism for propagating the disturbances responsible for the acoustic oscillation instability is pressure waves in contrast to density waves, which are discussed separately where the disturbance travels with the flow. Standing pressure waves (sound waves) are resonant where the frequency is determined by the sound speed and the length of the pipe that acts as an organ pipe. The frequency is usually high due to the high speed of sound waves which is sensitive to vapor content. The energy that feeds and sustains the instability is thermal in nature. In the compression phase, direct contact between the liquid phase and the heated surface is forced by collapsing a vapor film and heat transfer is enhanced, while in the rarefaction phase, the vapor film is reestablished, and the cycle is repeated. High velocity flow may also provide the mechanical energy to excite the standing waves.

Evaluation: There is no mechanism for feeding and sustaining this type of instability in the NPM ~~because the long pipe with geometry where an acoustic resonance is conceivable is the riser, which is adiabatic.~~ ~~2(a),(c),ECI~~ No high velocity flow is present in the NPM circulation loop.

Conclusion: No further consideration of acoustic instability is required in the stability analysis methodology since the mode cannot be sustained in the NPM.

4.3.2.3 Instability Mode: Density Waves

Description: Density wave instability is the most studied of instability mechanisms due to its relevance to BWRs. The instability may occur in vertical heated channels with or without boiling. The fundamental mechanism of the instability is that any flow perturbation at the inlet generates effects that propagate (wave) up the channel. A perturbation decreasing the inlet mass flow rate results in increasing the flow enthalpy,

which also lowers the density either by liquid expansion in the case of single-phase flow or through increased vapor generation. At steady state or quasi-steady state, or for low frequency perturbation, the inlet flow perturbation generates a negative feedback so that the system returns to its initial state and is stable. Specifically, a perturbation decreasing the inlet mass flow rate results in lowering the density in the channel, thus increasing the buoyancy pressure head, which tends to restore the original flow rate. However, the situation is different depending on the frequency of the perturbation in which delayed feedback, if sufficiently strong, can be destabilizing. The delay mechanism is the time it takes for the propagating density wave to transverse the heated channel length. There is a resonant frequency at which the delayed effects of the perturbation reach the channel exit at the time when the inlet perturbation reverses phase, and the original perturbation is reinforced. At this frequency, the system is destabilized, given sufficiently strong feedback, which can occur when the power is increased. For a single-phase heated channel, instability is conceivable only for long heated channels as the density change of liquid due to change in enthalpy is relatively small. Conversely, boiling increases the mixture density response to enthalpy change, making a boiling channel less stable compared to the single-phase case. In addition, in the two-phase case, the feedback from an initial inlet flow perturbation is not limited to density head, but includes the response of friction pressure drop, which is significant due to the two-phase multiplier.

The stability of density waves in a vertical boiling channel depends on the geometry and operating conditions of the system. Specifically, increasing power and decreasing flow are destabilizing. Axial power shapes skewed towards the inlet are also destabilizing. High pressure suppresses the density difference between the liquid and vapor phases and is therefore stabilizing. Increased inlet flow resistance is stabilizing, while increased exit resistance is destabilizing. The distinction is attributed to the phase difference of their respective effects due to the propagating wave. Inlet subcooling has a mixed effect; for highly subcooled flow, further increase of subcooling is stabilizing as it suppresses boiling in a larger part of the channel, but for low subcooling the system is destabilized by increasing inlet subcooling. ~~ff~~ The destabilizing effect of inlet subcooling has been demonstrated in both numerical and laboratory experiments, but has not been satisfactorily explained in phenomenological terms. An attempt to do so is given here by comparing the case of saturated inlet flow with a case of inlet subcooling. In the case of saturated inlet flow, the total vapor generation rate is constant depending on the channel power, but is not affected by flow perturbation. For the case of inlet subcooling, the vapor generation is modulated with the inlet flow at constant power as the part of the power needed to bring the subcooled liquid to saturation varies with the inlet mass flow rate, forcing the rest of the power that is used to generate vapor to vary in time with delayed effects due to wave propagation. ~~}}^{2(a),(c)}~~ By contrast, single-phase systems are insensitive to inlet subcooling and insensitive to pressure, as long as pressure does not drop to the point where vapor generation (flashing) may occur.

Evaluation: Density wave instability is seldom observed without compounding factors in nuclear systems. In a BWR, the phenomena are complicated by the nuclear reactivity feedback mechanisms and the time delay inherent in the heat conduction of fuel elements. While density waves are present normally in a heated channel, they can occur in a heated channel connected to a tall adiabatic riser as in simplified BWR's with natural circulation. Theoretically, the latter case is not particularly special if the adiabatic riser is

simply considered as part of a single channel with varying geometry where the heating axial distribution is pushed down. Another compounding effect is flashing. Flashing may occur in a tall riser located atop a heated section because the reduced static head lowers the pressure below the saturation point corresponding to the liquid enthalpy at the heated section exit, and induces vapor generation as the liquid travels up the riser. By analogy, flashing has the same effect on stability as a heat source generating vapor, making the riser effectively no longer adiabatic in this aspect.

Conclusion: Density wave phenomena are important for assessing the stability of both the primary coolant flow and the secondary side of the SG of the NPM. Density wave instability is a concern for the flow in the secondary side of the SG of the NPM and must be addressed. Density waves in the primary circuit are part of a compound interconnected phenomena of a potential natural circulation riser instability and must be addressed as an integral process with various components in the stability analysis methodology.

4.3.2.4 Instability Mode: Xenon Oscillations

Description: Xenon oscillation instability is a pure neutronic phenomenon. The products of U^{235} fission include isotopes that are high neutron absorbers or decay into other isotopes that are high neutron absorbers. In this way, fission product poisoning creates a delayed feedback system. A fission product of particular interest is iodine (I^{135}), which is radioactive and decays into Xe^{135} . The latter is a neutron poison with a large neutron absorption cross-section. Thus, decay of I^{135} generates Xe^{135} that is removed by either decaying or absorbing a neutron.

The neutron absorption reaction that removes Xe^{135} constitutes a positive feedback process in which increased fission power leads to increased reactivity, which reinforces the original power increase perturbation. However, the power increase perturbation also generates I^{135} , which decays into Xe^{135} and introduces negative reactivity, a delayed negative feedback process.

Detailed analysis of the xenon reactivity indicates the possibility of unstable power oscillations with a large period. These oscillations may involve the total reactor power or a spatial mode of the power distribution. These spatial modes are the radial (first azimuthal neutron flux mode) and the axial modes. For large PWR cores, the most susceptible mode is the axial oscillations in which the power swings from the top to the bottom of the core. In some PWRs with large cores, direct control to dampen axial xenon oscillations is accomplished using axial shaping control rods. Small cores are more stable in comparison.

Evaluation: Xenon stability calculations for the NPM core demonstrate that these oscillations are highly stable as a pure instability mode. The oscillation period is longer than two days, which is greater than the time scale of any thermal-hydraulic phenomenon in the NPM. ~~2(a),(c),ECI~~ Thus, interaction between the xenon oscillation and thermal-hydraulic feedback is precluded.

Conclusion: Xenon oscillations are unconditionally stable in the NPM core and no further consideration is required in connection with compounding other possible instability modes within the stability analysis methodology.

4.3.2.5 Instability Mode: Natural Circulation Instability

Description: Flow instability in a natural circulation loop bears some resemblance to that of density waves. While the density wave refers to the flow in a heated channel with fixed or prescribed boundary conditions, the natural circulation system includes two legs: a riser and a downcomer. The dynamics of the flow in the two legs depends on the heater design and the heat sink (exchanger) and their respective location. The natural circulation instability mechanism described in this report is for a natural circulation loop in which the heater is located under a tall riser and the cooling heat exchanger is located near the top of the cold leg. In steady state, the temperature in the riser is uniform and higher than the temperature downstream of the heat exchanger, and the corresponding difference in their respective densities create the force driving the flow. The steady-state temperature difference is proportional to the power-to-flow ratio and the friction pressure drop around the loop is proportional to the square of the flow rate; therefore, the steady-state natural circulation flow is proportional to the cubic root of the power. A perturbation increasing the flow rate results in a reduction in the heater exit temperature and an increase in its density. The density perturbation travels up the riser and there is a time delay before the new density is distributed throughout the entire length of the riser. This delayed feedback is negative because the difference in temperature between the riser and the cold leg is diminished and consequently reduces the density difference that drives the flow. If this delayed negative feedback is sufficiently strong, the flow is destabilized and undergoes growing oscillations. In the case of high friction in the loop that reduces flow, or if power input is sufficiently increased, boiling in the riser can be induced. The density response to an enthalpy perturbation is higher in the case of phase change than the case of single-phase thermal expansion by nearly a factor of six for water at the NPM operating pressure. The boiling natural circulation loop can be destabilized more readily than a single-phase loop.

The most idealized natural circulation loop in the literature is the Welander problem (References 12.1.10, 12.1.13, and 12.1.14). The Welander loop is symmetric with the heater located at the bottom of the loop and the heat sink at the top of the loop, thus there is no preference for the direction of the steady-state flow. The flow can be destabilized and oscillate with increasing magnitude and when flow reversal occurs, the flow transitions to oscillating around a negative flow rate point; these transitions were found to exhibit chaotic behavior. The Welander problem is a one-dimensional version of the older Bénard problem of a horizontal layer of fluid heated from below (Reference 12.1.15). While the Welander problem is a simple one, the numerical results were reported to vary and deviate from the experimental observations due to truncation errors and application of diffusive algorithms.

Evaluation: Reference 12.1.16 provides a more detailed analytical evaluation of the natural circulation loop with simplifying assumptions.

Conclusion: Natural circulation instability is a possible mode for the NPM and needs to be evaluated in depth in the stability analysis methodology. The evaluation in this report addresses this mode as well as other compounding phenomena. These compounding phenomena include the feedback from nuclear reactivity and the dynamics of the heat exchanger. Detailed numerical algorithms and models are used to avoid artificial damping, which overestimates the stability of the physical system.

4.3.2.6 Instability Mode: Thermal Stratification Oscillations

Description: For purposes of the NPM, thermal stratification oscillations are a specific extension of natural circulation instability that may occur in an ill-designed system, such as when the heat source is located in a higher elevation than the cooling sink. In such a configuration, heating of the water does not induce a reliable buoyancy-induced flow. Instead, the liquid becomes stratified and a periodic back-and-forth oscillatory flow occurs.

Evaluation: The necessary condition of having the heat source positioned higher than the cooling source does not occur in the NPM. The nuclear core is located sufficiently low in the system that SG heat removal and ambient heat losses out of the vessel do not result in thermal stratification oscillations. ~~ff~~In addition, the CVCS charging line used to inject hot water during NPM heatup is located low in the riser which prevents the effect. ~~ff~~^{2(a),(e),ECI}

Conclusion: No further consideration of this instability mode is required within the stability analysis methodology since the necessary conditions to cause this mode to occur do not exist in the NPM.

4.3.3 Coupled (Compound) Instability Modes

Fundamental, or pure, instability modes that have been presented above can manifest themselves in systems with the geometry and physical properties that permit the mechanisms for the respective mode to operate without interference of other phenomena. By contrast, the compound instability modes include secondary phenomena that influence or modify the primary mechanism significantly. The secondary phenomena may be geometric in nature, or physical processes that interact with the primary mechanisms through feedback that may reinforce or weaken the primary instability or modify its nature. The stability of engineering devices are more likely to require the study of compound instability phenomena, unlike laboratory experiments, which are often performed on simplified apparatuses to resolve the fundamental mechanisms.

4.3.3.1 Instability Mode: Parallel Channel Instability

Description: When a fundamental instability mechanism is possible in a single heated channel (e.g., density waves), the situation is complicated by having several such channels connected to common plena. The common plena alter the boundary conditions under which a single channel would have operated. The common pressure drop boundary condition allows for multiple oscillation modes depending on the phase

difference among the oscillations in each channel. For example, if the flow in all channels oscillates in phase, the stability of the group of channels would be the same as a single channel. However, for two channels oscillating out of phase, the common pressure drop fluctuation is eliminated (in the linear limit) as the effects of the flow oscillations in the two channels cancel out. The fixed pressure drop boundary condition is destabilizing and therefore a set of two channels connected in parallel are less stable than a single one. In the case of three channels, the preferred phase difference is 120 degrees to maintain constant pressure drop between the plena (Reference 12.1.6). For four tubes, two preferred mode possibilities exist: either the channels oscillate with a phase difference of 90 degrees from one to the next, or two groups of two channels each oscillate out of phase while the channels in each group oscillate in phase with one another. The parallel channel instability mode is not necessarily tied to density waves. The compound effect is purely geometrical if the channels are identical, but a richer spectrum of phenomena can be expected in the more general case in which the channels differ in geometry or the power level and distribution.

Evaluation: ~~ff~~ There are two subsystems in the NPM in which investigation of parallel channel instability is required. The first subsystem is the tubes of the SG where the tubes are connected in parallel to two common plena, and the flow inside them is two-phase and subject to density wave instability. Appendix A addresses SG instability with a focus on its interaction with the primary-side flow.

The second subsystem where parallel channel instability needs to be investigated is the NPM core itself. The fuel assemblies in the core are not equipped with channels like BWR fuel assemblies. Crossflow is possible among neighboring fuel assemblies. As a conservative idealization for the sake of simplicity, the flow in each fuel assembly is assumed to be one-dimensional without lateral mixing, as if the fuel assemblies are channeled. The individual fuel assemblies are thus arranged in a parallel heated channel configuration subject to a common constant pressure drop between the upper and lower plena. ~~ff~~^{2(a),(c),ECI} It was shown in Reference 12.1.17 that this type of instability is dispositioned for PWR conditions using the simplified conservative model of Ishii (Reference 12.1.18). The neutron reactivity feedback is not needed for analyzing this mode as the destabilization leading to flow oscillations in a single channel does not significantly excite a reactor power response.

Conclusion: Parallel channel instability in the ~~ff~~ flow inside the tubes of the SG, if it occurs, is benign because it does not result in resonant coupling to the primary coolant flow or power oscillations. Sufficiently high inlet throttling to individual tubes prevents density wave oscillations. This throttling guarantees smooth operation of the SG. Further consideration of the stability of the SG secondary flow is outside the scope of this report. ~~ff~~^{2(a),(c),ECI}

The parallel channel instability in the NPM core has been shown not to be a concern and further consideration is not required in the stability analysis methodology.

4.3.3.2 Instability Mode: Primary Circuit Flow Coupling to Secondary Side Steam Generator

Description: ~~ff~~ Density wave oscillations in the SG tubes (the secondary side), if they are in phase, would result in an oscillating heat transfer coefficient and a corresponding oscillation in the rate of heat removal from the primary coolant flow. The resulting fluctuations in the heat sink correspond to cold leg density fluctuations and the flow of the coolant in the primary circuit is induced to oscillate in response. Primary coolant flow oscillations also induce core power oscillations. The oscillating primary coolant flow results in an oscillating heat transfer coefficient on the primary side, which affects the heat source to the oscillating secondary side flow and the feedback loop is closed. ~~ff~~^{2(a),(c),ECI}

Evaluation: This primary-secondary coupling is of interest if the unstable oscillations in the SG tubes are in phase, which is not the case because the tubes are coupled together through common plena. This forces out-of-phase oscillations that cancel out the net heat sink oscillations. Appendix A addresses additional aspects of this compound phenomenon.

SG secondary side flow coupling to the primary system-side flow is restricted to the effects of the total secondary flow. Out-of-phase flow oscillations in the tubes are self-cancelling and result in no net oscillatory effects. A change of the secondary flow by a forcing function boundary condition influences the primary coolant flow, but the reverse is not possible.

Conclusion: The feedback loop between the SG and the primary side is broken in the NPM. Therefore, no further consideration of possible destabilizing effects of primary-secondary resonances is required in the stability analysis methodology. However, the effects of an externally driven oscillation in the SG are addressed to show their influence on the primary system. Section 8.2.7 addresses the effects of oscillating feedwater flow.

4.3.3.3 Instability Mode: Neutronic Coupling to Natural Circulation Instability

Description: Natural circulation instability was described earlier only considering thermal-hydraulic phenomena. This mechanism is evaluated as a compound instability by taking the effects of the neutron reactivity feedback into account. In response to a flow increase perturbation at the core inlet, the core exit temperature is reduced if the core power is kept constant. The reduction of the average coolant (moderator) temperature introduces positive reactivity and the power is increased for the condition of a negative moderator reactivity feedback. The power increase offsets the core exit temperature reduction and the reactivity response becomes milder (reduced gain). However, the time delay involved in these processes could result in reinforcing the perturbation if the resulting phase shift is large. The case of BWR neutronic coupling destabilizes density waves because the fluctuation in the energy added to the coolant through heat flux at the surface of the fuel rods is delayed relative to the originating fluctuation in the fission heat generation due to the radial heat conduction in the fuel rods. This time delay is ~~ff~~ significant given a conduction time constant in the order of 2 to 3 seconds and the resulting phase shift is close to 90 degrees, which is destabilizing. The reason for this large phase ~~ff~~^{2(a),(c),ECI}

shift is that the period of the density wave oscillation in BWR cores is 1.5 to 3 seconds. By contrast, the oscillation period of the primary coolant flow in the NPM is at least an order of magnitude larger than the BWR period, and therefore the conduction delay does not result in a significant phase shift.

Evaluation: The conduction time delay between a fission power oscillation and the resulting heat flux oscillation at the outer fuel rod surface is small compared to the NPM flow oscillation period and therefore the negative moderator reactivity feedback is stabilizing (opposite the effect in a BWR). The negative power feedback is shown to be stabilizing in the analytical study given in Reference 12.1.16. Results of detailed numerical studies presented in Section 8.0 confirm this result. Positive moderator feedback which may be present under certain conditions, has a destabilizing effect for NPM and this effect is limited by the Doppler feedback. ~~2(a),(c),ECI~~

Conclusion: The reactivity-to-power and power-to-heat flux phenomena are important for the NPM stability performance and are included in the stability analysis methodology.

4.3.3.4 Instability Mode: NuScale Natural Circulation Instability

Description: The components of this compound instability were presented earlier. Specifically, the stability of the flow in a natural circulation loop is first considered with simplifying assumptions of constant heater power and constant density cold leg (due to an idealized perfect heat exchanger/SG). The added phenomena include the reactivity-to-power feedback. Further, the ideal SG assumption is relaxed where realistic modeling of the heat transfer dynamics is considered. ~~2(a),(c),ECI~~

~~2(a),(c),ECI~~ The system may include parts in which the flow is two-phase due to subcooled boiling in the core and flashing in the riser, depending on the operating conditions under investigation. The combination of the core with neutronic power feedback, an adiabatic riser where density waves propagate with possible flashing, and ~~2(a),(c),ECI~~ constitute a dynamical system that is best modeled numerically.

Evaluation: The main instability mode is the NPM natural circulation instability, also called riser instability mode. The evaluations rely on detailed numerical techniques where a dynamical system is constructed using the:

- nonlinear differential equations governing the conservation of mass, momentum, and energy of the generally two-phase flow field
- equations governing the fission power dynamics
- equations governing heat transfer

Section 5.0 describes the model. Sections 8.0 and 9.0 present results for various representative operating conditions and sensitivity cases.

density head. {{

}}^{2(a),(c),ECI}

3. Power generation in the core is represented by a point kinetics model. Accordingly, the axial power shape is invariant, which is a reasonable approximation given that only minimal subcooled voiding is possible.
4. {{

}}^{2(a),(c),ECI}

5. The flow in the primary coolant loop is modeled as non-equilibrium two-phase flow in which a drift flux formulation accounts for mechanical (velocity) differences between the liquid phase and the vapor phase if vapor exists. Thermal non-equilibrium allows the liquid to be in a subcooled, saturated, or superheated state, but the vapor is restricted to the saturation state. Closing relations governing mass, momentum, and energy exchange between the phases and the solid structures are adaptations from commonly used correlations. The algorithms do not account for the possibility of reverse flow.
6. The flow in the secondary side of the SG is modeled {{

}}^{2(a),(c),ECI}

7. The pressurizer is not modeled. Pressure is specified by input and the dependence of thermodynamic properties on pressure is uniform. This approximation implies that pressure waves cannot be simulated where the sound speed is infinite. Given the long transport times for fluid transit around the primary coolant loop and the low frequency of the oscillations following any perturbation of the steady state, the impact of this approximation on the stability calculation is negligible. {{

}}^{2(a),(c)}

{{

}}^{2(a),(c),ECI}

In the next subsections, the time-dependent conservation equations are written and adapted to the one-dimensional finite volume geometry. Constitutive relations and boundary conditions are also presented.

5.5.1 Conservation Equations

5.5.1.1 Mass Balance

The differential form of the vapor mass balance is written as

$$\frac{\partial}{\partial t}(\alpha \rho_g) + \nabla \cdot (\alpha \rho_g \vec{v}_g) = \Gamma''' \quad \text{Eq. 5-1}$$

where

t	=	time
α	=	void fraction
ρ_g	=	vapor density (a function of local conditions at the reference pressure)
\vec{v}_g	=	vapor velocity (vector)
Γ'''	=	rate of vapor mass generated per unit volume

Integrating over the volume of a finite control volume and applying Gauss's theorem, considering that the flow velocity is perpendicular to the cross-section area of the control volume, the mass balance equation becomes

$$\frac{\partial}{\partial t}(V \alpha \rho_g)_n + (A \alpha \rho_g v_g)_{n+1/2} - (A \alpha \rho_g v_g)_{n-1/2} = (\Gamma''' V)_n \quad \text{Eq. 5-2}$$

where

A	=	cross-section area
V	=	volume

and the subscript n refers to the average or bulk of the control volume, and $n \pm 1/2$ refers to the inlet and outlet boundaries of the control volume, respectively.

The differential form of the one-dimensional vapor mass conservation equation can be obtained for a generally varying cross-section area along the flow direction,

the secondary fluid along the axial length of the SG. The code user specifies {{

}}^{2(a),(c)}

Within the structure of the analysis model described in this section, the SG model encompasses modeling of the secondary fluid conditions, conduction through the SG tubes, and heat transfer at the primary-side and secondary-side tube surfaces. The SG is incorporated into the analysis model via the rate of heat removal from each primary node in the region of the SG, variable \dot{Q}_n of the energy balance shown in Eq. 5-9. At each time step, the current-time primary temperature and flow rate associated with each node of the SG is used {{

}}^{2(a),(c),ECI}

A single column of nodes, assuming the mass flow in the SG tubes is the same in each, represents fluid in the secondary side of the SG. Total flow area within the SG tubes and average tube length are used in the modeling. {{

}}^{2(a),(c),ECI} The heat transfer area of primary and secondary control volumes associated with thermal conduction through the tubes and heat transfer on the surfaces of the tubes is determined by the dimensions of the inclined helical geometry of the SG tubes.

{{

}}^{2(a),(c)} The enthalpy in each node of the secondary is used to determine the fluid temperature and heat transfer regime associated with heat transfer on the inside of the SG tubes.

As noted in the assumptions and limitations described in Section 5.2, the total heat transfer performance of the SG is effectively defined {{

}}^{2(a),(c)}

The cylindrical conduction equation for the SG tube walls is solved consistent with the description in Section 5.6.3.

The primary and secondary sides interact by exchanging heat through the SG tube walls. Conditions for forced convective heat transfer on the primary side use single-phase correlations appropriate for crossflow heat transfer on the exterior of the tubes (two-phase models are not included). The modeling is consistent with the NRELAP5 heat transfer package for primary-side crossflow heat transfer and has the following form,

$$Nu = C Re^n Pr^m \quad \text{Eq. 5-45}$$

where

Nu	=	Nusselt number
Re	=	Reynolds number
Pr	=	Prandtl number

⌘ The Reynolds and Nusselt numbers are based on a characteristic length taken as the tubes' outer diameter consistent with the correlation definition. The area basis is the minimum flow area (corresponding to the maximum fluid velocity) between tubes. The correlation coefficients of Eq. 5-45 are given in the NRELAP5 documentation and verified based on NuScale testing results with NRELAP5 are as follows;

$$C = 0.211$$

$$n = 0.651$$

$$m = 0.34$$

The coefficients are user-input, and other values may be applied if warranted by testing. ⌘^{(a),(e)}

Heat transfer modeling on the secondary side (inside the SG tubes) covers the entire range from subcooled single-phase liquid to superheated vapor. The Dittus-Boelter correlation is used for single-phase liquid and vapor forced convection heat transfer from Eq. (8.59) of Reference 12.1.24

$$Nu = 0.023 Re^{0.8} Pr^{0.4} \quad \text{Eq. 5-46}$$

where the Reynolds and Nusselt numbers are based on a characteristic length taken as the tubes' inner diameter.

Boiling heat transfer is modeled with the form of the Chen correlation extended to subcooled boiling as proposed by Collier, Eq. (12-33) of Reference 12.1.25. Accordingly, the heat flux is obtained from

$$f_{1\phi} = \begin{cases} f_{L,1\phi} & \text{laminar region} & \text{Re}_{1\phi} \leq \text{Re}_{low} \\ f_{Tran,1\phi} & \text{transition region} & \text{Re}_{low} < \text{Re}_{1\phi} \leq \text{Re}_{high} \\ f_{T,1\phi} & \text{turbulent region} & \text{Re}_{high} < \text{Re}_{1\phi} \end{cases} \quad \text{Eq. 5-52}$$

where

$$\begin{aligned} \text{Re}_{low} &= \text{Reynolds number lower limit for the laminar-to-turbulent transition region} \\ \text{Re}_{high} &= \text{Reynolds number upper limit for the laminar-to-turbulent transition region} \end{aligned}$$

The transition from laminar to turbulent regimes is consistent with Reference 12.1.29. The value for these limits is user-input. The values described in Reference 12.1.29 are 2200 and 3000, respectively. The friction factor in the transition region is obtained by ~~ff~~ interpolation between the laminar and turbulent values. The friction factor for the three regions are the following:

$$f_{L,1\phi}(\text{Re}_{1\phi}) = \frac{C_{lam}}{\text{Re}_{1\phi}} \quad \text{Eq. 5-53} \quad \text{ff}^{2(a),(c)}$$

$$\text{ff} \quad f_{Tran,1\phi}(\text{Re}_{1\phi}) = \left(1 - \frac{\text{Re}_{low}}{\text{Re}_{1\phi}}\right) \left(\frac{\text{Re}_{high}}{\text{Re}_{high} - \text{Re}_{low}}\right) \left(f_{T,1\phi}(\text{Re}_{high}) - f_{L,1\phi}(\text{Re}_{low})\right) + f_{L,1\phi}(\text{Re}_{low}) \quad \text{Eq. 5-54}$$

$$\frac{1}{\sqrt{f_{T,1\phi}(\text{Re}_{1\phi})}} = -2 \log_{10} \left(\frac{\varepsilon}{3.7D_H} + \frac{2.51}{\text{Re}_{1\phi}} \left(1.14 - 2 \log_{10} \left(\frac{\varepsilon}{D_H} + \frac{21.25}{\text{Re}_{1\phi}^{0.9}} \right) \right) \right) \quad \text{Eq. 5-55}$$

where

$$\varepsilon = \text{relative-pipe roughness}$$

The numerical value $C_{lam} = 64$ typically described for laminar flow is for flow in a round pipe. However, as described in Chapter 9 Section IV.B of Reference 12.1.25, the coefficient depends on geometry. According to Eq. (9.82) and Table 9-3 of Reference 12.1.25 for a rod bundle,

$$C_{lam} = 35.55 + 263.7 \left(\frac{\lambda}{d} - 1 \right) - 190.2 \left(\frac{\lambda}{d} - 1 \right)^2 \quad \text{Eq. 5-56}$$

where λ/d is the pitch-to-rod diameter, resulting in $C_{lam} = 102$ for $\lambda/d = 1.33$ for the typical NPM fuel bundle geometry. ~~ff~~ ^{2(a),(c)}

5.5.6.2.2 Two-Phase Friction Factor

With single-phase friction factors evaluated based on liquid and vapor properties, the Reference 12.1.27 approach is used to model the two-phase transition between these conditions.

The single-phase friction factors are obtained from Eq. 5-52. ~~ff~~The mixture friction factor is obtained as

$$f_m = \left(f_l + 2x \left(f_v \frac{\rho_l}{\rho_v} - f_l \right) \right) (1-x)^{1/3} + f_v \frac{\rho_l}{\rho_v} x^3 \quad \text{Eq. 5-57}$$

where

x = flow quality

~~ff~~^{2(a),(e)}

5.5.6.3 Pressure Drop for Local Form Losses

The generally two-phase form loss coefficient needed for evaluating pressure drop in Eq. 5-32 is correlated as function of the mixture Reynolds number. The latter is defined from

$$\text{Re}_{2\phi} = \frac{\dot{m} D_H}{\mu_m A} \quad \text{Eq. 5-58}$$

where the mixture viscosity is obtained from a quality-weighted interpolation of liquid and vapor viscosities [Cicchitti et al. relation shown in Eq. (11-80b) of Reference 12.1.25] as

$$\mu_m = x\mu_v + (1-x)\mu_l \quad \text{Eq. 5-59}$$

The loss coefficient as a function of the two-phase Reynolds number in Eq. 5-58 takes the form

$$\xi_{loc} = \left(\frac{A}{A_{ref}} \right)^2 \left[a \left(\frac{A}{A_{ref}} \right)^b \text{Re}_{2\phi}^b + c \right] \quad \text{Eq. 5-60}$$

where the coefficients a , b , and c are user-input along with a reference area A_{ref} associated with the loss coefficients.

5.5.6.4 Drift Flux Parameters

The drift flux parameters used in formulating the flow equations are the concentration parameter, C_0 , and the drift velocity, V_{gj} . Homogeneous flow conditions can be imposed by specifying $C_0 = 1$ and $V_{gj} = 0$.

For non-homogeneous flow, the values of the drift flux parameters are user-input. A correlation for the drift flux parameters is obtained from Eq. (3.10) of Reference 12.1.30. Accordingly, $\{$

$$C_0 = 1.13 \quad \text{Eq. 5-61}$$

$$V_{gj} = 1.41 \left[\frac{(\rho_f - \rho_g) \sigma g}{\rho_f^2} \right]^{0.25} \quad \text{Eq. 5-62}$$

where σ is surface tension.

The numerical value $V_{gj} = 0.14$ m/s is calculated at the nominal NPM operating pressure and it has only a weak dependence on pressure. $\}}^{2(a),(c)}$

5.5.6.5 Evaporation and Condensation

The correlation for phase change (evaporation and condensation) is adapted $\{$

$\}}^{2(a),(c)}$

{{

}}^{2(a),(c)} A boiling coefficient of $\gamma=5000 \text{ kg/m}^3\text{s}$ is the default value, where the user can change it by input. }}

}}^{2(a),(c)}

 {{

 }}^{2(a),(c)}

After converging to a steady-state solution that is not necessarily stable, the transient calculations are performed as follows:

- The point kinetics model is solved implicitly to update the fission energy term.
- The fraction of the fission energy deposited in the pellets is used in the pin heat conduction model to calculate the heat transfer at the clad surface. This term is added to the direct energy deposition to obtain the energy source term in the coolant. The conduction model is also used to get pellet temperature for Doppler reactivity to be used in the subsequent time step.
- The SG model is integrated to get the heat transfer from the primary coolant loop control volumes in contact with the SG secondary side.
- The core heat source term and the SG heat sink term are used in the thermal-hydraulic explicit solution of the fluid flow conservation equations. Mass flow rate, void fraction, and temperature fields are calculated. The coolant temperature in the core section is used to calculate the moderator temperature reactivity term for using in the subsequent time step point kinetics solution.

The stability of the calculated flow is optionally examined by introducing a user-defined perturbation. This perturbation is typically accomplished by ~~ff~~ assigning a nonzero pressure residual term for a small period of time, but can also be accomplished with a reactivity perturbation. The perturbed flow oscillates and the oscillations either grow if the system is unstable or decay to return to the pre-perturbation state eventually. The stability parameters, decay ratio and frequency, are calculated by a separate program using the mass flow rate time series output generated by the PIM code. ~~}}^{2(a),(c)}~~

The operating states and events covered include:

- Stability of various steady-state operating power levels (at the corresponding natural circulation flow) is analyzed to demonstrate the operating behavior with regard to the stability of the NPM during power operations. Stability at BOC and EOC conditions are verified, which addresses moderator reactivity variations in a representative design.
- Stability during transients is analyzed to demonstrate the operating behavior of the NPM during operational events, such as minor changes in feedwater flow, that may occur during normal operations and during AOOs. Also considered is the behavior of the plant to respond to gradual trends in feedwater flow, in which core thermal power responds to changing primary coolant conditions. Specifically, in the calculations presented, the plant is demonstrated to return to stable plant operations, possibly at a new power/flow condition, for any situation in which the riser subcooling is maintained (riser subcooling is protected by the hot leg trip setpoint).
- Stability during heatup at subcritical conditions is analyzed to demonstrate the operating behavior of the NPM during heatup using a non-nuclear heat source. Specifically, the calculations presented show that the plant does not experience unstable flow conditions as the system is brought to conditions necessary for initial criticality. This demonstration includes the effects of the non-nuclear heat source.

8.1 Stability Analysis for a Range of Steady-State Operating Conditions

The scope of this section is to demonstrate the stability performance of the NPM during power operations for a range of power and flow conditions in case of a small perturbation in the plant operations. In each analysis, the natural circulation flow rate is commensurate with power level. Primary system flow, core inlet temperature, secondary inlet flow and temperature, and the secondary steam pressure conditions are specified at each power level. Modeling incorporates the effects of ambient heat losses and heat loss through the non-regenerative heat exchange in the CVCS described in Section 3.6 to ensure consistent thermodynamic modeling of plant operations. ~~}}~~In modeling the CVCS, ~~}}~~ ^{2(a),(c)} of primary system coolant is assumed to be withdrawn from the downcomer and returned to the riser at evaluated power levels. Because supplementary heating is not provided to the CVCS water, the water returned to the riser is colder than the water taken out of the downcomer as a result of heat removal by the non-regenerative heat exchanger indicated in Section 3.4. ~~}}~~^{2(a),(c),ECI}

The entire range of conditions described in Section 3.6 is considered. However, calculations described in detail in this section are performed at representative thermal power levels of 160, 120, 80, 40, 32, and 1.6 MW. These conditions are equivalent to 100, 75, 50, 25, 20, and 1 percent of rated power, respectively. The power level of 32 MW is considered to address effects related to activation of the turbine and feedwater heater system.

After reaching steady state in each calculation, a small perturbation is applied to the steady conditions ~~ff~~ by the following approaches:

- A momentary (1 second) increase in pressure loss residual in the natural circulation primary coolant circuit – The momentary pressure residual perturbation is chosen as the main approach for its reliable effect on initiating a system-wide response and for exciting all possible modes in the NPM.
- A one-cycle sinusoidal oscillation of pressure loss residual with specified oscillation periods – This approach is used to selectively excite particular oscillation periods.
- A change in the secondary feedwater conditions that results in a primary system flow disturbance – The feedwater perturbation is provided to illustrate an alternate approach for perturbing the system in elected cases. This perturbation is also consistent with a technique used in the NIST-1 testing.

~~ff~~^{2(a),(e)}

After the primary system flow is disturbed, the transient response is calculated and time series signals are recorded in output files for examining the system behavior and evaluating its stability. The stability is deduced from the core inlet flow as function of time, and the signal is selected in a time interval during which the signal clarity is optimal. ~~ff~~ There are two different considerations in interpreting the transient response:

- The short window immediately after the perturbation highlights the apparent decay ratio of the system to a perturbation. This apparent decay ratio illustrates the rapid response of the system to a perturbation and in effect combines all possible modes. The system quickly attempts to return to the initial conditions.
- The relatively long-term transient response of the system is to show very small magnitude oscillations relative to the initial response to a sharp perturbation. These oscillations are related to loop dynamics, in which the longest period oscillation is characterized by the overall time for fluid to transit about the natural circulation loop. Modes of shorter periods, in principle, may persist longer. ~~ff~~^{2(a),(e),EC1}

Brief consideration for the early response and the resulting apparent decay ratio is given in this section. However, the overall effect of any small perturbation that allows the system to return to the initial condition is bounded by the response to operational events described in the next section. The primary emphasis of this section is to demonstrate the stability of the long-term transient response.

Analyses are performed at each condition for a duration that represents approximately ten circuits of coolant in the primary system. The time for coolant to make one circuit corresponds to the primary system coolant mass (not including water in the pressurizer) divided by the flow rate. ~~ff~~ Values of the primary system transit times are provided in Table 8-1. This analysis duration is selected to allow sufficient time for the short-lived effects to dampen, leaving a clean indication of the longer-lived effects. ~~ff~~^{2(a),(e)}

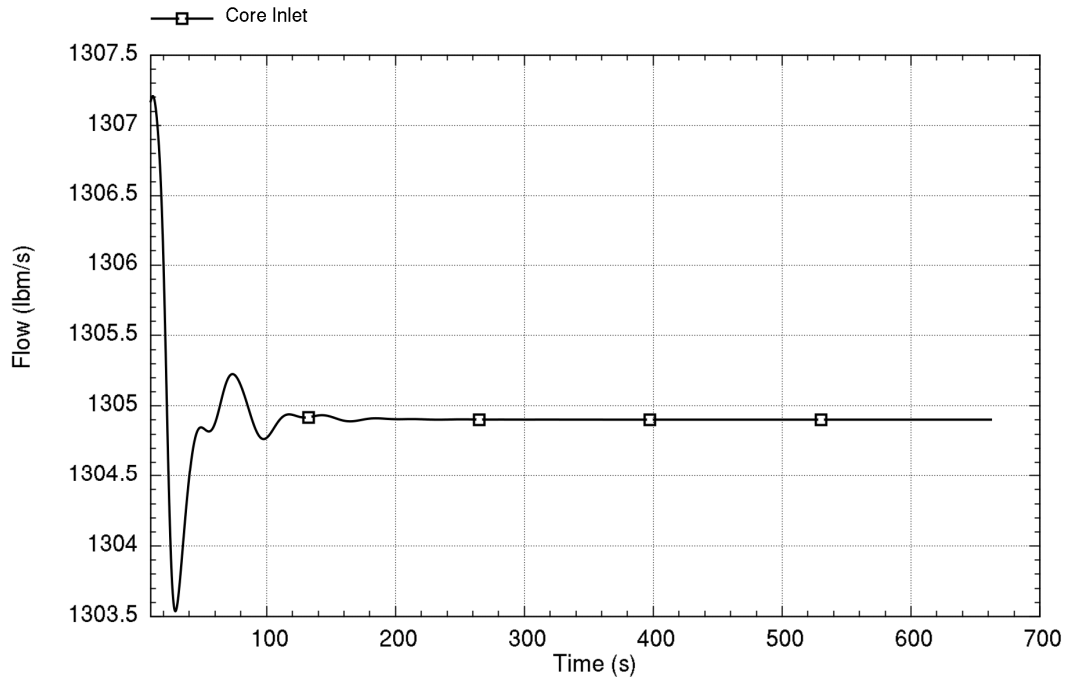
In applying the perturbation for determining stability performance, it is important to recognize that the magnitude of the resulting initial disturbance is not important as long as the disturbance is small enough to introduce no nonlinear effects or to cause flow regime or heat transfer transitions. What is considered is the relative change of a signal as the disturbance propagates in time.

8.1.1 Stability at Rated Power

Starting at 160 MW core power with the core at BOC cycle exposure (closest moderator reactivity to zero), a pressure residual perturbation is introduced at time zero. Figure 8-1 depicts the primary coolant flow response starting 10 seconds after the perturbation and shows highly-damped oscillations in the early time window that vanish on the plot scale by 250 seconds. The early system damping is so strong that showing predictions starting at 0.0 seconds results in scaling the y-axis of the graph so large that little detail is discernable after 200 seconds.

Figure 8-2 shows the corresponding graph of power for fission plus decay heat and heat removal by SG and ambient losses. This graph also illustrates the highly-stable response. In inspecting the figures, the relative change in oscillation magnitude with time is the main figure of merit, not the absolute change; the size of the perturbation and absolute scale on the y-axis are not important. ^{(a),(c),ECI}

ff

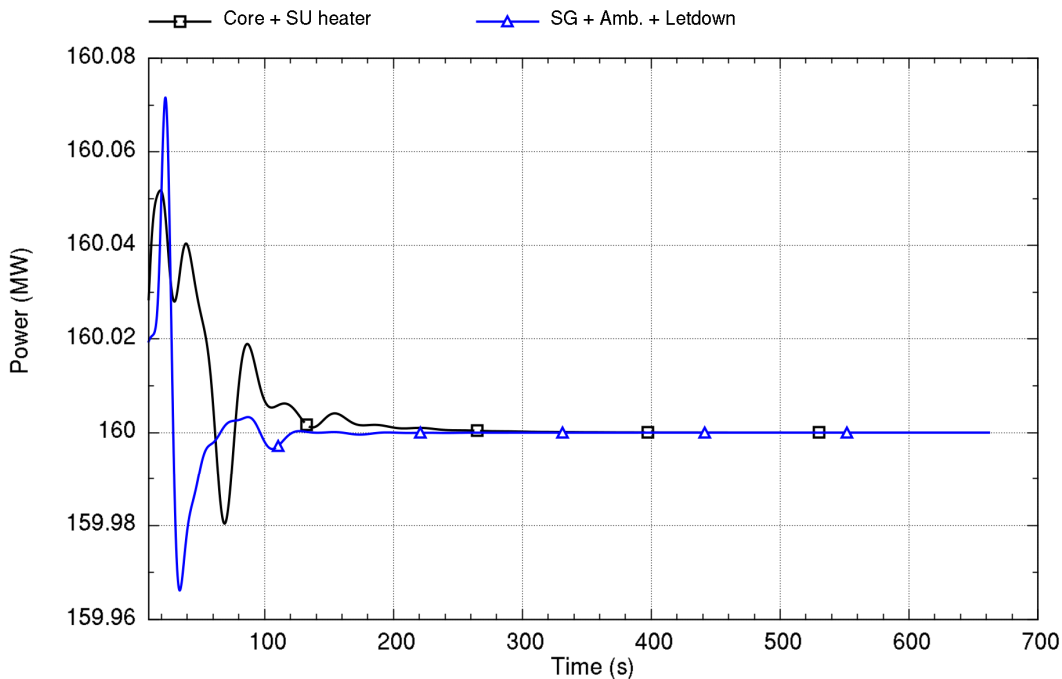


Run ID: Run on Jun/01/2016 at 01:05:55 with PID 017816

ff 2(a),(e),ECI

Figure 8-1. Time trace of primary coolant flow response to a perturbation at rated conditions and beginning-of-cycle reactivity

ff



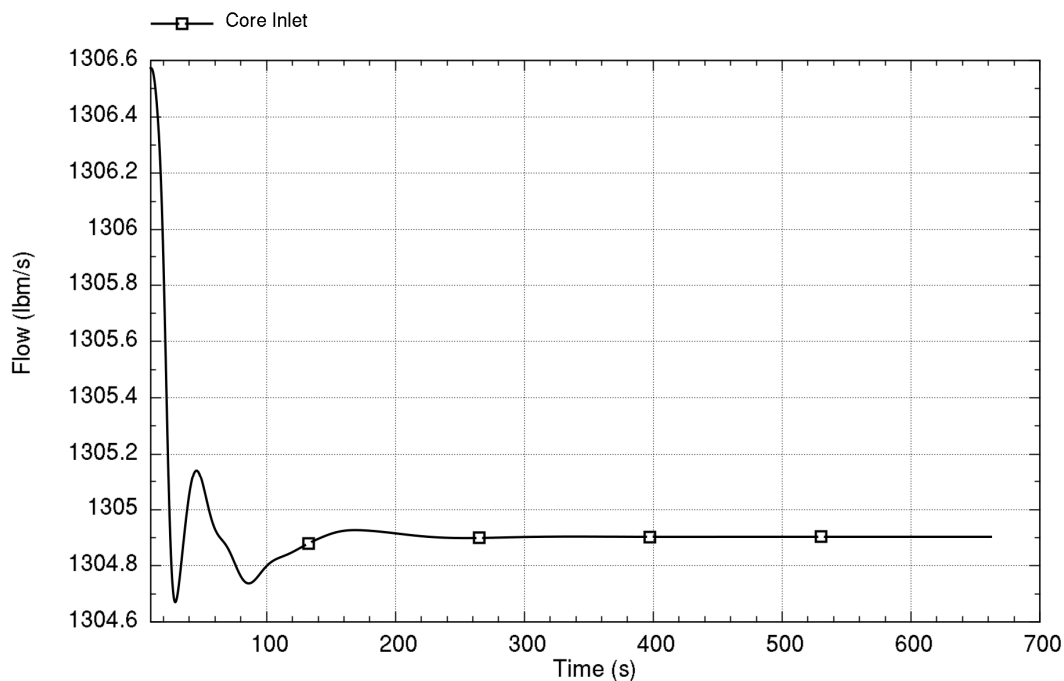
Run ID: Run on Jun/01/2016 at 01:05:55 with PID 017816

ff2(a),(e),ECI

Figure 8-2. Time trace of heat addition and heat removal response to perturbation at rated conditions and beginning-of-cycle reactivity

ff-The sensitivity of the stability at the rated conditions is examined for the effect of the reactivity-to-power feedback related to core burnup. Figure 8-3 shows the primary coolant flow rate following a perturbation at rated power for EOC reactivity conditions (most negative moderator reactivity value). The system is again shown to be stable and the oscillation damping is generally stronger (e.g., the system is more stable) for this case than at BOC. In this analysis, the point kinetics parameters and fuel rod burnup level are also changed to EOC conditions. ff2(a),(e),ECI

ff



Run ID: Run on Jun/01/2016 at 01:13:05 with PID 013056

}}2(a),(c),ECI

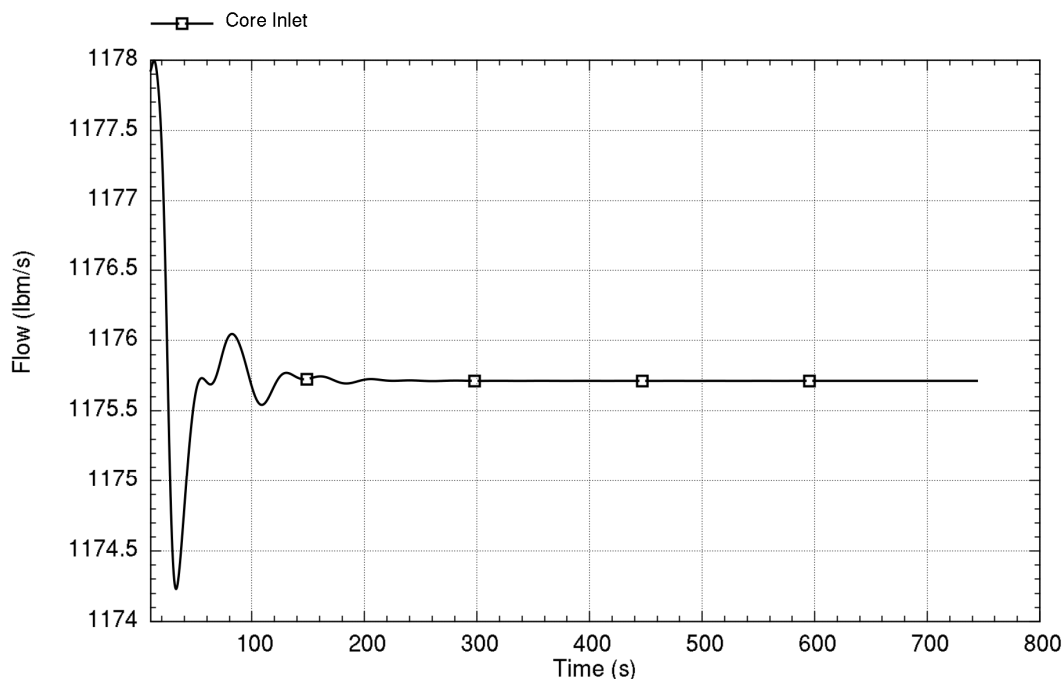
Figure 8-3. Time trace of primary coolant flow response to a perturbation at rated conditions and end-of-cycle reactivity

ff Comparing the effects of BOC vs. EOC conditions, the neutron kinetics feedback from negative reactivity effects at EOC provides a stabilizing effect (i.e., the more negative the reactivity, the more stabilizing the effect). }}2(a),(c),ECI

8.1.2 Stability at 120 MW

ff Starting at 120 MW core power (75 percent of rated power) for BOC reactivity conditions, a pressure perturbation is introduced at time zero. Figure 8-4 depicts the primary coolant flow response 10 seconds after the perturbation and shows highly-damped oscillations that vanish on the plot scale by 250 seconds. }}2(a),(c),ECI

ff



Run ID: Run on Jun/01/2016 at 01:05:10 with PID 007652

ff^{2(a),(e),ECI}

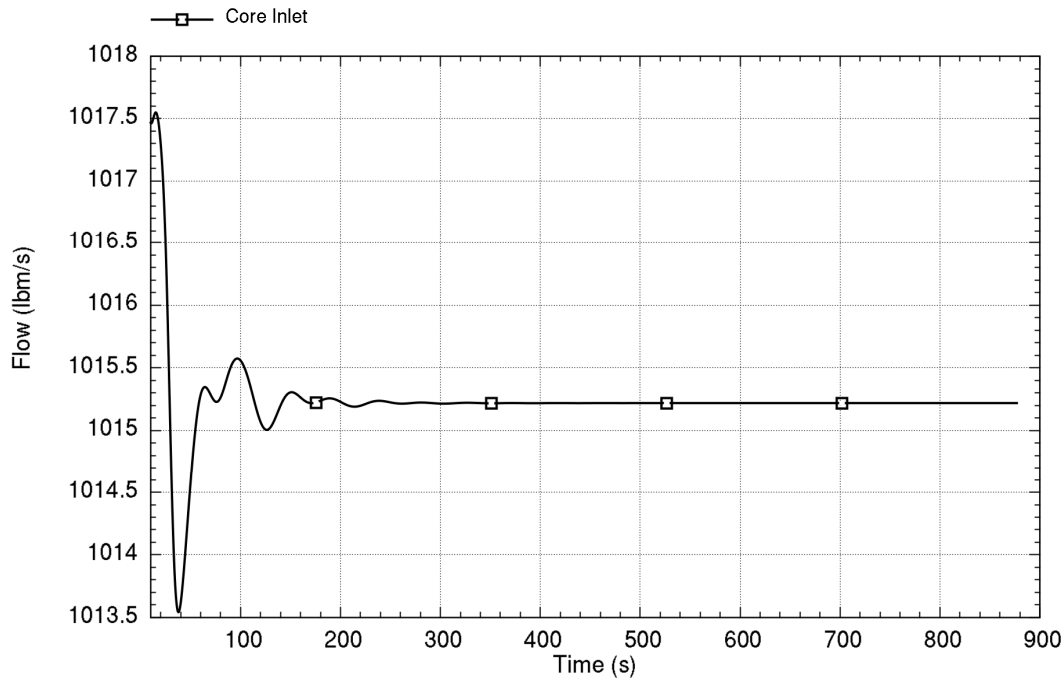
Figure 8-4. Time trace of primary coolant flow response to a perturbation at 120 MW and beginning-of-cycle reactivity

ff The flow response is highly stable at this power level, in which careful inspection relative to Figure 8-1 shows slight increase in oscillatory behavior, but nothing of interest. Results for EOC at this power level are consistent; less oscillation than BOC at this power level and slight increase in oscillatory behavior relative to EOC at rated power shown in Figure 8-3. ff^{2(a),(e),ECI}

8.1.3 Stability at 80 MW

ff Stability at 80 MW core power (50 percent of rated power) for BOC reactivity conditions is now evaluated. Figure 8-5 depicts the primary coolant flow response 10 seconds after the perturbation and shows highly-damped oscillations that vanish on the plot scale by 350 seconds. ff^{2(a),(e),ECI}

ff



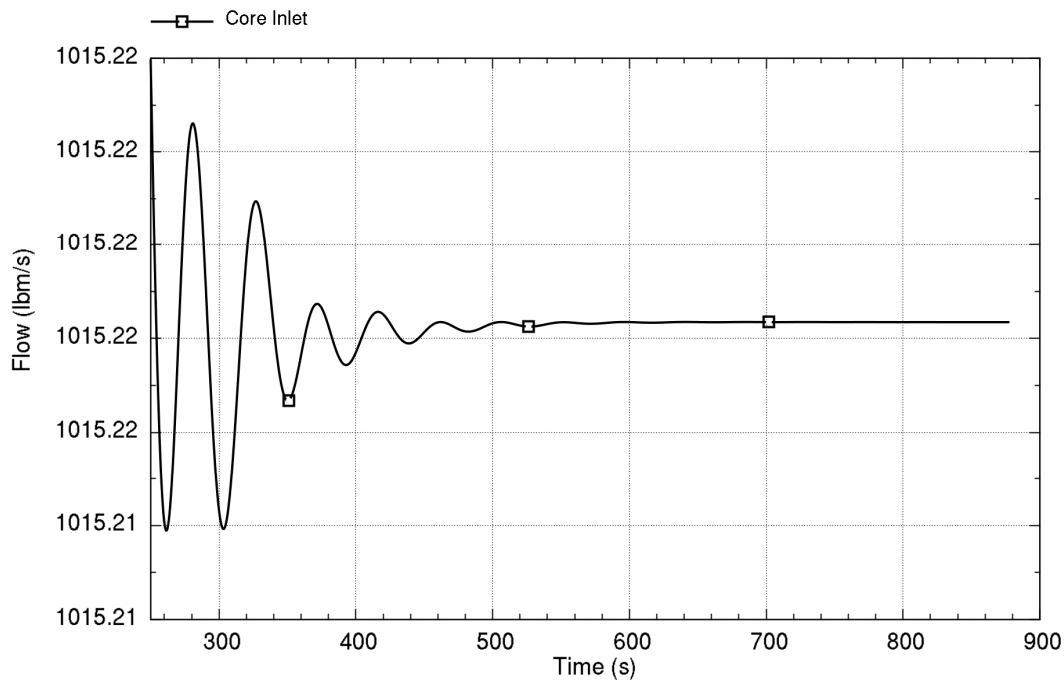
Run ID: Run on Jun/01/2016 at 01:04:25 with PID 002536

ff^{2(a),(e),ECI}

Figure 8-5. Time trace of primary coolant flow response to a perturbation at 80 MW and beginning-of-cycle reactivity

ff The flow response is highly stable at this power level, but with the smallest hint of oscillation at 250 seconds on the plot scale. This is illustrated by graphing the core flow starting at 250 seconds in Figure 8-6 and scaling the y-axis to highlight the oscillations. The intent of Figure 8-6 is to show the relative change in oscillation magnitude with time, so the absolute scale on the y-axis is not important. ff^{2(a),(e),ECI}

ff



Run ID: Run on Jun/01/2016 at 01:04:25 with PID 002536

ff^{2(a),(c),ECI}

Figure 8-6. Time trace of primary coolant flow response to a perturbation at 80 MW and beginning-of-cycle reactivity after 250 seconds

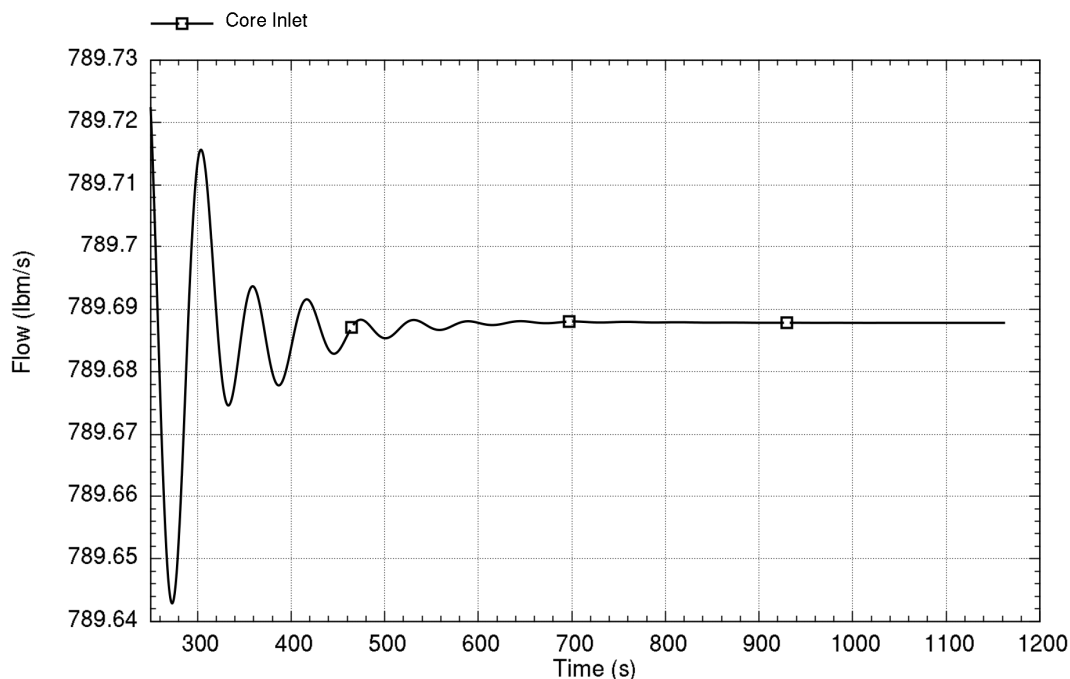
ff Figure 8-6 indicates that some long-lived oscillations persist after 250 seconds. The oscillation period is approximately 45 seconds, as seen by looking at successive peaks in the figure, and the decay ratio is clearly less than 1.0.

Results for EOC at this power level are consistent with earlier results; there is less oscillation than BOC at this power level and slight increase in oscillatory behavior relative to EOC at higher power. ff^{2(a),(c),ECI}

8.1.4 Stability at 40 MW

ff Stability at 40 MW core power (25 percent of rated power) for BOC reactivity conditions is now evaluated. Figure 8-7 depicts the primary coolant flow response 250 seconds after the perturbation. Results before 250 seconds are consistent with earlier figures. This figure shows damped oscillations that vanish on the plot scale by 800 seconds. ff^{2(a),(c),ECI}

ff



Run ID: Run on Jun/01/2016 at 01:03:42 with PID 017912

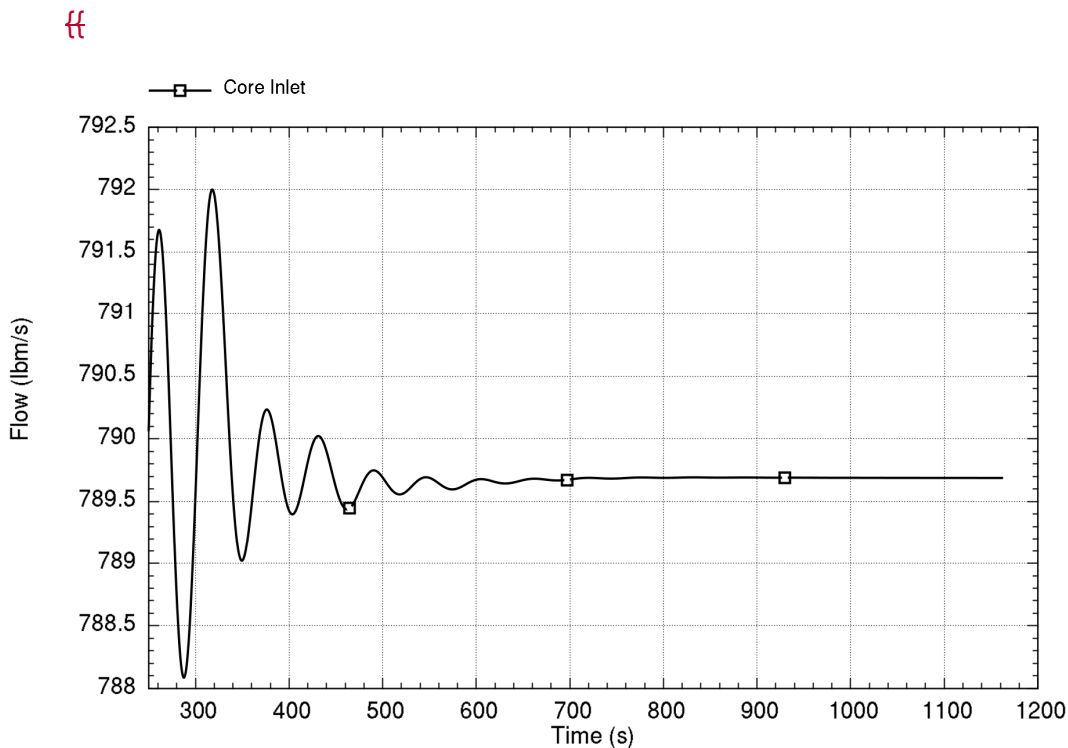
ff2(a),(e),ECI

Figure 8-7. Time trace of primary coolant flow response to a perturbation at 40 MW and beginning-of-cycle reactivity after 250 seconds

ff-The flow response is stable at this power level. However, oscillations persist and a measureable decay ratio is present. The oscillation period of the observed oscillations is approximately 57 seconds and the decay ratio is estimated to be 0.58 based on analyzing the long-lived flow response from approximately 550 seconds through the end of the analysis.

The result in Figure 8-7 provides the first clear indication of the relatively long-term transient response of the system. Results for an alternate pressure residual perturbation approach using a one-cycle sine variation with period of approximately 57 seconds are shown in Figure 8-8. The purpose of this perturbation is to specifically excite the long-lived oscillation observed with the short-pressure perturbation with sufficient energy that it can be clearly observed. The resulting period and decay ratio are consistent with earlier results in Figure 8-7, and this confirms the long-lived response is not a numerical artifact.

An additional sensitivity for a perturbation period coincident with the loop time constant at this power shows the long-term response of the system returns to a similar period as described above, so the long-term response is self-selecting of the system cannot be imposed. ff2(a),(e),ECI

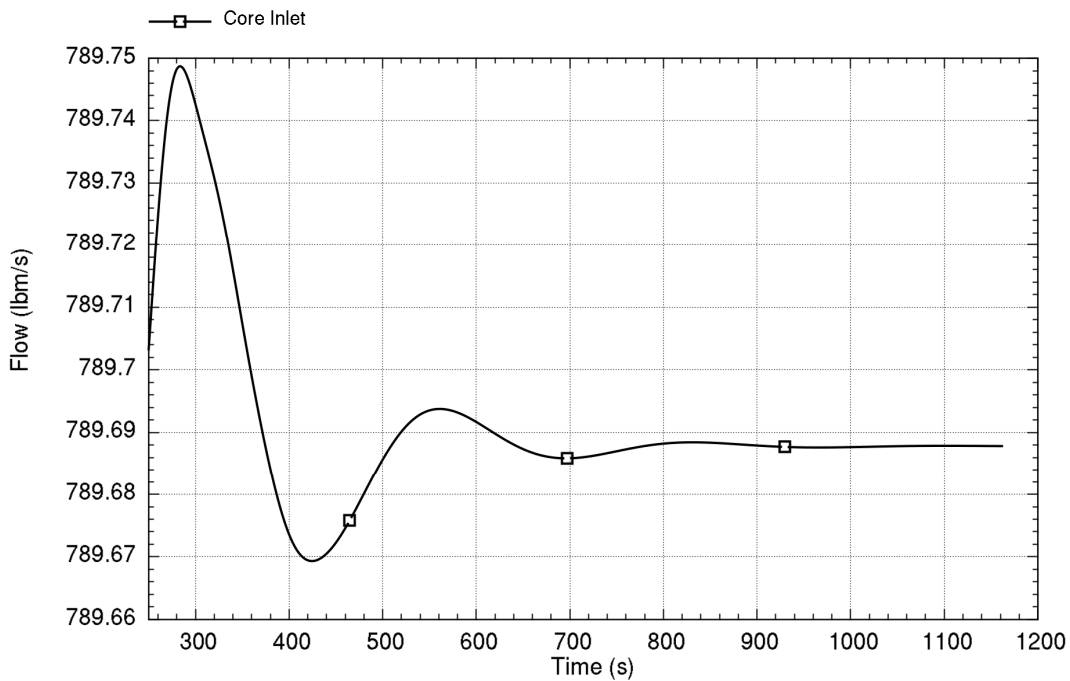


ff^{2(a),(e),ECI}

Figure 8-8. Time trace of primary coolant flow response to a sine perturbation with period of 57 seconds at 40 MW and beginning-of-cycle reactivity after 250 seconds

ff—Results for EOC at 40 MW are consistent with earlier results; EOC conditions are more stable than BOC conditions as shown in Figure 8-9. In this figure, an oscillation of an approximate 270-second period is observed. This oscillation is the feedback effect of large negative moderator reactivity in core, which can be seen by inspecting the fission power in Figure 8-10. The effect of negative moderator feedback is more clearly observable when inspecting the operational events in Section 8.2. ff^{2(a),(e),ECI}

ff

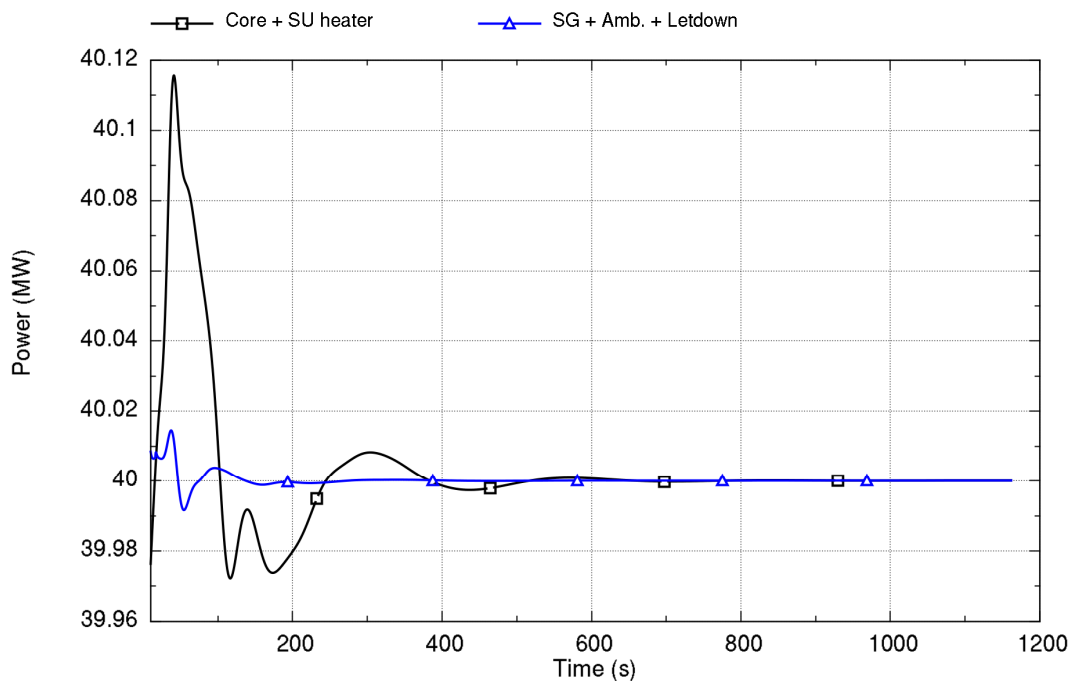


Run ID: Run on Jun/01/2016 at 01:11:00 with PID 007396

ff2(a),(e),ECI

Figure 8-9. Time trace of primary coolant flow response to a perturbation at 40 MW and end-of-cycle reactivity after 250 seconds

ff



Run ID: Run on Jun/01/2016 at 01:11:00 with PID 007396

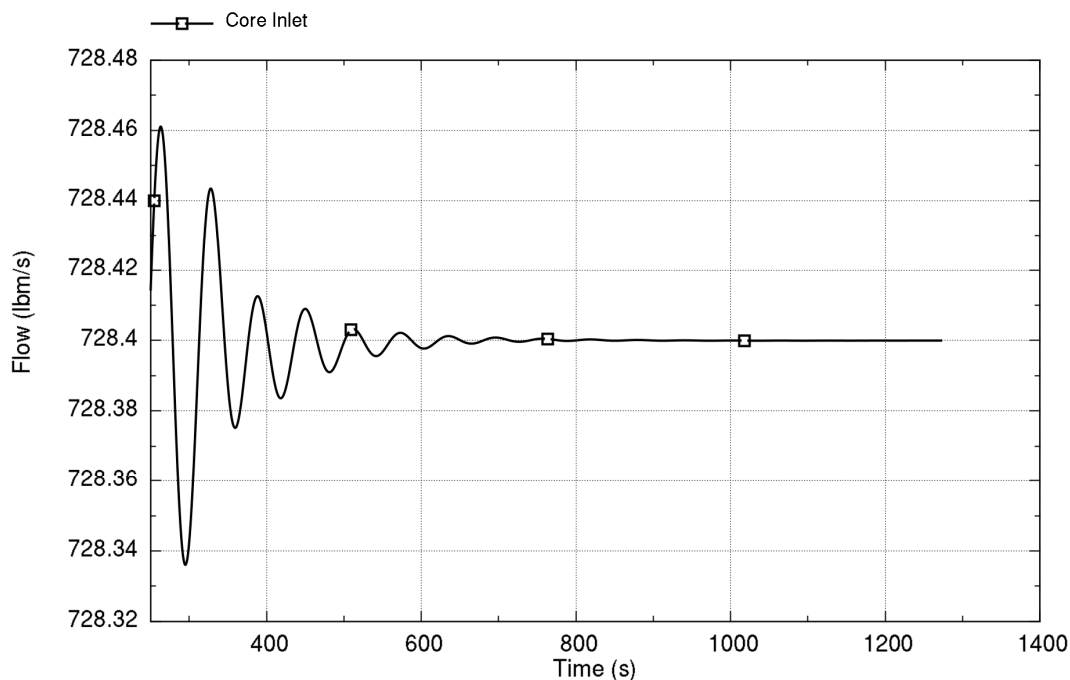
ff^{2(a),(e),ECI}

Figure 8-10. Time trace of heat addition and heat removal response to a perturbation at 40 MW power and end-of-cycle reactivity

8.1.5 Stability at 32 MW

ff—Stability at 32 MW core power (20 percent of rated power) with a feedwater temperature of 50 degrees-F for BOC reactivity conditions is now evaluated. Figure 8-11 depicts the primary coolant flow response 250 seconds after the perturbation and shows damped oscillations with a period of approximately 62 seconds. ff^{2(a),(e),ECI}

}}



Run ID: Run on Jun/01/2016 at 01:03:24 with PID 011676

}}^{2(a),(c),ECI}

Figure 8-11. Time trace of primary coolant flow response to a perturbation at 32 MW and beginning-of-cycle reactivity

}}

This figure illustrates the extent of the oscillations. Damping of the oscillations after 400 seconds corresponds to a decay ratio of approximately 0.53. This case with feedwater temperature of 50 degrees-F shows a slightly more unstable behavior than the same case performed at 200 degrees-F. The two different feedwater temperatures correspond to the conditions before and after the turbine and feed-water heater system are brought online as described in Section 3.6. Results for EOC at this power level are consistent with earlier results. }}^{2(a),(c),ECI}

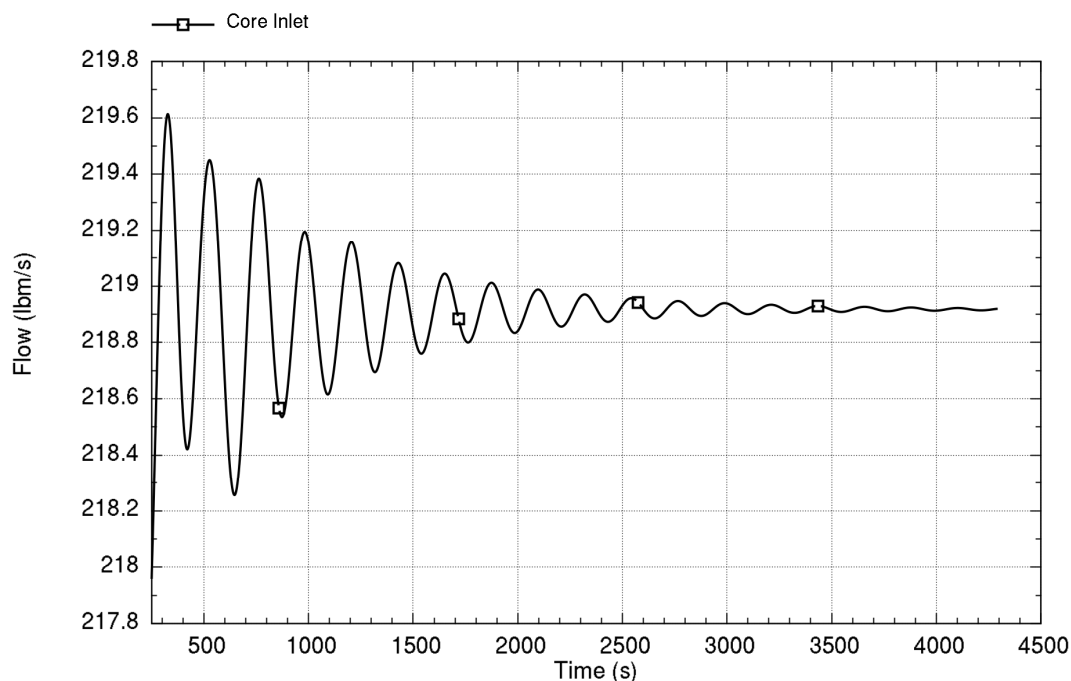
8.1.6 Stability at 1.6 MW

}}

Stability at 1.6 MW core power (1 percent of rated power) at BOC reactivity conditions is now evaluated. This condition has a core inlet temperature a little above 420 degrees-F. At this temperature, the moderator reactivity feedback is slightly positive at BOC as described in Section 5.6.1.2; however, the overall net reactivity is negative as a result of the fuel Doppler coefficient.

The CVCS is active and results in }} ^{2(a),(c)} of heat removal. Ambient heat losses consistent with primary system temperature are also included. These effects result in the total heat removal by the SG of approximately }} ^{2(a),(c),ECI}

Figure 8-12 depicts the primary coolant flow response 250 seconds after the perturbation and shows damped oscillations with a period of approximately 223 seconds. A decay ratio of approximately 0.74 is calculated, which is less stable than the higher power cases.



Run ID: Run on Jun/01/2016 at 01:02:51 with PID 020088

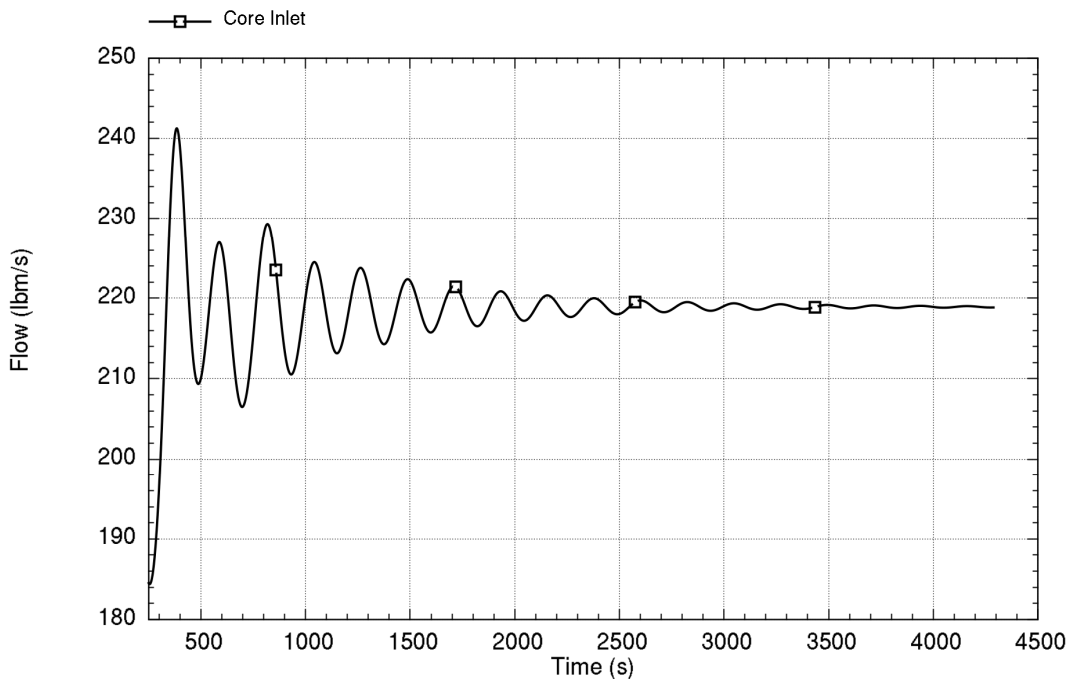
2(a),(e),ECI

Figure 8-12. Time trace of primary coolant flow response to a perturbation at 1.6 MW and beginning-of-cycle reactivity

The decay ratio in this condition is larger than seen at higher power levels. The result in Figure 8-12 shows the relatively long-term transient response of the system. Figure 8-13 shows results for an alternate pressure residual perturbation approach using a one-cycle sine variation with a period of approximately 223 seconds. The resulting period and decay ratio are consistent with earlier results in Figure 8-12, which confirms the long-lived response is not a numerical artifact, but is consistent with the results for 40 MW.

An additional sensitivity for a perturbation period coincident with the loop time constant at this power shows the long-term response of the system at 1.6 MW returns to a similar period as described above, thus the long-term response is confirmed to be self-selecting of the system and cannot be imposed. 2(a),(e),ECI

ff



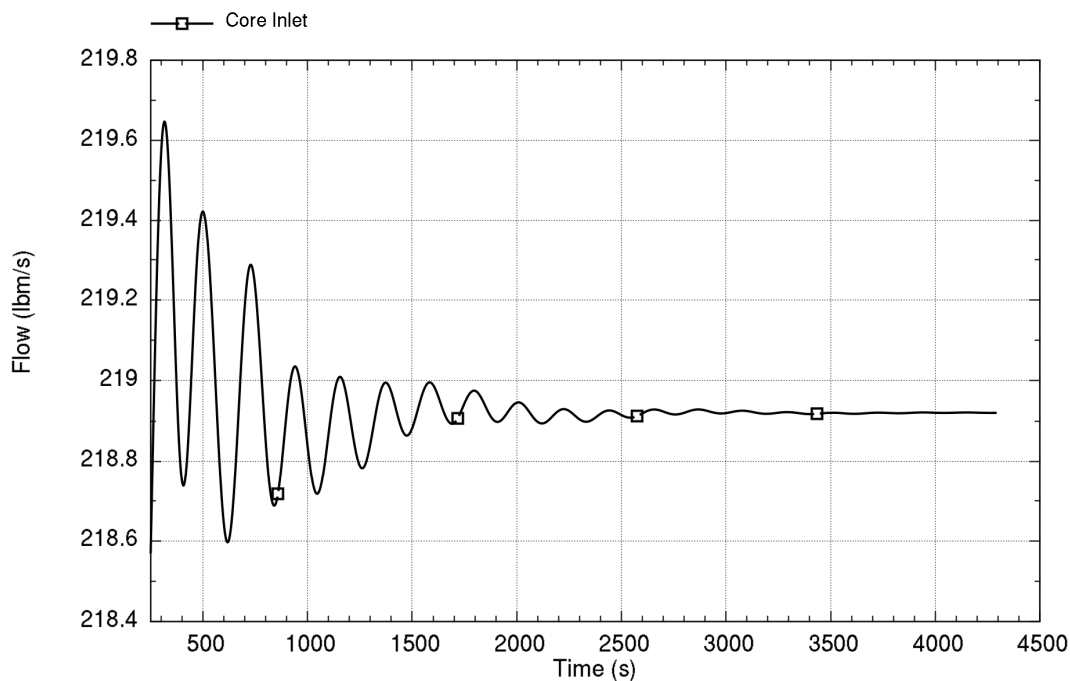
Run ID: Run on Jun/01/2016 at 01:31:54 with PID 001268

ff^{2(a),(e),ECI}

Figure 8-13. Time trace of primary coolant flow response to a sine perturbation with a period of 223 seconds at 1.6 MW and beginning-of-cycle reactivity after 250 seconds

ff Results for EOC at this power level are consistent with earlier results; the behavior is more damped than BOC conditions in Figure 8-14. Figure 8-14 depicts the primary coolant flow response 250 seconds after the perturbation. ff^{2(a),(e),ECI}

ff



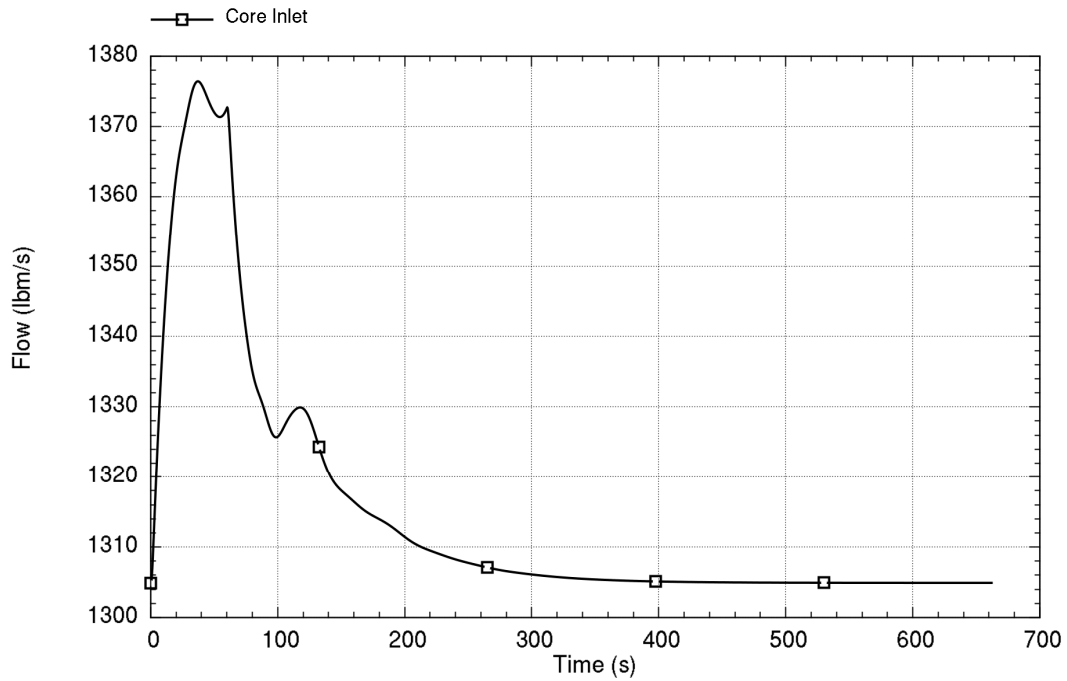
ff2(a),(e),ECI

Figure 8-14. Time trace of primary coolant flow response to a perturbation at 1.6 MW and end-of-cycle reactivity

8.1.7 Stability at Rated Power with Feedwater Perturbation

ff—Starting at 160 MW core power with the core at BOC cycle exposure (smallest moderator reactivity), the feedwater flow rate is increased by 20 percent for 60 seconds, then returned to the original value. Figure 8-15 depicts the primary coolant flow response starting at 0 seconds. Inspecting the results, one notable increase in primary system flow occurs at approximately 110 seconds. After that time, the primary system flow gradually returns to the initial value. The corresponding graph of power for fission plus decay heat and heat removal by SG and ambient losses is shown in Figure 8-16. This graph also illustrates the highly-stable response. ff2(a),(e),ECI

ff

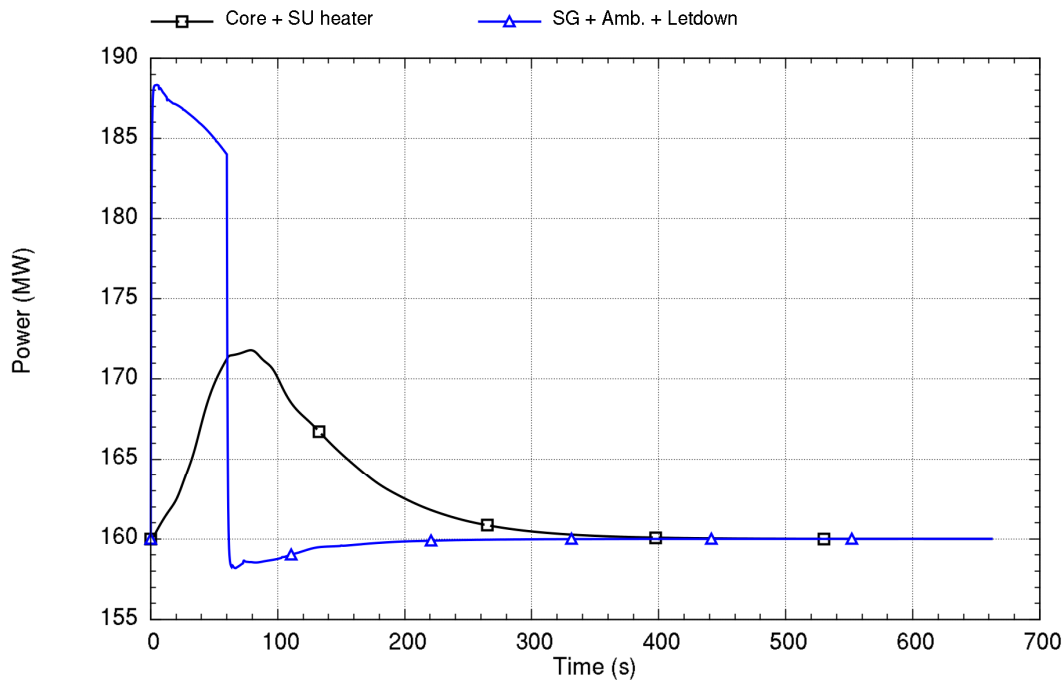


Run ID: Run on Jun/01/2016 at 16:45:28 with PID 005388

ff2(a),(e),ECI

Figure 8-15. Time trace of primary coolant flow response to a 60-second feedwater perturbation at rated conditions and beginning-of-cycle reactivity

ff



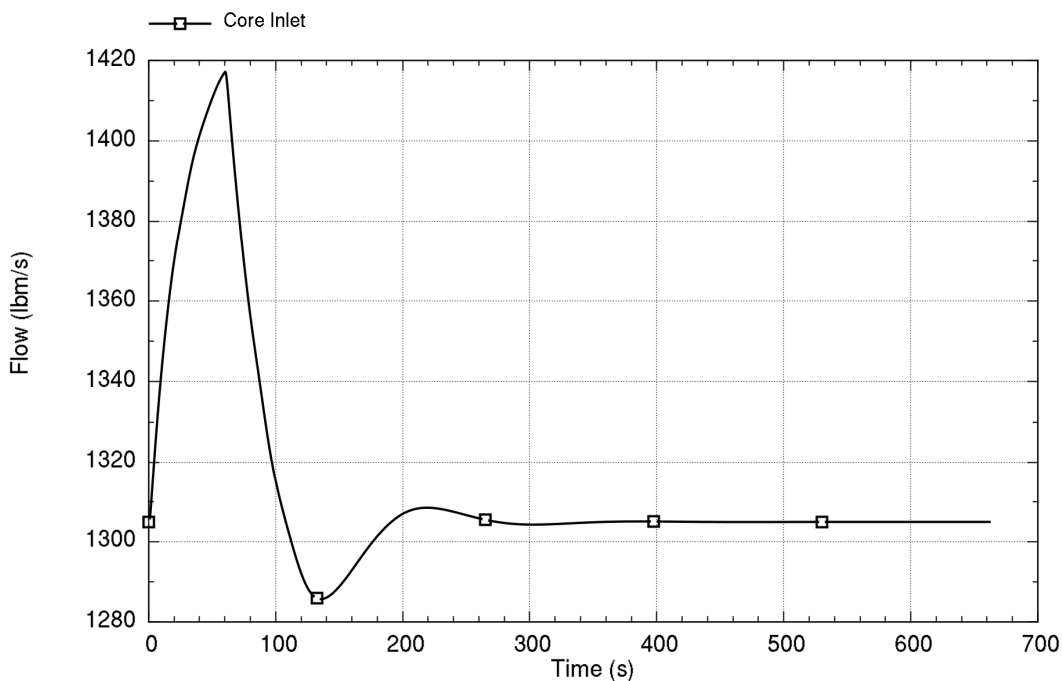
Run ID: Run on Jun/01/2016 at 16:45:28 with PID 005388

ff^{2(a),(e),ECI}

Figure 8-16. Time trace of heat addition and heat removal response to a 60-second feedwater perturbation at rated conditions and beginning-of-cycle reactivity

ff—The sensitivity of the stability at the rated conditions to the same feedwater perturbation is illustrated for the effect of EOC reactivity in Figure 8-17 for the primary coolant flow rate. The stronger negative moderator reactivity strongly dampens the flow response as seen in earlier sections. ff^{2(a),(e),ECI}

ff



Run ID: Run on Jun/01/2016 at 16:58:49 with PID 005744

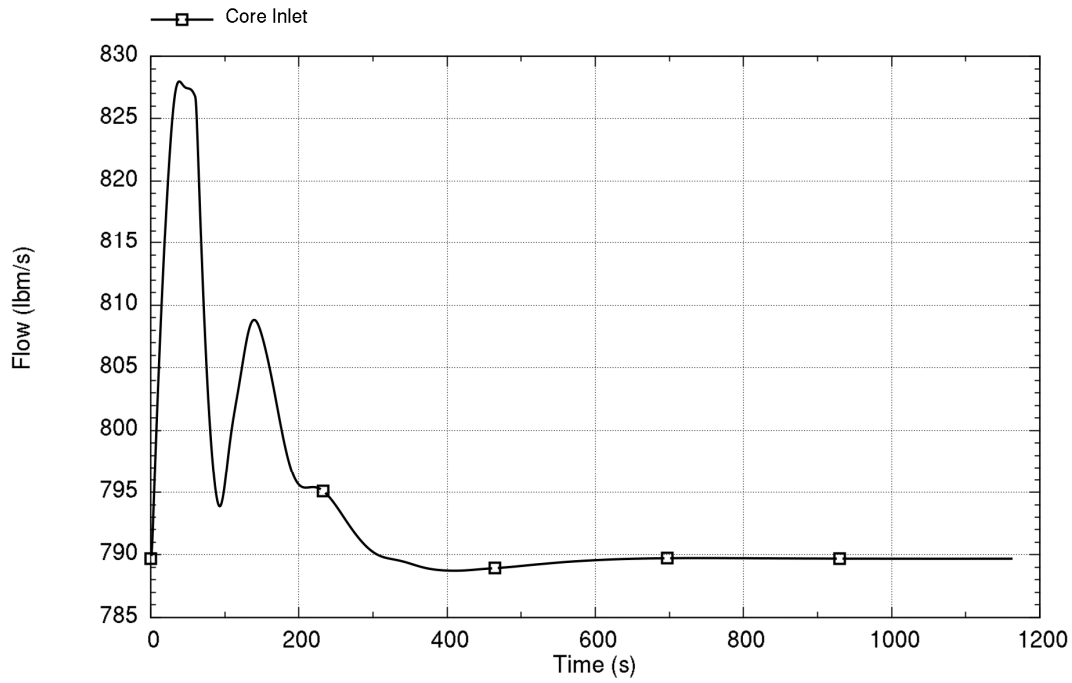
}}2(a),(c),ECI

Figure 8-17. Time trace of primary coolant flow response to a perturbation at rated conditions and end-of-cycle reactivity

8.1.8 Stability at 40 MW with Feedwater Perturbation

ff—Starting at 40 MW core power with the core at BOC cycle exposure (smallest moderator reactivity), the feedwater flow rate is increased by 20 percent for 60 seconds, then returned to the original value. Figure 8-18 depicts the primary coolant flow response starting at 0 seconds. The corresponding graph of power from fission plus decay heat and heat removal by SG and ambient losses is shown in Figure 8-19. Overall, the response is consistent with rated conditions, but with a larger flow increase after the feedwater perturbation. It is important to note that the relative magnitude of the initial primary system flow response is sufficiently large that the long-lived oscillations illustrated in Section 8.1.4 are not discernable in these results.}}2(a),(c),ECI

ff

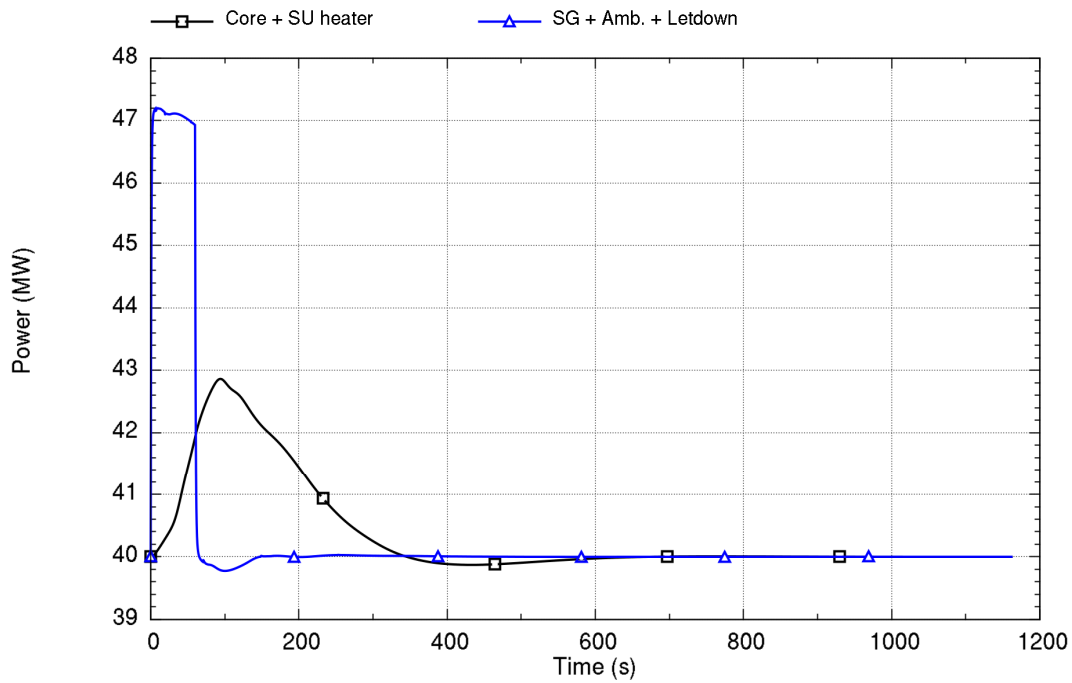


Run ID: Run on Jun/01/2016 at 16:43:24 with PID 014312

ff 2(a),(e),ECI

Figure 8-18. Time trace of primary coolant flow response to a 60-second feedwater perturbation at 40 MW and beginning-of-cycle reactivity

ff



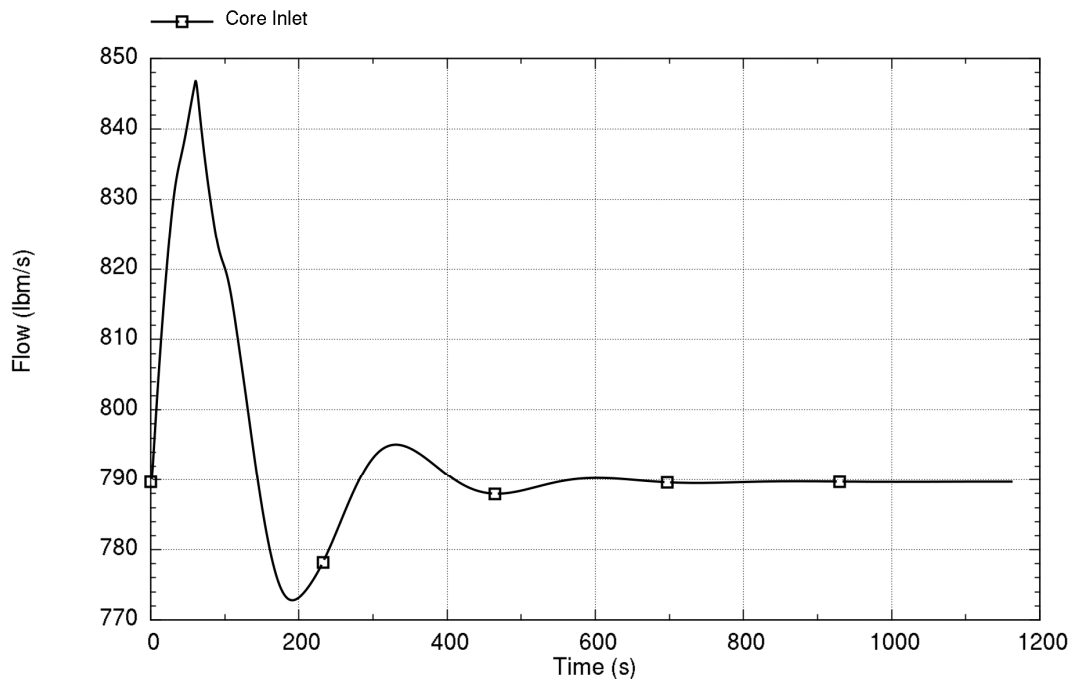
Run ID: Run on Jun/01/2016 at 16:43:24 with PID 014312

ff2(a),(e),ECI

Figure 8-19. Time trace of heat addition and heat removal response to a 60-second feedwater perturbation at 40 MW and beginning-of-cycle reactivity

ff—The sensitivity of the stability at the rated conditions to the same feedwater perturbation is illustrated for the effect of EOC reactivity in Figure 8-17. The stronger negative moderator reactivity strongly dampens the flow response as seen in earlier sections. ff2(a),(e),ECI

ff



Run ID: Run on Jun/01/2016 at 16:56:16 with PID 004156

}}2(a),(c),ECI

Figure 8-20. Time trace of primary coolant flow response to a perturbation at rated conditions and end-of-cycle reactivity

8.2 Stability Analysis for Operational Events

ff—Because primary system flow of the NPM is dictated by natural circulation principles, the range of flow for which the plant can operate in steady state at a given power level is narrow, and governed by effects such as pressure losses and the helical-coil once-through SG pressure and level. The system stability performance as representative of fixed points along the power-flow operating line has been described in Section 8.1. It remains to examine state points other than these steady-state points. In effect, the system may pass through conditions (defined by power, flow, and other state variables) in a transitory way that fall outside the evaluated steady state conditions. The purpose of this section is to show the behavior of the NPM in transiting through these conditions and the behavior at the event end point. Alternatively, the MPS will mitigate any potentially unstable conditions before instability can occur. Section 9.0 evaluates the identified situations in more detail.

The type of stability investigation performed in this section widens the scope of the inquiry beyond the strict requirement of initial conditions near a fixed point. }}2(a),(c),ECI

However, the nature of the natural circulation system performance narrows the analysis down to examining transients that are credible and realizable in the physical NPM. For this, a set of operational events is investigated, in which externally imposed boundary conditions are applied to influence the system response. These boundary conditions may include reactivity insertion (either directly in the core or by changes in primary system conditions) and plausible changes in primary and secondary conditions.

While not intended to be the final event evaluation, results are presented to demonstrate proper behavior of the code and to identify an acceptable operating region for the NPM. Formal application of the stability methodology is expected to address and disposition plausible events associated with the licensing basis of the NPM. Events considered fall into the following general classifications:

- increase in heat removal by the secondary system
- decrease in heat removal by the secondary system
- decrease in reactor coolant system (RCS) flow rate
- increase in reactor coolant inventory
- reactivity and power distribution anomalies
- decrease in reactor coolant inventory

The operational events addressed here are related to licensing basis AOOs. However, typical licensing basis AOO scenarios are selected for their sizable system response and reliance of the reactor protection system (including reactor trip) to mitigate the effects of the scenario. Here, the focus is on events that do not instigate a reactor trip in order to show the stable nature of the NPM. This condition is a key consideration because any event quickly resulting in MPS trip will not experience instability, but a relatively mild event within the limits of an MPS trip needs to be ensured not to progress toward unstable operation.

The PIM code provides the NPM system response, which demonstrated system stability at initially steady-state operation in Section 8.1. It should be noted that, unlike starting from a steady state (fixed point), there is no need to apply an artificial perturbation. An input forcing function is applied to the appropriate boundary condition to initiate the transient, for example, user-specified feedwater flow changing as a function of time to simulate a decrease in heat removal by the secondary system.

In addition to the above event classes, several additional events are addressed that do not fall into the classifications. These events are identified based on a consideration for events that may occur in the NPM, but may typically be of low interest in the safety analysis because they show non-limiting transient response outside of stability considerations. The following events are also addressed: ~~112(a),(e),ECI~~

- ~~ff~~ effect of oscillating secondary system flow
- stability during gradual shutdown
- stability during non-nuclear heat-up (before criticality)

While a typically non-limiting operational event, effects of sinusoidal flow oscillations in the secondary system arising from a controller or valve behavior that may produce sinusoidal oscillations in feedwater flow, temperature, or steam pressure are considered. This sinusoidal behavior is addressed to evaluate the primary system response to an externally driven influence to show the NPM does not experience resonant response to the excitation that may lead to large oscillations in the primary system. In addition, the events related to gradual shutdown of the NPM by following changes in feedwater flow (load following) and the effects of non-nuclear heat sources used to heat the primary system before criticality are evaluated. ~~ff~~^{2(a),(e),ECI}

8.2.1 Increase in Heat Removal by the Secondary System

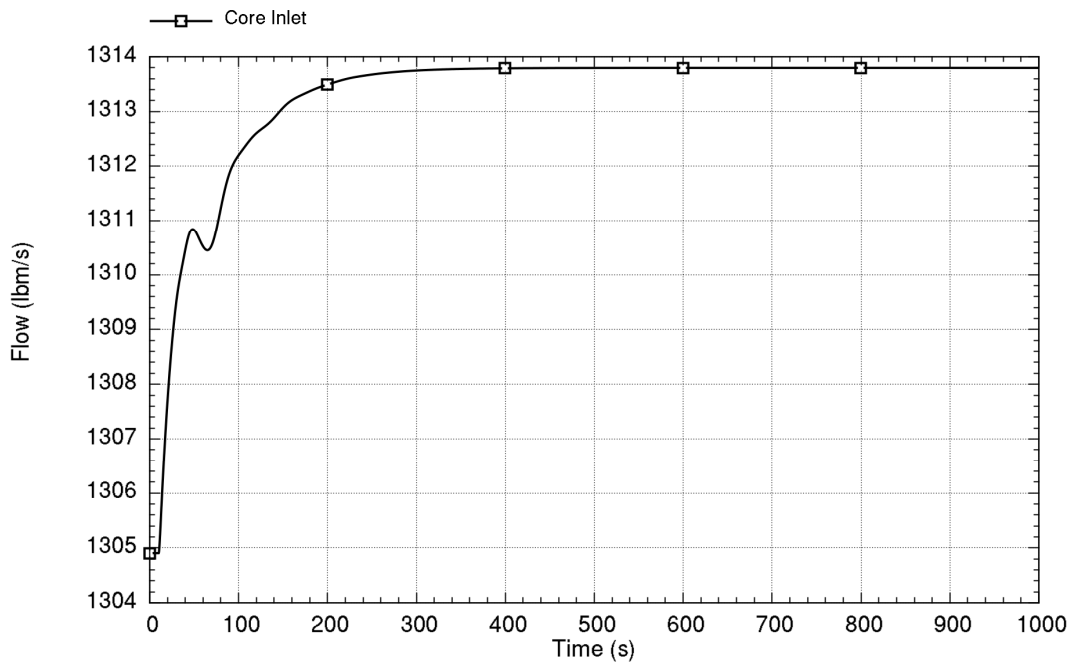
~~ff~~ Stability following an increase of feedwater flow is the event addressed in this class. In the event, a hypothetical rapid increase in feedwater flow occurs due to a feedwater pump speed increase, valve alignment changes, or other causes. However, the change is sufficiently small that the MPS does not actuate on the change and control systems, such as those for steam pressure, accommodate the change by maintaining other parameters at the original value.

Other causes of increased heat removal, such as decreasing feedwater temperature or decreasing steam pressure (that causes enhanced boiling in the SG), are bounded by changes in feedwater flow. This bounding effect is because the potential for change in feedwater temperature is more gradual when considering the entire feedwater system train (e.g., preheaters and piping lengths) and large rapid changes in steam pressure are expected to cause either compensating control actions or MPS trips. ~~ff~~^{2(a),(e),ECI}

8.2.1.1 Rated Power Conditions

~~ff~~ The figures below provide results for an event at rated power in which feedwater flow rapidly increases by 2.2 lb/s (1.0 kg/s) after 10 seconds. Both BOC and EOC reactivity conditions are considered. This relatively small change is chosen because larger changes would result in a reactor trip on high reactor power. Figure 8-21 through Figure 8-24 show the flow and power response for BOC and EOC core conditions. ~~ff~~^{2(a),(e),ECI}

ff

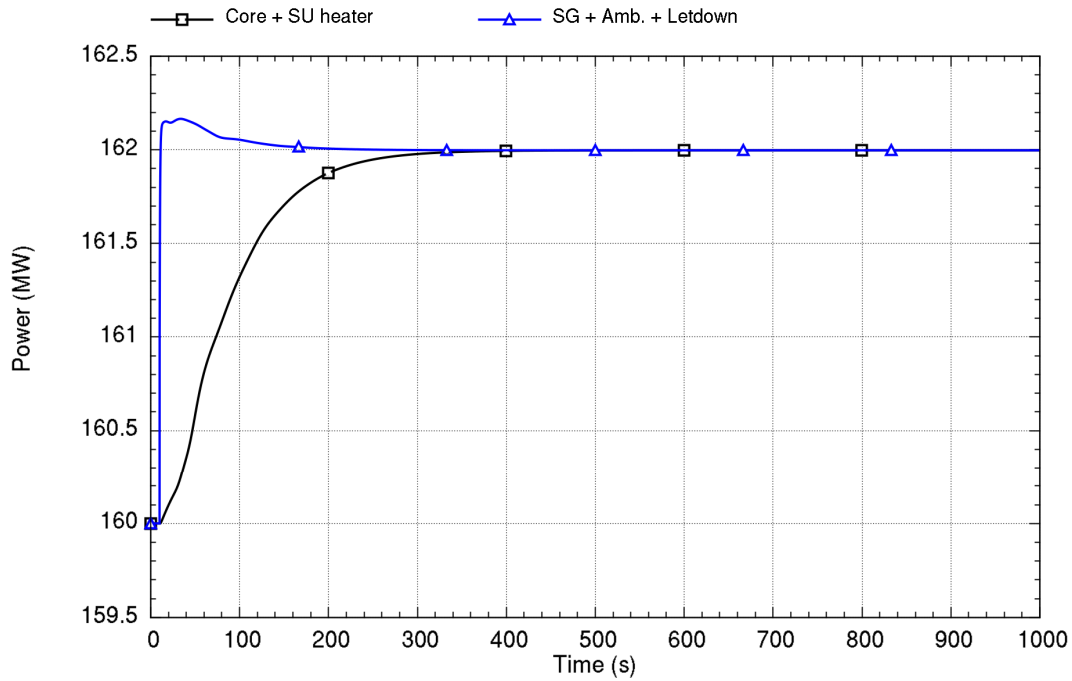


Run ID: Run on Jun/01/2016 at 21:33:47 with PID 010824

ff 2(a),(e),ECI

Figure 8-21. Time trace of primary coolant flow response to an increase in feedwater flow at rated power and beginning-of-cycle reactivity

ff

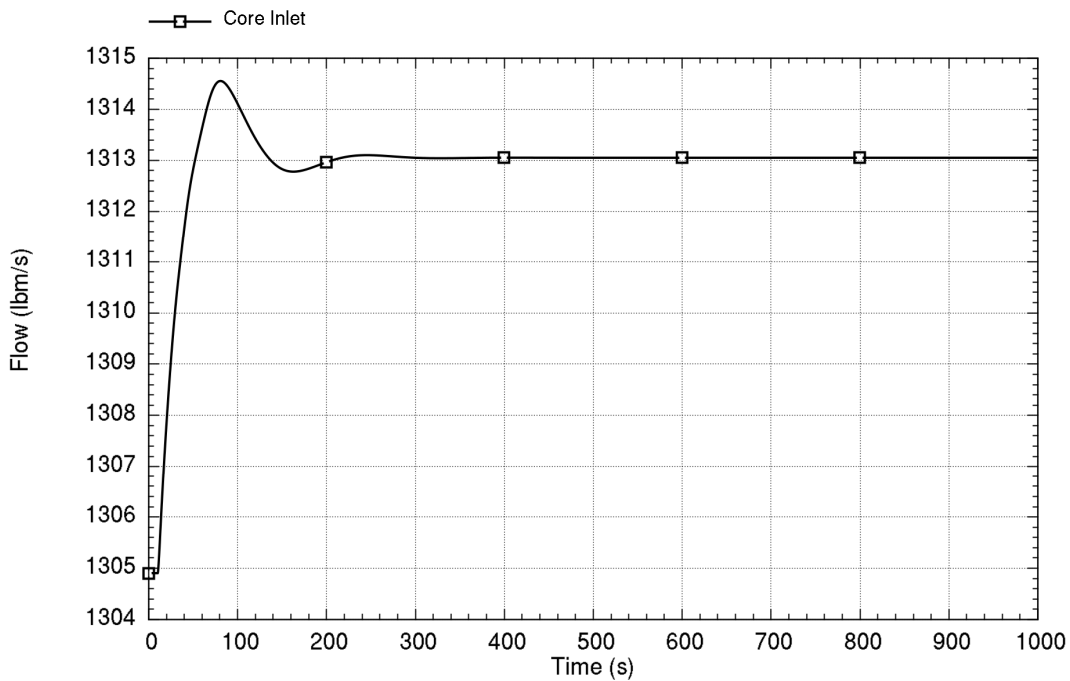


Run ID: Run on Jun/01/2016 at 21:33:47 with PID 010824

ff 2(a),(e),ECI

Figure 8-22. Time trace of heat addition and heat removal response to an increase in feedwater flow at rated power and beginning-of-cycle reactivity

ff

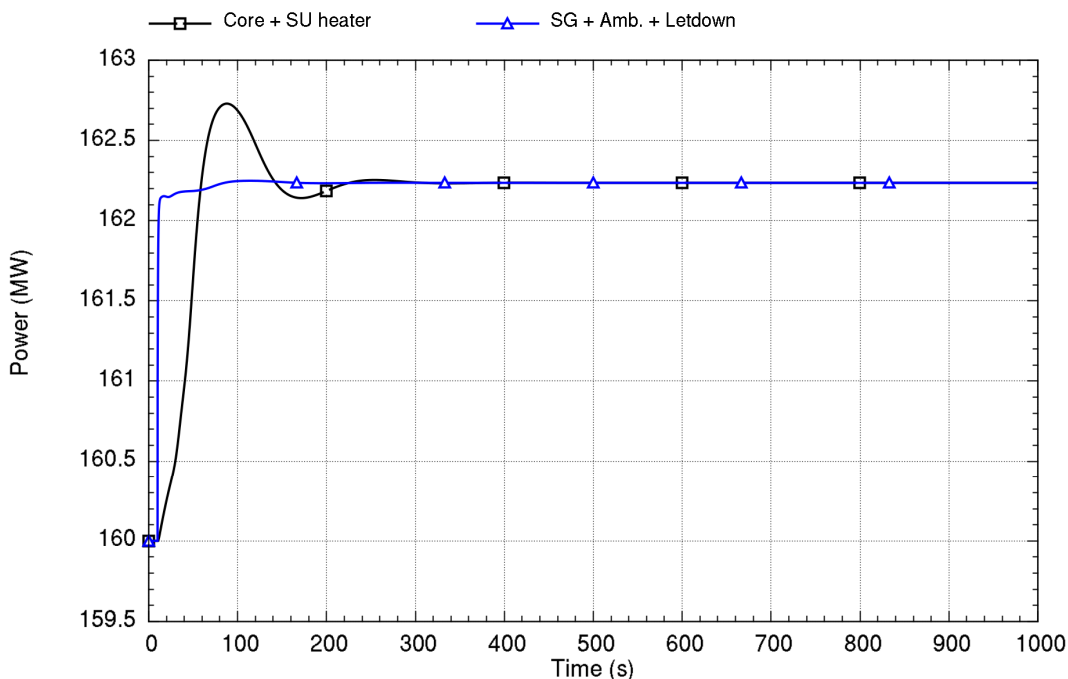


Run ID: Run on Jun/01/2016 at 21:34:02 with PID 009576

ff 2(a),(e),ECI

Figure 8-23. Time trace of primary coolant flow response to an increase in feedwater flow at rated power and end-of-cycle reactivity

ff



Run ID: Run on Jun/01/2016 at 21:34:02 with PID 009576

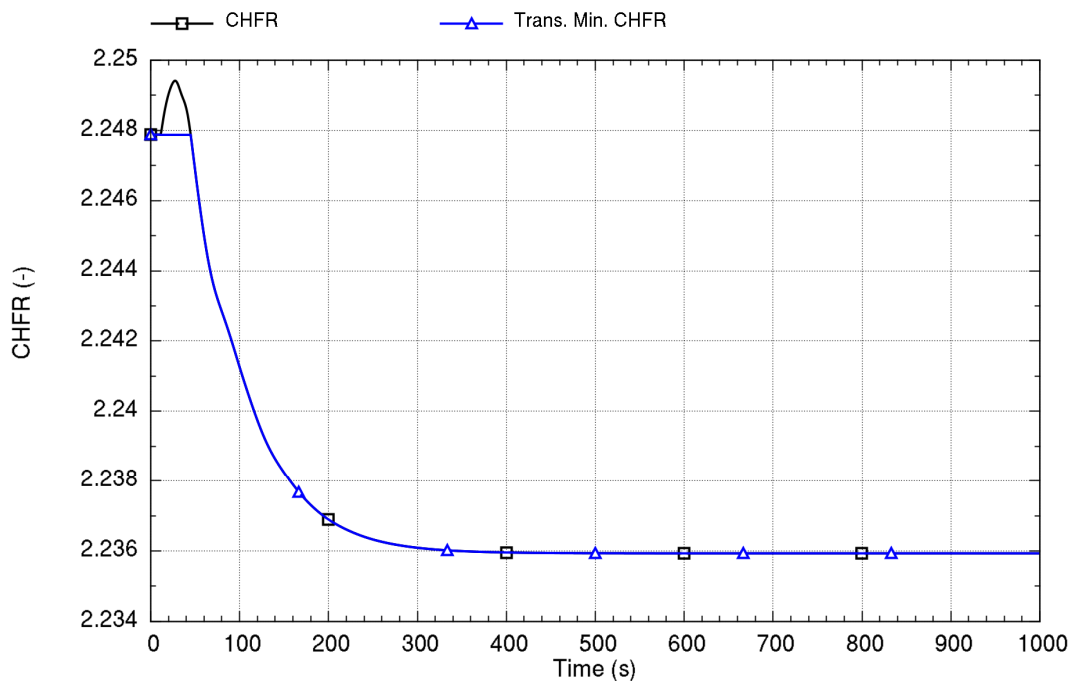
ff2(a),(c),ECI

Figure 8-24. Time trace of heat addition and heat removal response to an increase in feedwater flow at rated power and end-of-cycle reactivity

ff The results show that the NPM is highly stable at BOC and EOC conditions, but behaviors in the first 300 seconds illustrate the interactions between power and flow through the moderator reactivity feedback. One important observation is the effect of large negative reactivity at EOC. The NPM responds to the change in heat removal by the secondary system more rapidly than at BOC conditions. This response leads to an overshoot in the core power that is not observed in BOC conditions. The power overshoot is strongly damped in EOC conditions and there is no potential for instability from this mechanism for the modeled EOC reactivity coefficients.

Figure 8-25 and Figure 8-26 illustrate that both conditions maintain a large margin to CHF limits. Recall that these predictions of CHF are qualitative in nature and intended to screen the results based on the relative change of the CHF ratio compared with its initial value as described in Section 5.6.5. ff2(a),(c),ECI

ff

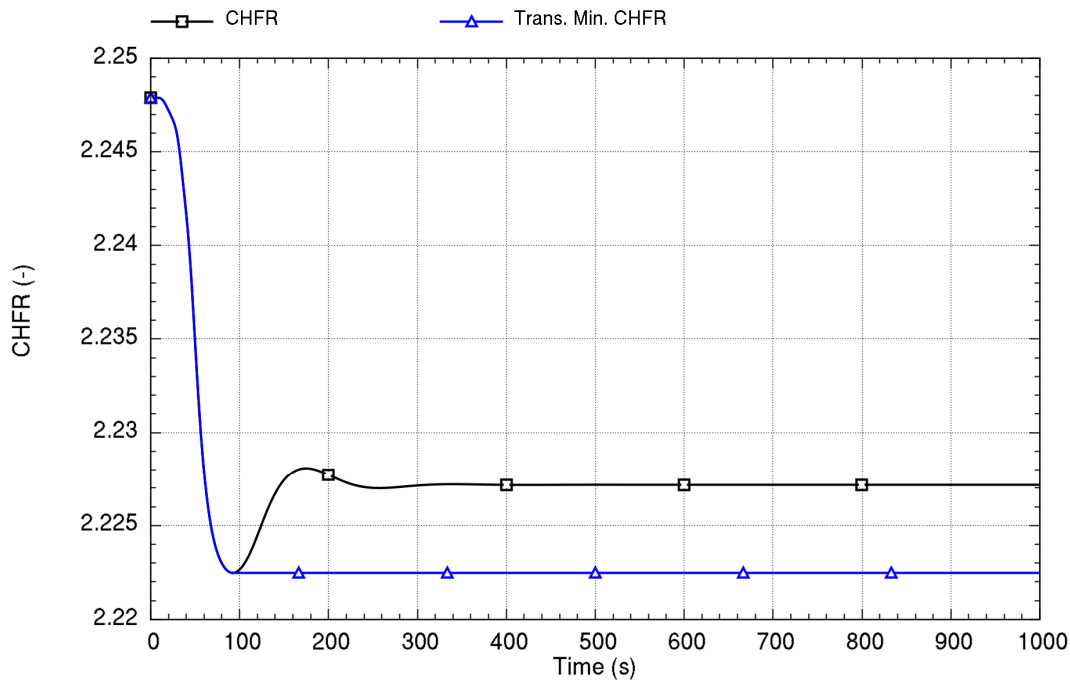


Run ID: Run on Jun/01/2016 at 21:33:47 with PID 010824

ff2(a),(e),ECI

Figure 8-25. Time trace of critical heat flux ratio response to an increase in feedwater flow at rated power and beginning-of-cycle reactivity

ff



Run ID: Run on Jun/01/2016 at 21:34:02 with PID 009576

ff2(a),(c),ECI

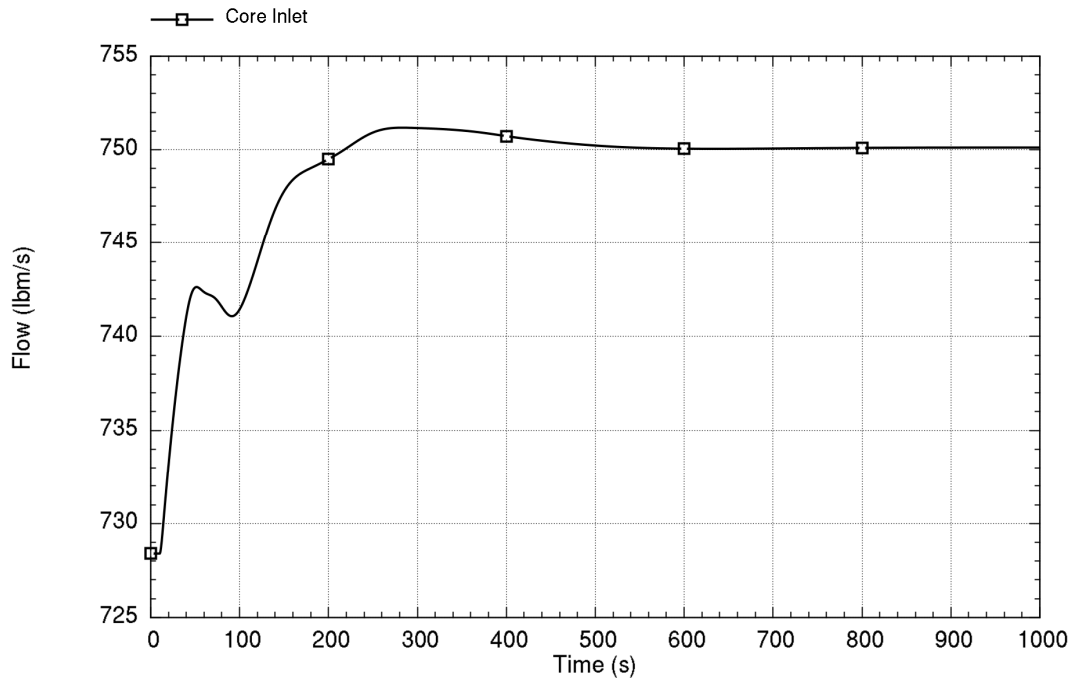
Figure 8-26. Time trace of critical heat flux ratio response to an increase in feedwater flow at rated power and end-of-cycle reactivity

8.2.1.2 Event at 32 MW Conditions

ff The figures below provide results for an event at 32 MW and 200 degrees-F feedwater temperature in which feedwater flow increases rapidly by 2.2 lb/s (1.0 kg/s) after 10 seconds. This condition is chosen to bound the lower limit of power where the turbine and feedwater heater system are on-line.

Both BOC and EOC reactivity conditions are considered. The approximate 8-percent change in feedwater flow is larger than considered at rated power. This power level and feedwater condition are selected for analysis in part because it is the expected power at which the turbine comes online and feedwater heating begins, as discussed in Section 3.6. Therefore, the changes in feedwater flow can be considered as normal operation. Figure 8-27 through Figure 8-30 show the flow and power for BOC and EOC reactivity coefficients. ff2(a),(c),ECI

ff

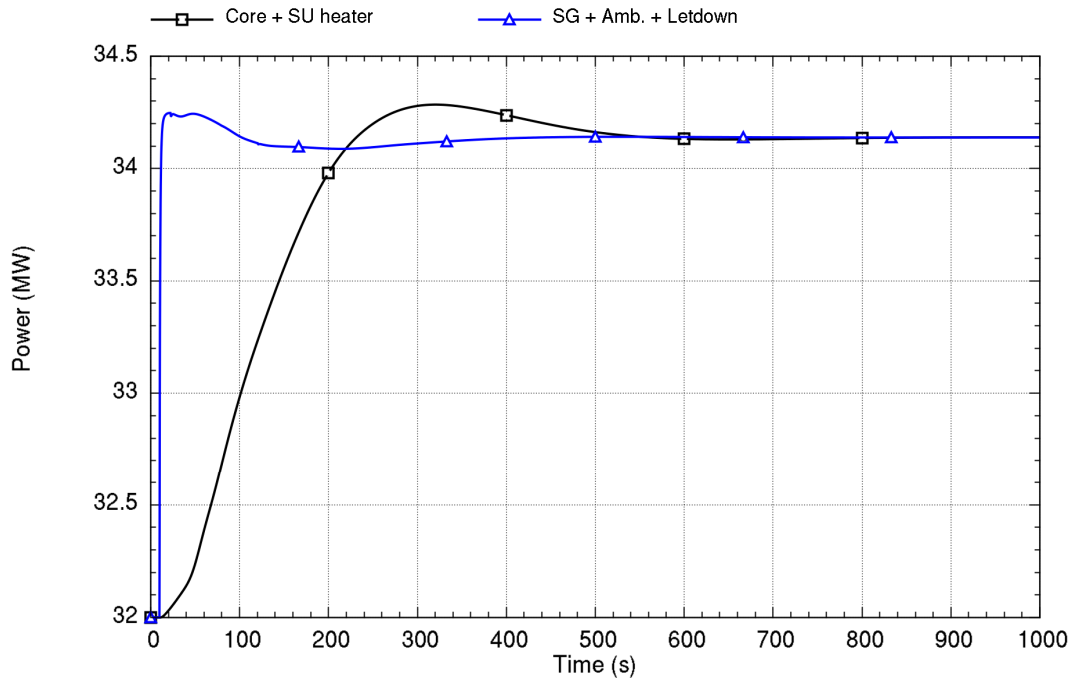


Run ID: Run on Jun/01/2016 at 21:35:33 with PID 010052

ff 2(a),(e),ECI

Figure 8-27. Time trace of primary coolant flow response to an increase in feedwater flow at 32 MW and beginning-of-cycle reactivity

ff

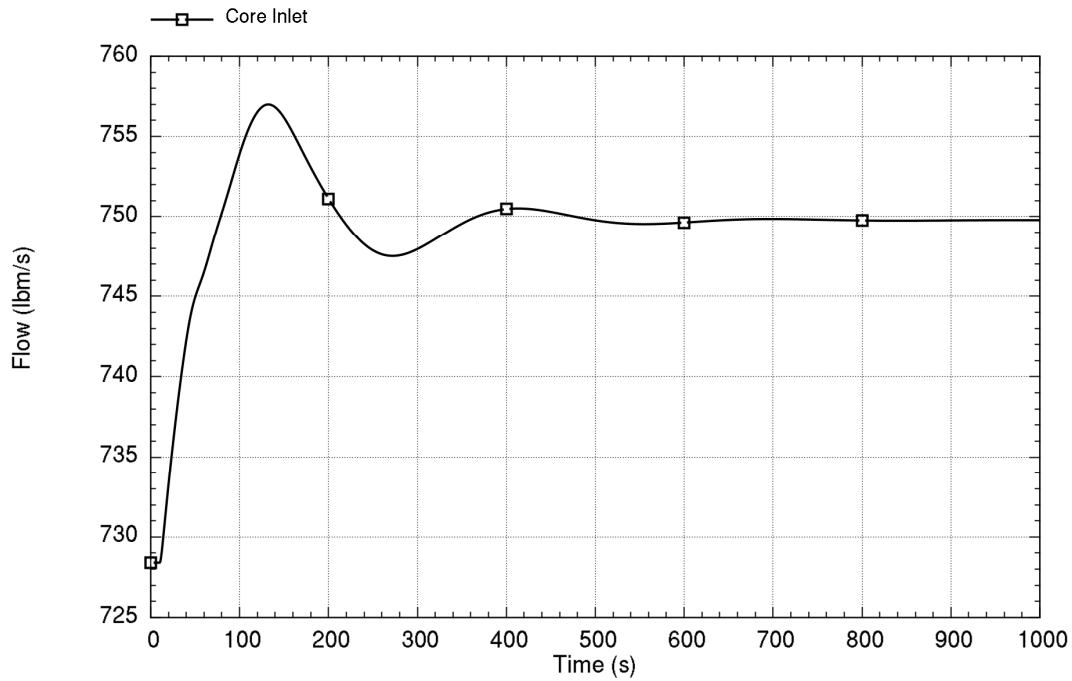


Run ID: Run on Jun/01/2016 at 21:35:33 with PID 010052

ff2(a),(e),ECI

Figure 8-28. Time trace of heat addition and heat removal response to an increase in feedwater flow at 32 MW and beginning-of-cycle reactivity

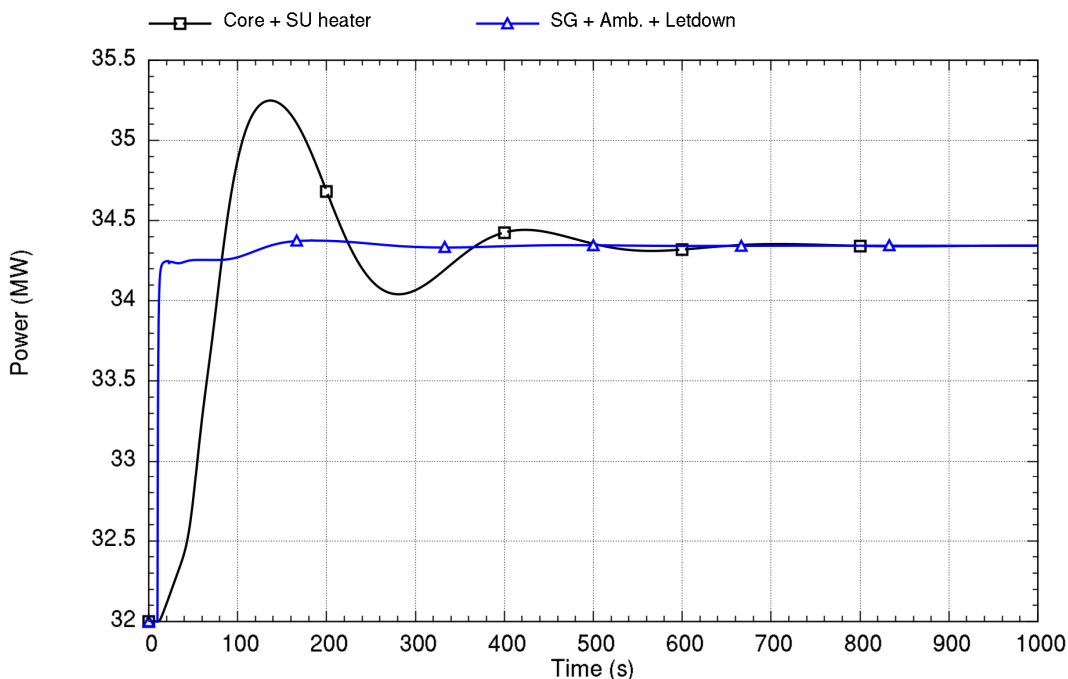
ff



ff 2(a),(e),ECI

Figure 8-29. Time trace of primary coolant flow response to an increase in feedwater flow at 32 MW and end-of-cycle reactivity

ff



Run ID: Run on Jun/01/2016 at 21:35:48 with PID 004524

ff^{2(a),(e),ECI}

Figure 8-30. Time trace of heat addition and heat removal response to an increase in feedwater flow at 32 MW and end-of-cycle reactivity

ff The results show that the NPM is stable at BOC and EOC conditions. Consistent with observations in Section 8.1, the results show oscillation damping is not as strong as rated power; this includes a more overshoot or undershoot in core power at EOC.

There is a large margin for CHF ratio at low power and the relative change in conditions is small; therefore, CHF ratio limits are not violated for the presented demonstration of this event. ff^{2(a),(e),ECI}

8.2.2 Decrease in Heat Removal by the Secondary System

ff Stability following a reduction of feedwater flow is the event addressed in this class. In the event, a hypothetical rapid decrease in feedwater flow occurs due to a feedwater pump speed change, valve alignment changes, or another cause. However, complete loss of feedwater is not considered because it would result in actuation of the MPS and a reactor trip.

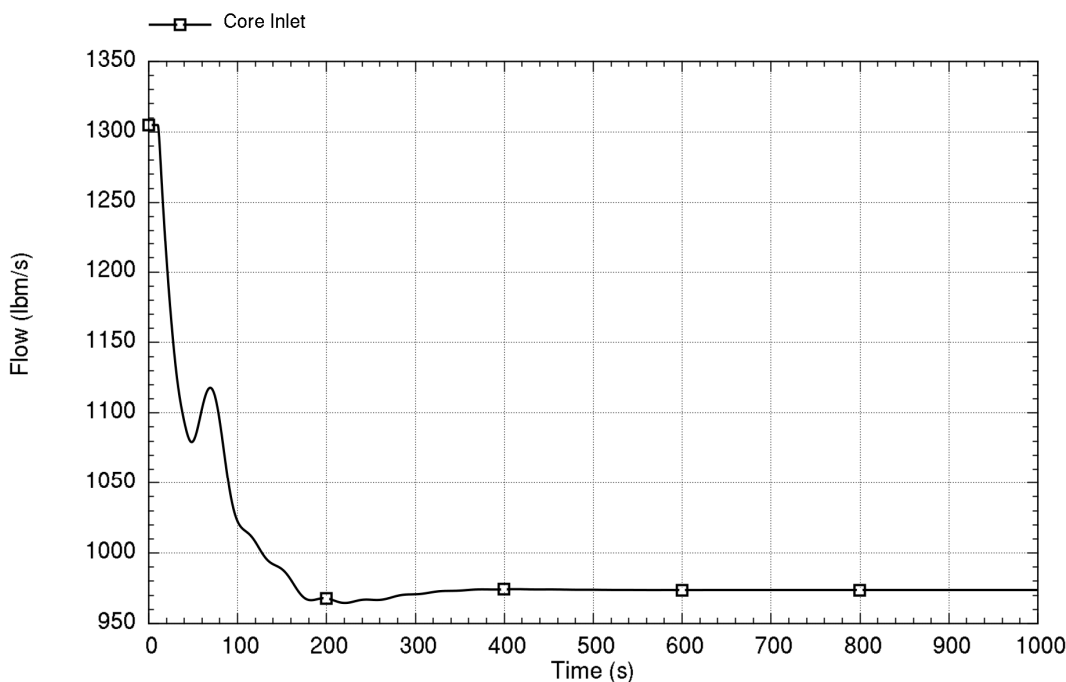
Other causes of decreased heat removal, such as increasing feedwater temperature or increasing steam pressure (that causes suppressed boiling in the SG), ff^{2(a),(e),ECI}

ff are generally bounded by changes in feedwater flow for similar reasons discussed in the last section. ~~}}2(a),(e),ECI~~

8.2.2.1 Rated Power Conditions

ff The figures below provide results for an event at rated power in which feedwater flow decreases rapidly by 50 percent after 10 seconds while maintaining feedwater temperature and steam pressure. Both BOC and EOC reactivity conditions are considered. This magnitude of change is selected to determine the acceptability of a partial loss of feedwater and a successful runback that avoids a reactor trip.

The reduction in heat removal from the primary coolant flow initiates a transient in which the primary coolant temperature starts to rise and negative moderator feedback affects the fission power. The combined reduction of the heat sink and core power restores the primary coolant temperature to a value above its initial value. The Doppler reactivity compensates for the difference and the net average reactivity is restored to zero. The density head driving the primary coolant flow is reduced and the flow is adjusted from its initial value to approximately 75 percent of its initial value. Figure 8-31 through Figure 8-34 show the flow and power for BOC and EOC reactivity

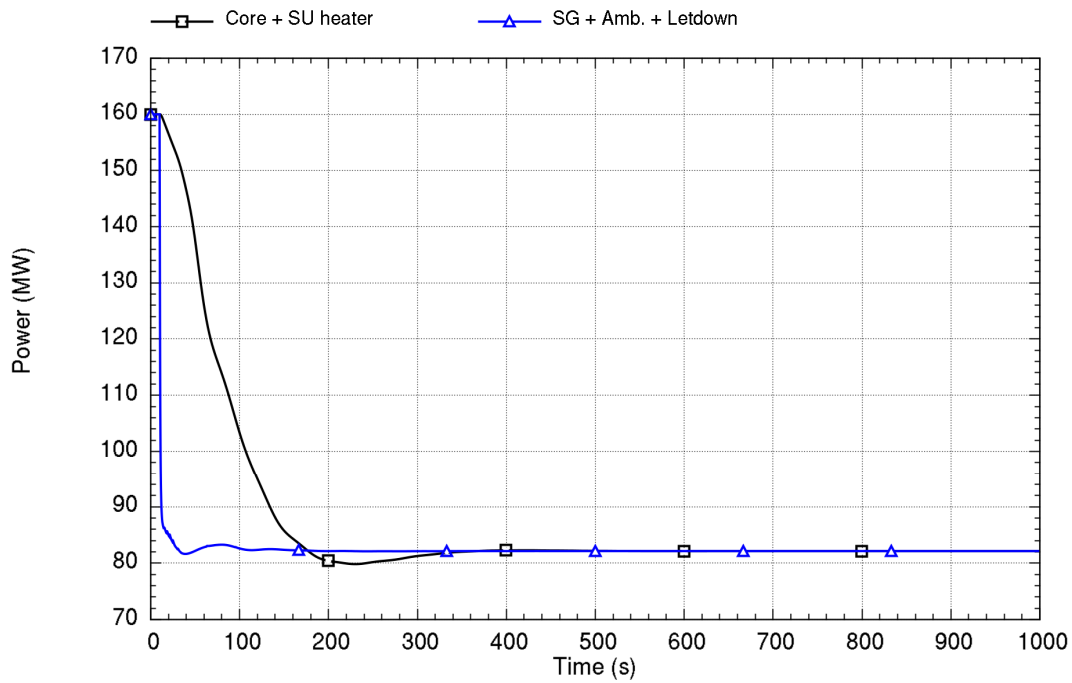


Run ID: Run on Jun/01/2016 at 21:34:17 with PID 003020

~~}}2(a),(e),ECI~~

Figure 8-31. Time trace of primary coolant flow response to a 50-percent decrease in feedwater flow at rated power and beginning-of-cycle reactivity

ff

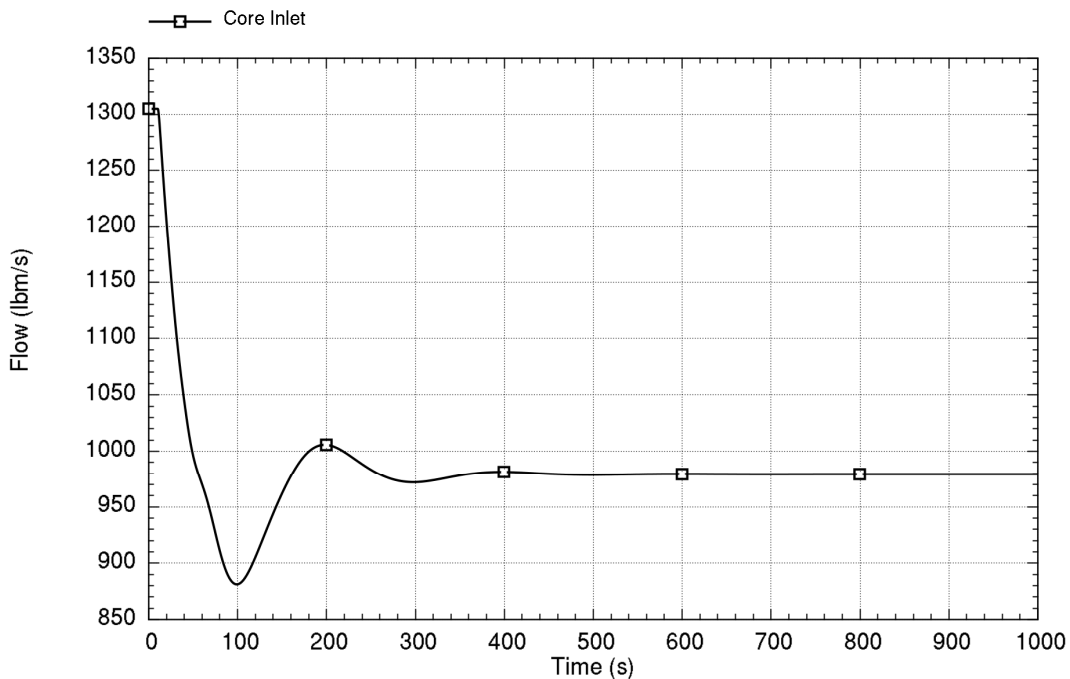


Run ID: Run on Jun/01/2016 at 21:34:17 with PID 003020

ff2(a),(e),ECI

Figure 8-32. Time trace of heat addition and heat removal response to a 50-percent decrease in feedwater flow at rated power and beginning-of-cycle reactivity

ff

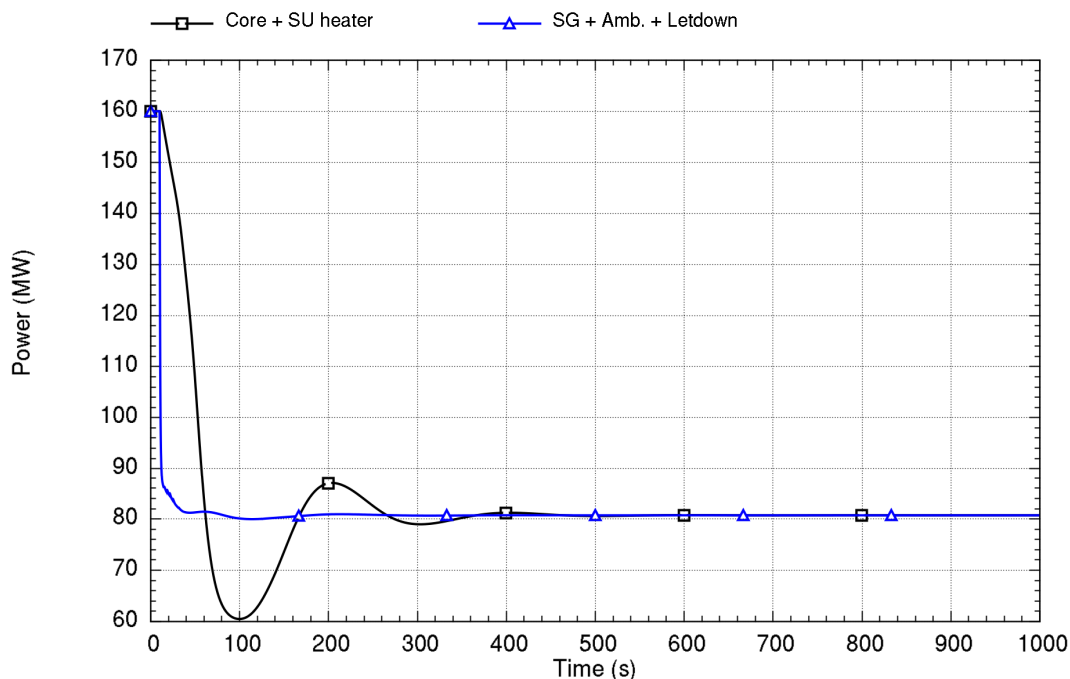


Run ID: Run on Jun/01/2016 at 21:34:47 with PID 007232

ff2(a),(e),ECI

Figure 8-33. Time trace of primary coolant flow response to a 50-percent decrease in feedwater flow at rated power and end-of-cycle reactivity

ff



Run ID: Run on Jun/01/2016 at 21:34:47 with PID 007232

}}2(a),(e),ECI

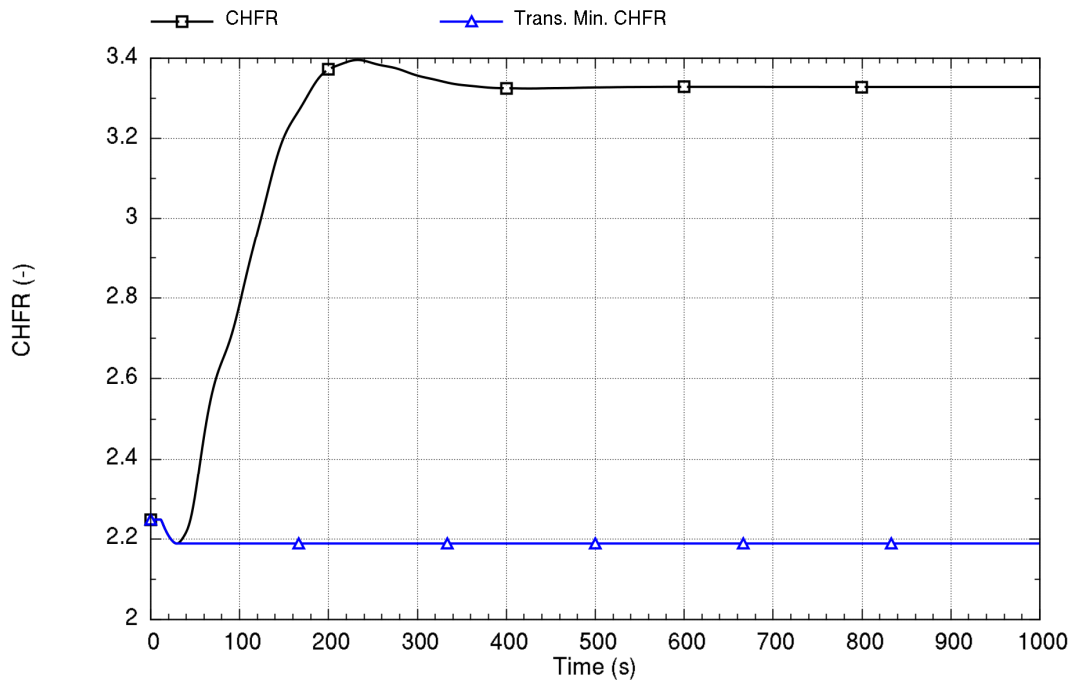
Figure 8-34. Time trace of heat addition and heat removal response to a 50-percent decrease in feedwater flow at rated power and end-of-cycle reactivity

ff—The results show stable behavior at BOC and EOC conditions for a decrease in secondary heat removal. Additionally, these figures are mirrors of their counterparts in Figure 8-21 through Figure 8-24, albeit the magnitude is larger considering the larger relative change in feedwater flow. Discussion related to the increased feedwater flow in the last section applies, including the (now undershoot or overshoot of power) effect of large negative reactivity.

It is important to recognize that the MPS may actuate during these events. Specifically, a reactor trip on large rate change in measured neutron flux may activate a reactor trip, where a typical trip setpoint ensures the flux does not change more than ± 15 percent of the rated thermal power per minute. Such a trip is not credited in these stability considerations, but provides additional assurance that rapidly changing fission power is detected and mitigated.

Figure 8-35 and Figure 8-36 illustrate both conditions maintain large margin to CHF limits. }}2(a),(e),ECI

ff

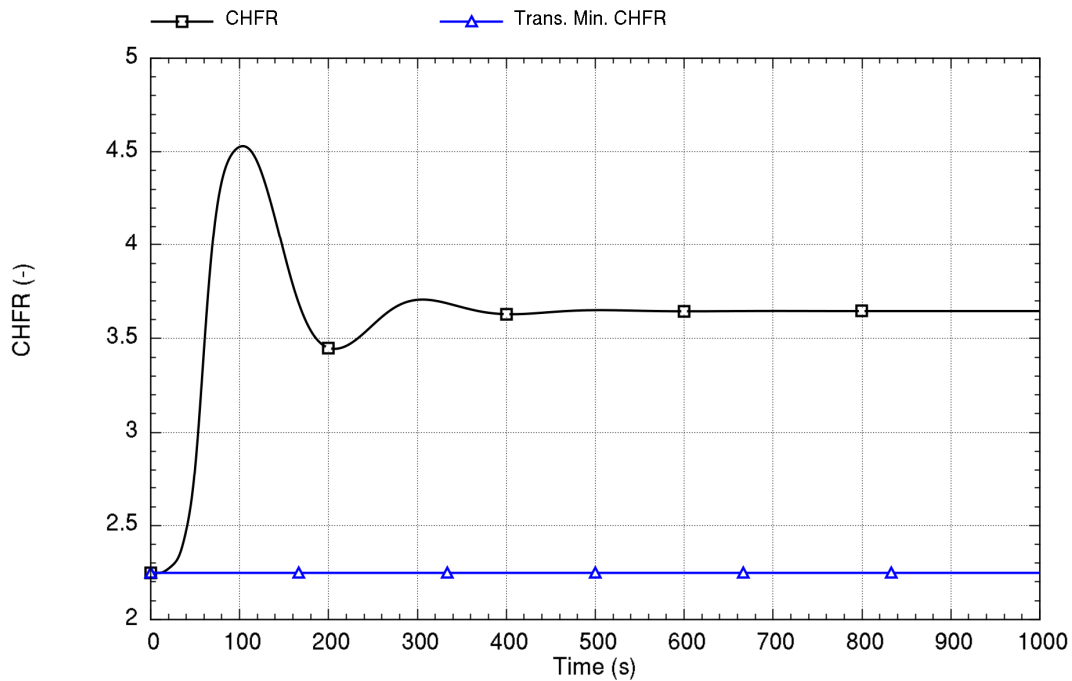


Run ID: Run on Jun/01/2016 at 21:34:17 with PID 003020

ff2(a),(e),ECI

Figure 8-35. Time trace of CHF ratio response to a 50-percent decrease in feedwater flow at rated power and beginning-of-cycle reactivity

ff



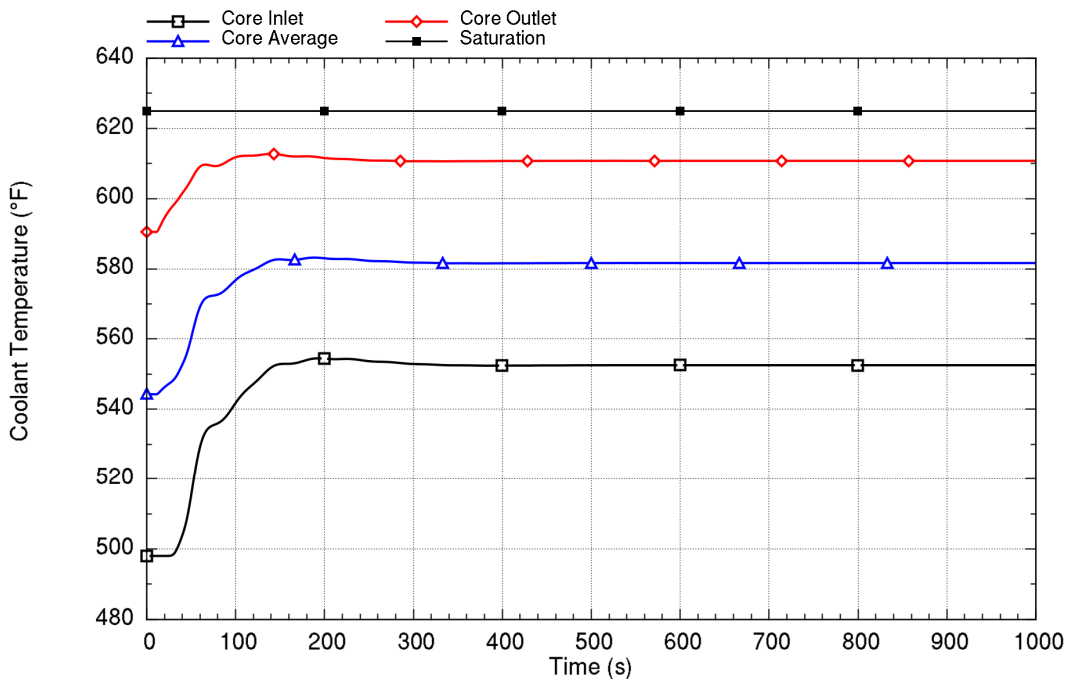
Run ID: Run on Jun/01/2016 at 21:34:47 with PID 007232

ff2(a),(e),ECI

Figure 8-36. Time trace of CHF ratio response to a 50-percent decrease in feedwater flow at rated power and end-of-cycle reactivity

ff-While the analyzed cases show stable behavior, varying the moderator feedback can bring the NPM to conditions in which instability may occur as a result of losing subcooling in the riser. Figure 8-37 and Figure 8-38 illustrate the coolant temperature response for BOC and EOC conditions. As illustrated, a loss of subcooled margin occurs for BOC conditions. This effect is the result of slower core power response seen in Figure 8-32 in comparison with the heat removal by the SG that leads to overall heatup of the primary coolant. ff2(a),(e),ECI

ff

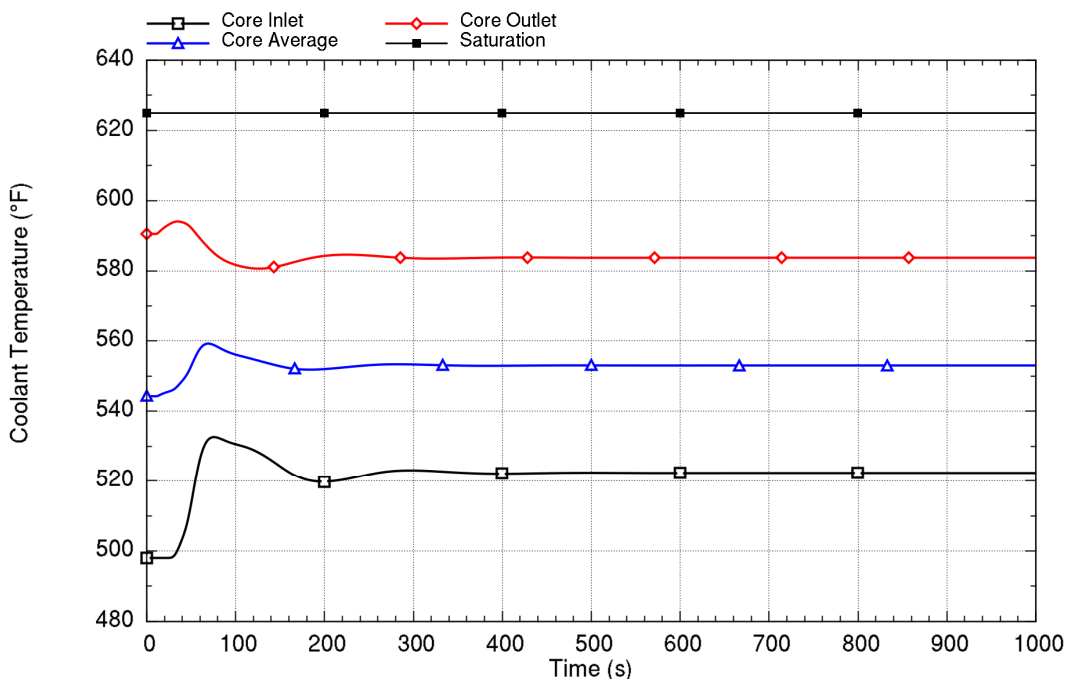


Run ID: Run on Jun/01/2016 at 21:34:17 with PID 003020

ff 2(a),(e),ECI

Figure 8-37. Time trace of coolant temperature response to a 50-percent decrease in feedwater flow at rated power and beginning-of-cycle reactivity

ff



Run ID: Run on Jun/01/2016 at 21:34:47 with PID 007232

ff^{2(a),(e),ECI}

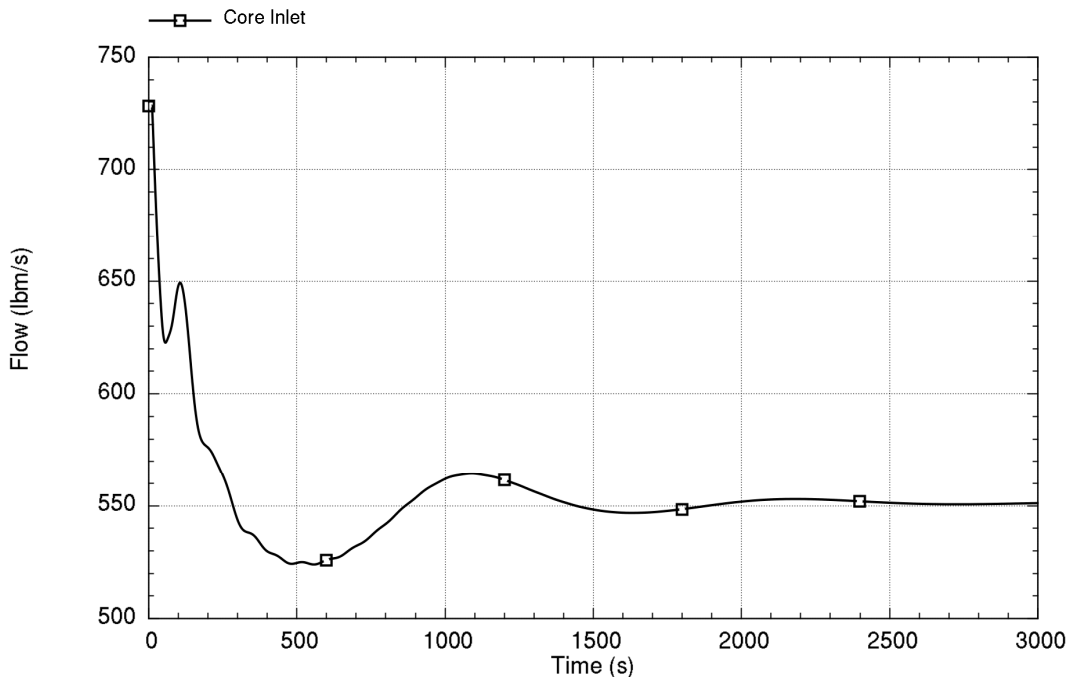
Figure 8-38. Time trace of coolant temperature response to a 50-percent decrease in feedwater flow at rated power and end-of-cycle reactivity

ff To bound the effect of losing subcooling in the riser, an analysis with zero moderator feedback for this event at rated power is addressed in Section 9.0 to show the MPS role in protecting the plant from undergoing an instability related to voiding in the riser.
ff^{2(a),(e),ECI}

8.2.2.2 Event at 32 MW Conditions with 35 Percent Initial Decay Heat

ff An event at 32 MW in which feedwater flow decreases rapidly by 50 percent after 10 seconds shows a behavior that is generally uninteresting when using a typical equilibrium decay heat fraction of approximately 7 percent. More pronounced results of an alternate event are shown in this section in which the plant is assumed to operate indefinitely at full power conditions, then core thermal power is rapidly reduced to 32 MW by control rods or other means. Once reaching this power, the feedwater flow immediately decreases rapidly by 50 percent before the decay heat associated with full-power has a chance to move significantly towards equilibrium from rated power to the lower power level at 32 MW. This hypothetical scenario increases the decay heat fraction to 35 percent of the 32 MW initial power level and it is held constant for the duration of the analysis. Because the decay heat is not affected by the ff^{2(a),(e),ECI}

Reactivity feedback mechanisms, the resulting effect is equivalent to a damping in both Doppler and moderator reactivity feedback because decay heat does not respond to changes in reactivity. Figure 8-39 through Figure 8-42 show the flow and power for BOC and EOC reactivity for this event.

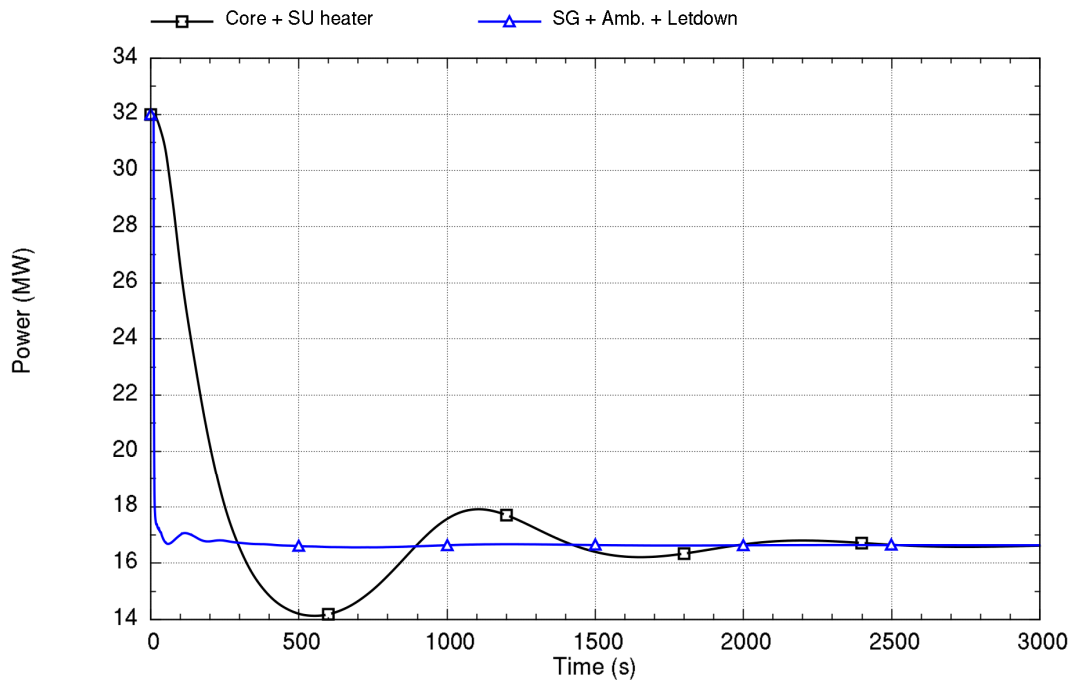


Run ID: Run on Jun/01/2016 at 21:36:18 with PID 008208

2(a),(c), ECI

Figure 8-39. Time trace of primary coolant flow response to a 50-percent decrease in feedwater flow at 32 MW and BOC reactivity with 35-percent decay heat

ff

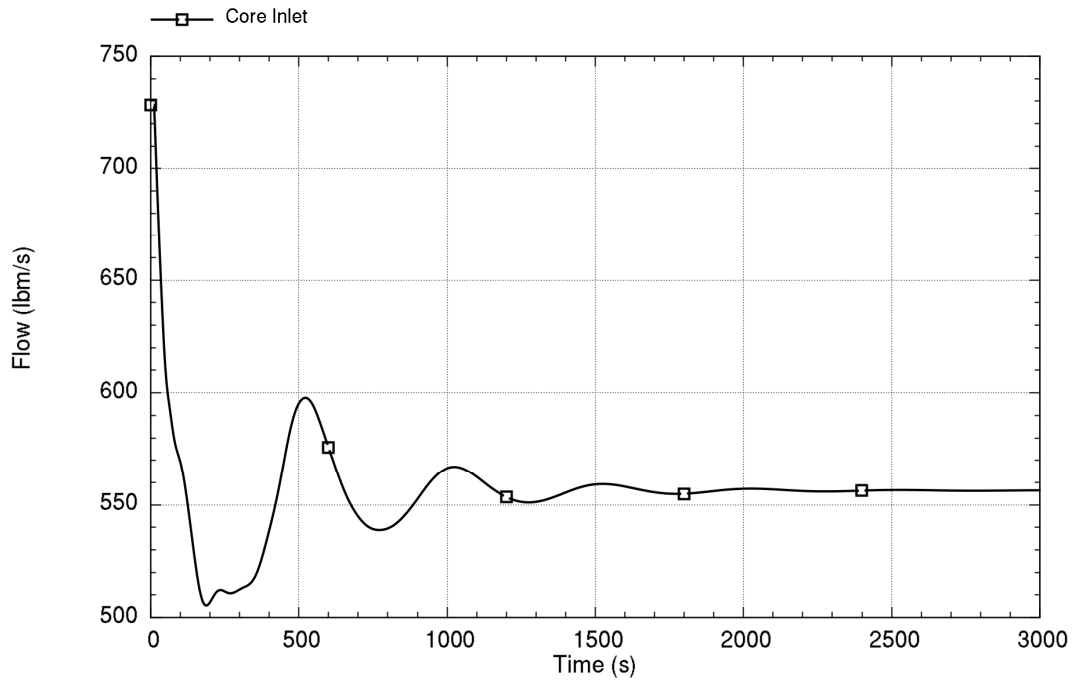


Run ID: Run on Jun/01/2016 at 21:36:18 with PID 008208

ff2(a),(e),ECI

Figure 8-40. Time trace of heat addition and heat removal response to a 50-percent decrease in feedwater flow at 32 MW and beginning-of-cycle reactivity with 35-percent decay heat

ff

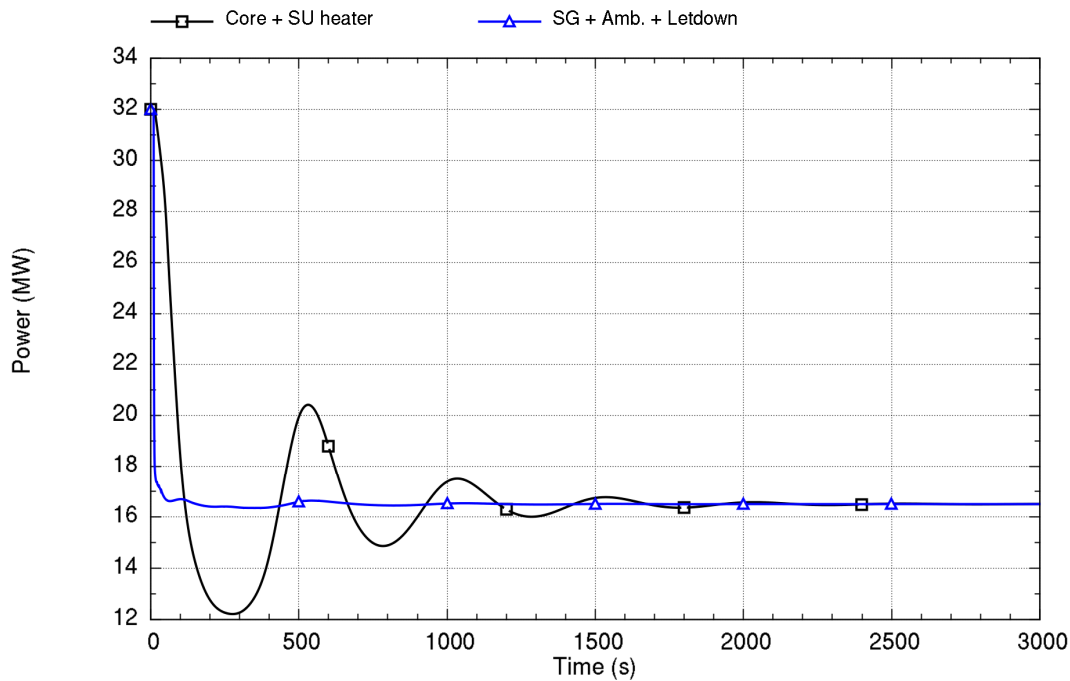


Run ID: Run on Jun/01/2016 at 21:36:33 with PID 010652

ff 2(a),(e),ECI

Figure 8-41. Time trace of primary coolant flow response to a 50-percent decrease in feedwater flow at 32 MW and end-of-cycle reactivity with 35-percent decay heat

ff



Run ID: Run on Jun/01/2016 at 21:36:33 with PID 010652

ff2(a),(e),ECI

Figure 8-42. Time trace of heat addition and heat removal response to a 50-percent decrease in feedwater flow at 32 MW and end-of-cycle reactivity with 35-percent decay heat

ff-The results demonstrate stable behavior at BOC and EOC conditions. Oscillations in flow that are observed in the results are emanating from changes in core power. While the choices of input (35 percent decay heat and maintaining decay heat constant through the analysis) are extreme, the results show the NPM behaves stably even under these extreme assumptions. ff2(a),(e),ECI

8.2.3 Decrease in Reactor Coolant System Flow Rate

ff-The effect of a decrease in primary system flow rate (in isolation of other effects) is not considered a credible event for stability analysis. This determination is because there is no source for changing the primary system flow without other influences, because there are no primary system pumps in the NPM to directly influence primary system flow. ff2(a),(e),ECI

8.2.4 Increase in Reactor Coolant Inventory

Effects of increasing RCS inventory (for its effect in increasing system pressure) are not important in the stability assessment. This determination is because additional subcooled margin in the riser is obtained by the increase in primary system pressure and overall stability behavior is not sensitive to pressure changes for a single-phase system.

The effect of adding cold water from the CVCS during an increasing RCS inventory event is generally bounded by analyses of increased heat removal by the secondary system, even when considering the potential for minor reduction in primary system flow resulting from adding cooler water to the riser. This effect is due to the relatively small cooldown that may occur at high power conditions and the long time for coolant to transit from the CVCS return line located in the riser, around the primary system, and into the core during low-power operations. ^{2(a),(c),ECI}

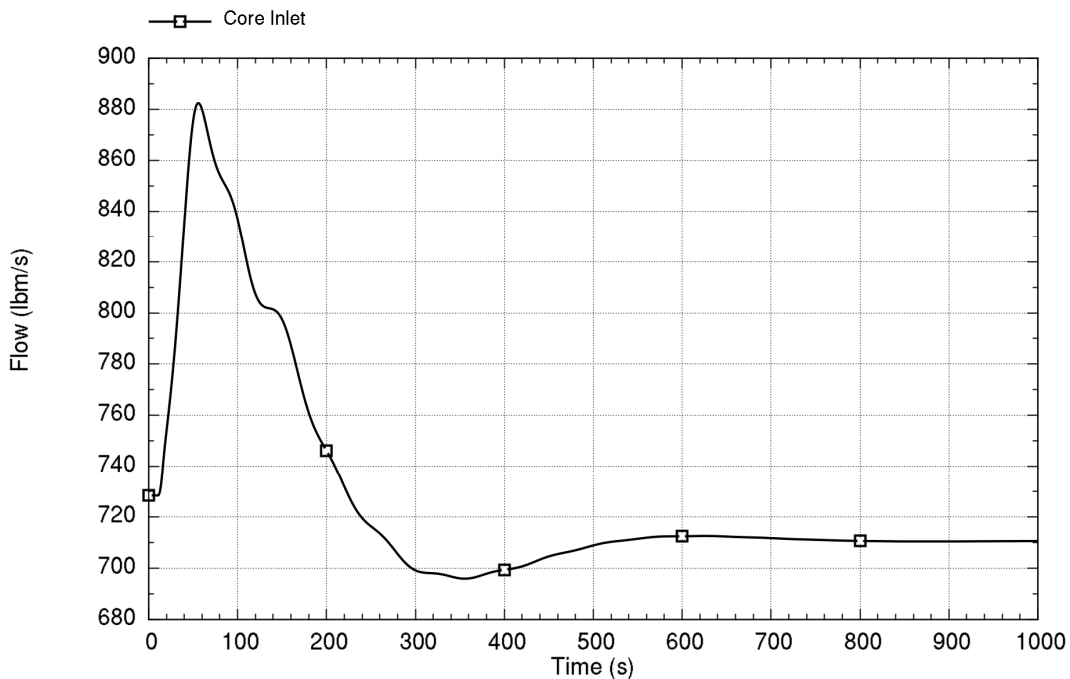
8.2.5 Reactivity and Power Distribution Anomalies

The effect of a reactivity anomaly associated with adding or reducing boron concentration via the CVCS is generally bounded by other analyses. This effect is due to the relatively slow change in core inlet boron concentration as a result of mixing in the RCS. Effects of changing moderator reactivity due to changing boron concentration are generally bounded by considering both BOC and EOC conditions.

An uncontrolled control rod assembly withdrawal or similar at-power event may occur that results in reactivity insertion. Such events are analyzed in the safety analysis, including the size of reactivity change and the rate at which it can be added, and are thus outside the scope of this report. Specifically, control rod drive mechanisms are designed to limit the rate of withdrawal to protect core thermal limits. From the perspective of stability assessment, reactivity increases that do not result in a reactor trip on high flux or high rate change in flux are expected to be relatively slow and generally bounded by effects of increasing heat removal from the secondary side that are described in Section 8.2.1. In addition, slow reactivity insertion events tend to trip on high pressurizer pressure in low-power conditions when pressurizer level is being controlled.

The results provided below demonstrate the stability behavior for an event at 32 MW and 200 degrees-F feedwater temperature where, starting at 10 seconds, 0.25 of reactivity is added to core in 5 seconds through user input while other reactivity components are calculated as normal. Both BOC and EOC core reactivity conditions are considered. The choice of 32 MW is to allow margin to the reactor trip setpoint and the high flux rate trip is not considered. Figure 8-43 through Figure 8-46 show the flow and power for BOC and EOC core reactivity conditions. ^{2(a),(c),ECI}

ff

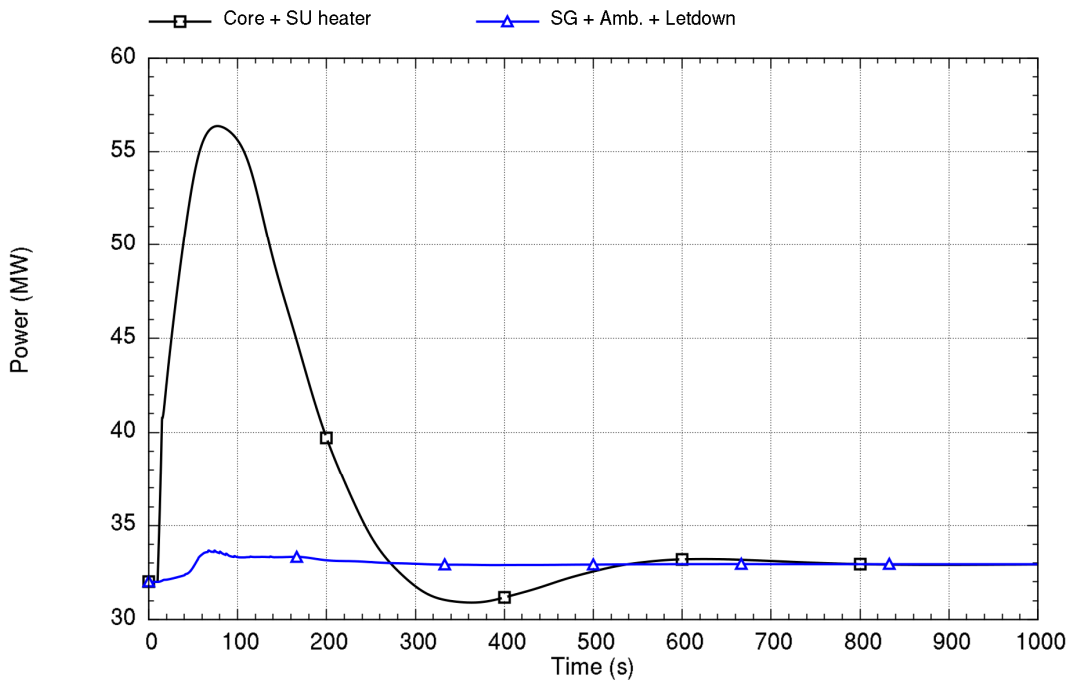


Run ID: Run on Jun/01/2016 at 21:37:03 with PID 007760

ff2(a),(e),ECI

Figure 8-43. Time trace of primary coolant flow response to an increase in core reactivity at 32 MW and beginning-of-cycle reactivity

ff

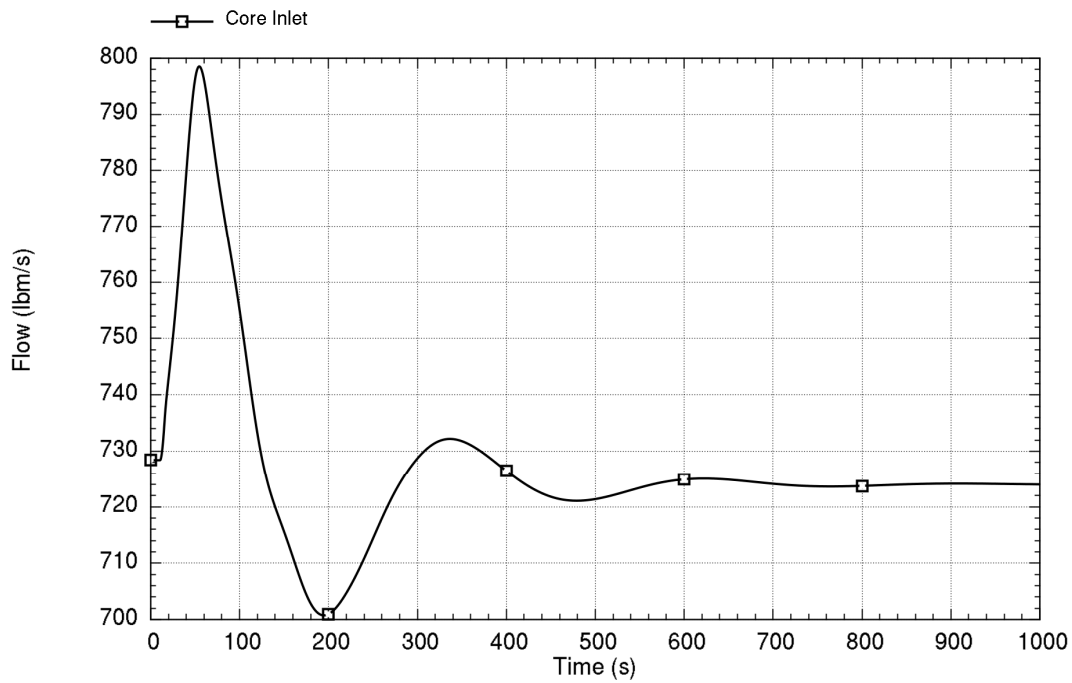


Run ID: Run on Jun/01/2016 at 21:37:03 with PID 007760

ff2(a),(e),ECI

Figure 8-44. Time trace of heat addition and heat removal response to an increase in core reactivity at 32 MW and beginning-of-cycle reactivity

ff

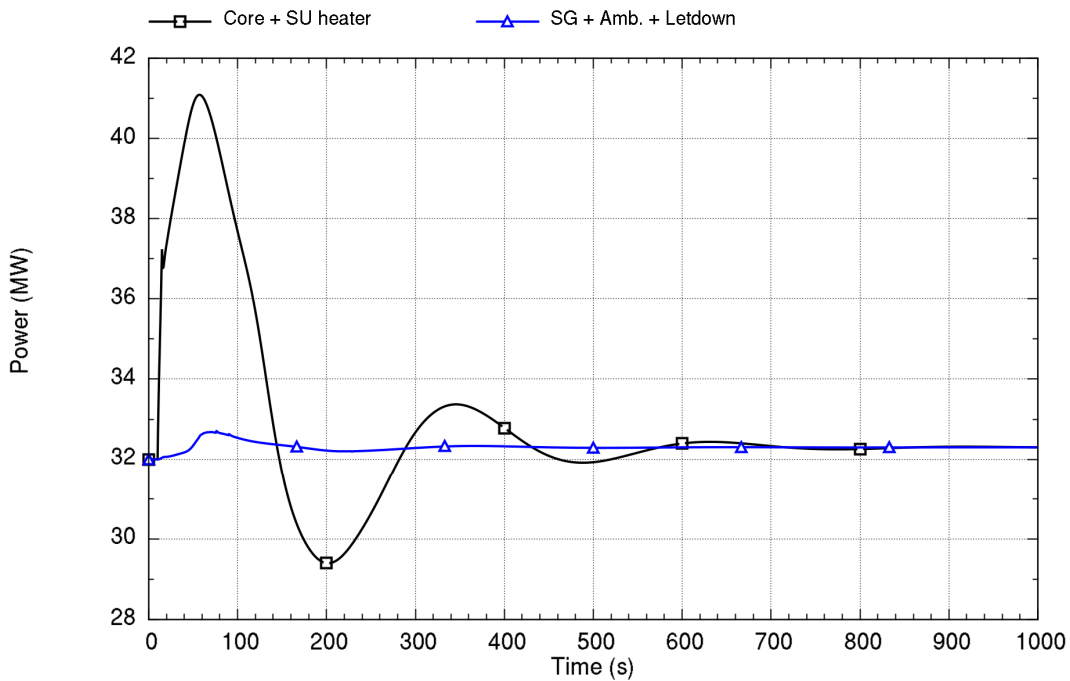


Run ID: Run on Jun/01/2016 at 21:37:18 with PID 007372

ff2(a),(e),ECI

Figure 8-45. Time trace of primary coolant flow response to an increase in core reactivity at 32 MW and end-of-cycle reactivity

ff



Run ID: Run on Jun/01/2016 at 21:37:18 with PID 007372

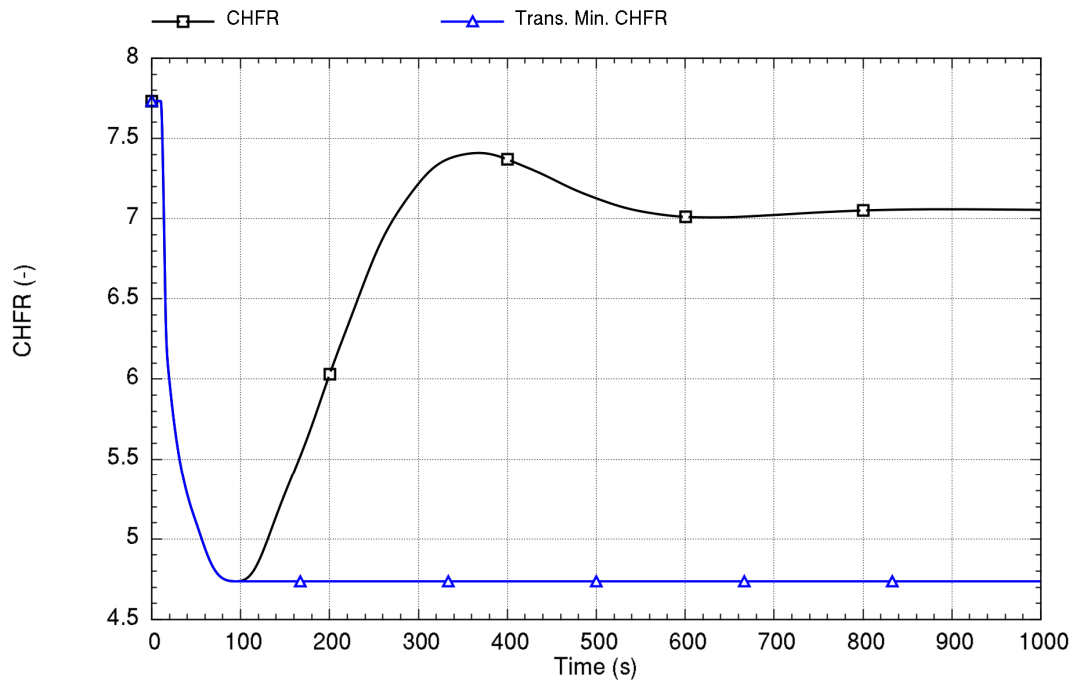
ff 2(a),(e),ECI

Figure 8-46. Time trace of heat addition and heat removal response to an increase in core reactivity at 32 MW and end-of-cycle reactivity

ff The results indicate stable behavior at BOC and EOC conditions for this addition of reactivity. There is nothing notable about the results beyond what was previously stated specifically, effects of strong negative reactivity on the overshoot or undershoot of core power.

Figure 8-47 and Figure 8-48 illustrate that large margin-to-CHF limits is maintained.
ff 2(a),(e),ECI

ff

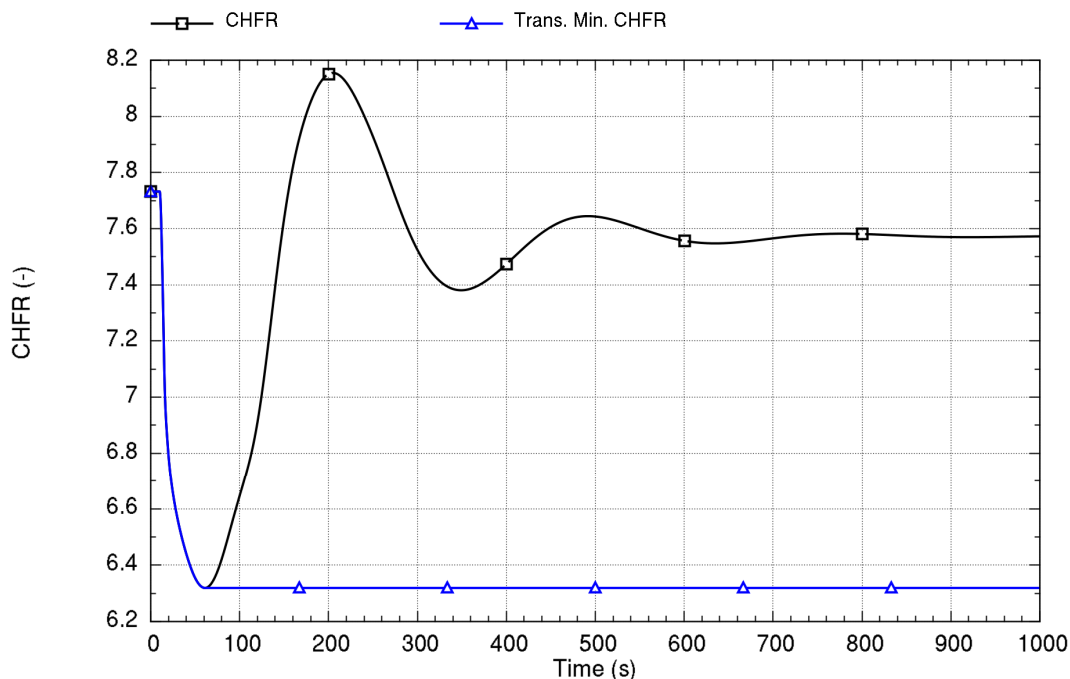


Run ID: Run on Jun/01/2016 at 21:37:03 with PID 007760

ff 2(a),(e),ECI

Figure 8-47. Time trace of critical heat flux ratio response to an increase in core reactivity at 32 MW and beginning-of-cycle reactivity

ff



Run ID: Run on Jun/01/2016 at 21:37:18 with PID 007372

}}2(a),(e),ECI

Figure 8-48. Time trace of critical heat flux ratio response to an increase in core reactivity at 32 MW and end-of-cycle reactivity

8.2.6 Decrease in Reactor Coolant Inventory

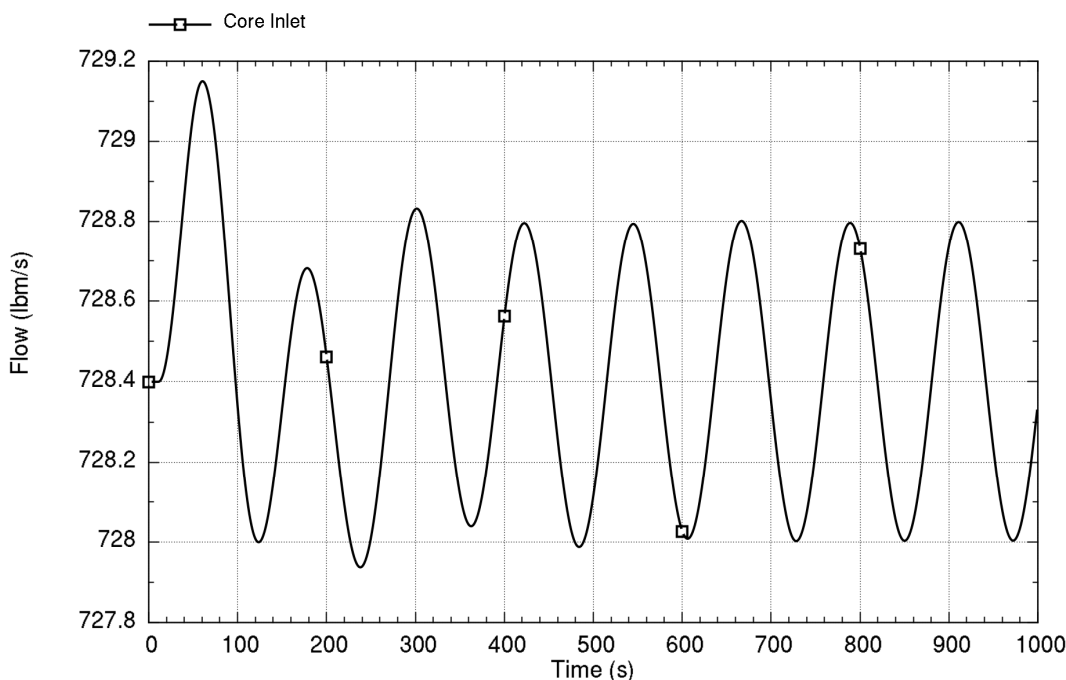
ff Effects of decreasing RCS inventory with constant primary pressure are not important in the stability assessment. The protection system trips on low pressurizer level before any appreciable effect regarding stability, so no consideration is made for this event.

Decreasing reactor coolant inventory that results in decreasing pressure (but does not result in a level trip) is expected to produce no significant effect on stability as long as the primary coolant in the riser remains subcooled. As described in Section 3.7, the MPS includes measurement of hot leg temperature and system pressure, which generates MPS trip signals that protect against an instability event before loss of riser subcooling can occur. Further depressurization beyond the trip setpoint that results in riser voiding is expected to destabilize the system. Therefore, because the trip protects the plant from experiencing instability, Section 9.0 discusses the analysis and results. The existing systems are shown to protect the plant against instability, including consideration of effects of sensor and hardware delays. }}2(a),(e),ECI

8.2.7 Effect of Oscillating Feedwater Flow

The feedwater flow response for a step increase and decrease were considered earlier. The case of oscillating feedwater flow that may result from cycling a feedwater pump, valve, or other component is of interest to examine the magnitude of the effect on the primary coolant flow particularly when the oscillating feedwater period is chosen to resonate with the primary coolant flow period. Recall that net heat sink oscillation feedback to the primary system caused by unstable density waves in the individual SG tubes are not possible because the out-of-phase tube oscillations cancel out as discussed in Section 4.3.3.2.

The 5-percent 0.05 kg/sec feedwater flow oscillation is imposed as a boundary forcing function at 32 MW and EOC conditions, where the large negative reactivity allows the core power to follow the flow more closely than at BOC. The oscillation period is selected as 122 seconds consistent with the loop transit time for this power level. Figure 8-49 and Figure 8-50 show the results for flow and power.

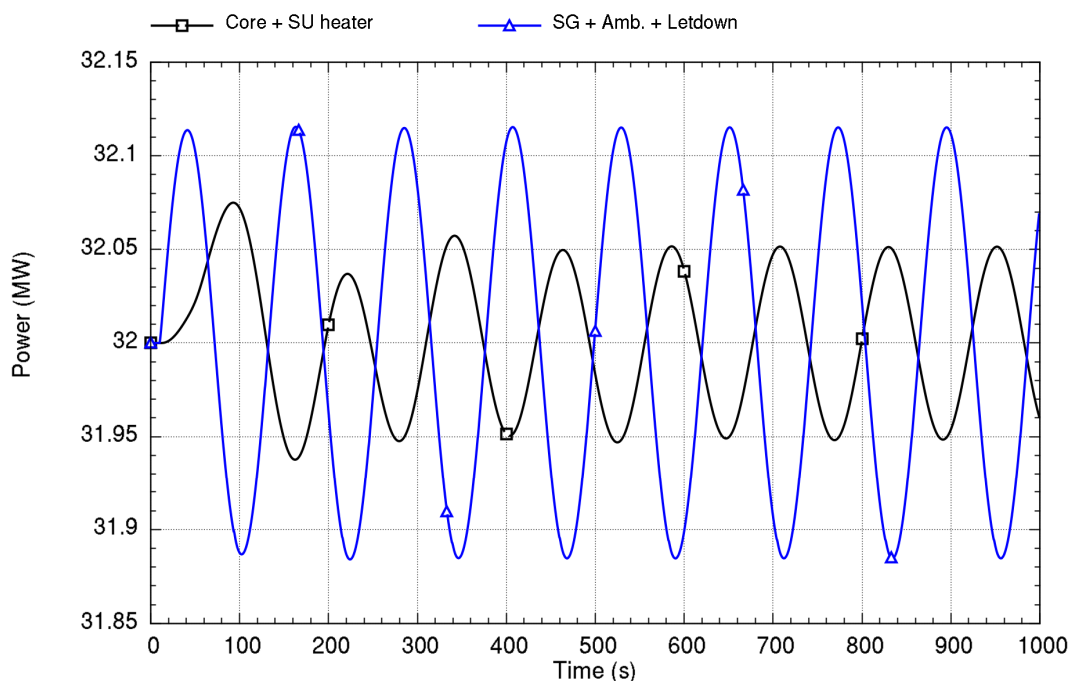


Run ID: Run on Jun/01/2016 at 21:38:48 with PID 007716

2(a),(c), ECI

Figure 8-49. Time trace of primary coolant flow response to feedwater flow oscillation with 122-second period and end-of-cycle conditions

ff



Run ID: Run on Jun/01/2016 at 21:38:48 with PID 007716

ff2(a),(e),ECI

Figure 8-50. Time trace of heat addition and heat removal response to feedwater flow oscillation with 122-second period and end-of-cycle conditions

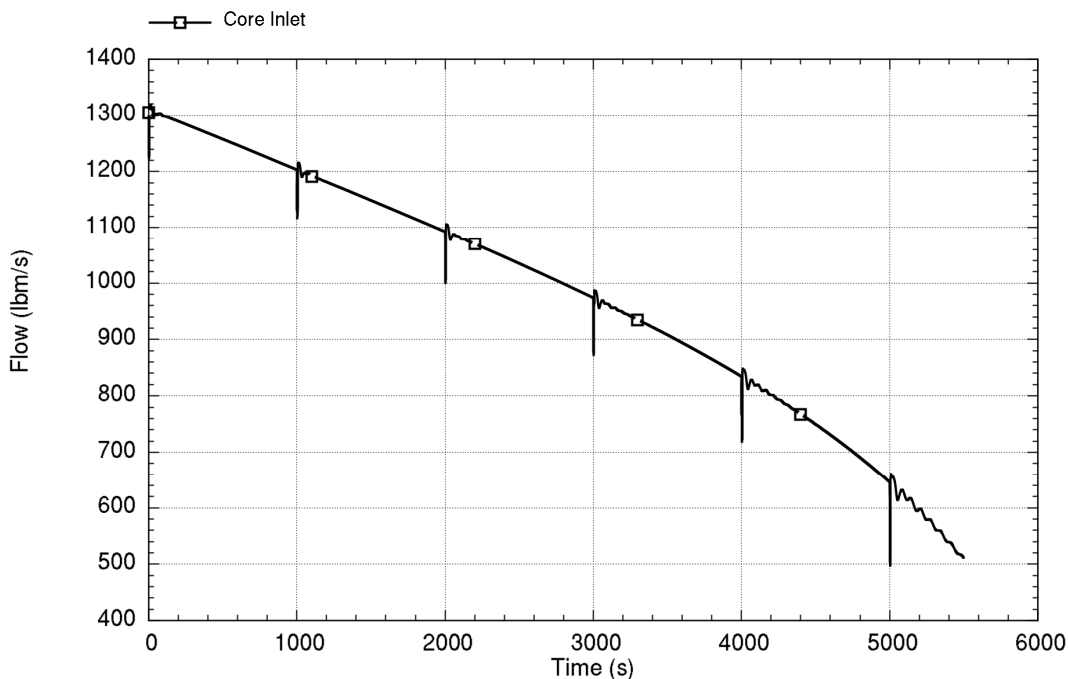
ff The results show that the primary flow is not responding with a resonance that might otherwise induce large-amplitude primary flow oscillations. In addition, core power is responding with damped oscillations relative to the SG heat removal as seen in Figure 8-50. This behavior demonstrates the coupling of the SG and core power. Sensitivities at BOC conditions with a 32-second and a 62-second oscillation period show even more damping of flow and core power than illustrated here.

Evaluation of the oscillatory response shows that the NPM does not undergo a resonant excitation that may cause large primary system oscillations. ff2(a),(e),ECI

8.2.8 Stability During Shutdown by Feedwater Reduction

ff Gradual shutdown of the fission power in response to changes in the feedwater system is analyzed to illustrate the expected behavior in a load-following event. Starting from rated-power conditions with BOC core reactivity in which response of power to changing primary coolant temperature is slow compared to EOC, the feedwater flow is reduced at the arbitrary rate of approximately 1 percent per minute, while feedwater temperature is held constant. Unlike the case with a large sudden reduction of feedwater flow, the slow reduction of feedwater produces no oscillations. Therefore, ff2(a),(e),ECI

Artificial pressure perturbations are applied every 1000 seconds to provide an indication if the system has transited into unstable conditions. The primary coolant flow and power are shown in Figure 8-51 and Figure 8-52. In addition to these, Figure 8-53 provides a zoom on the flow oscillations occurring after an artificial perturbation at 5000 seconds. The zoom illustrates the nature of oscillations that may occur during the decreasing power trend; they are in line with oscillations seen in Section 8.1 at power below 32 MW.

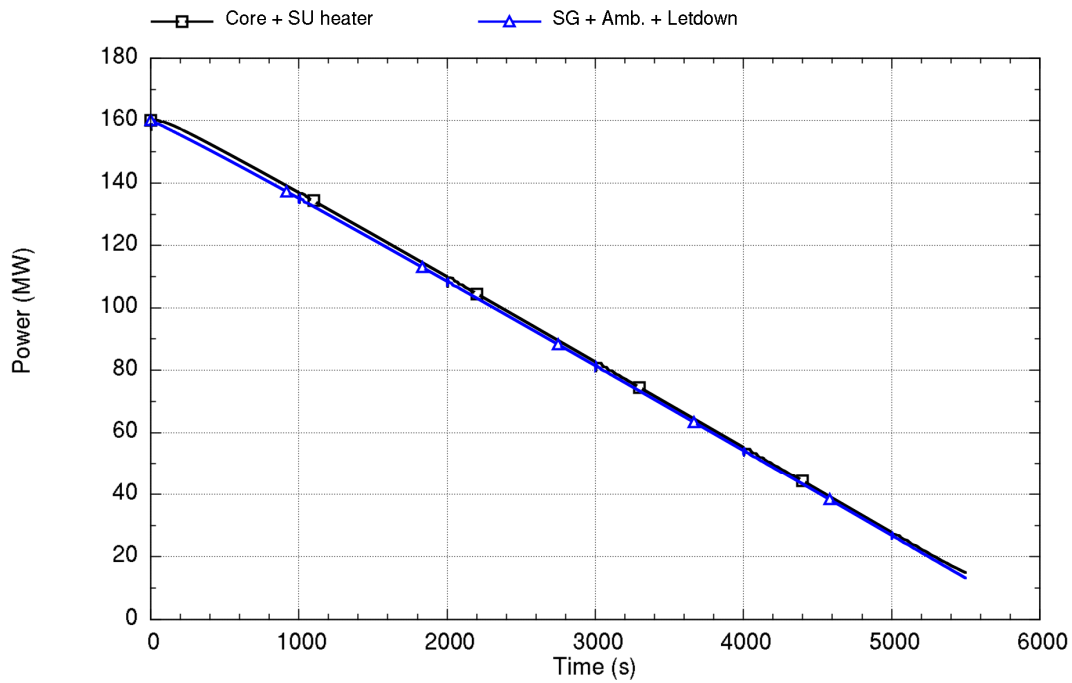


Run ID: Run on Jun/01/2016 at 21:39:49 with PID 009880

2(a),(e),ECI

Figure 8-51. Time trace of primary coolant flow response for gradual feedwater reduction at beginning-of-cycle reactivity

ff

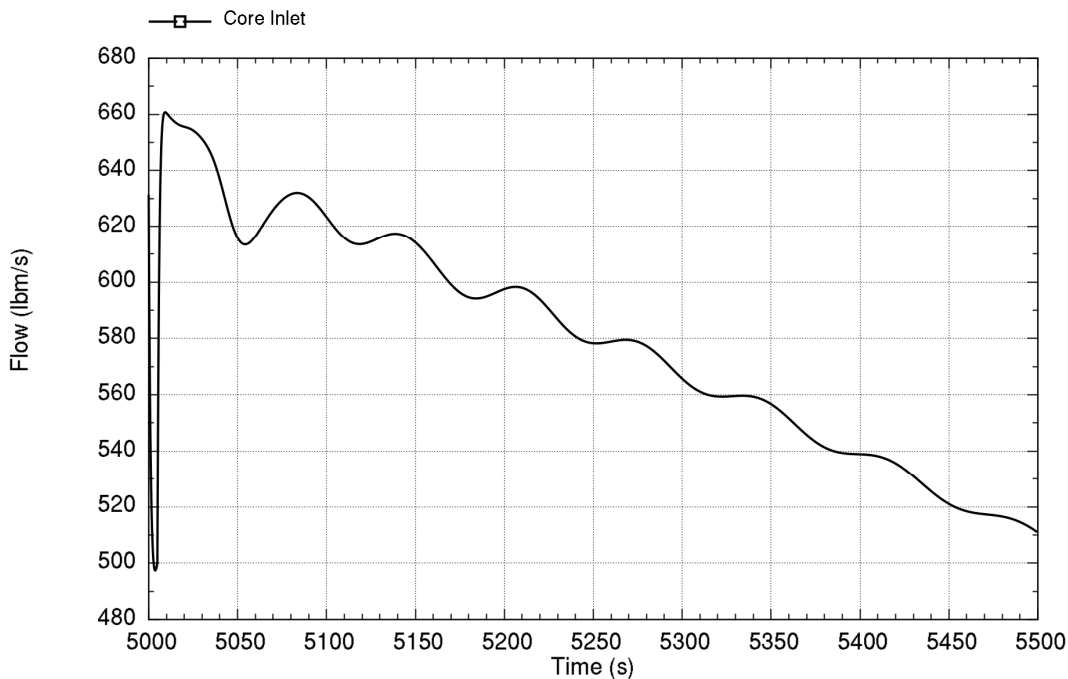


Run ID: Run on Jun/01/2016 at 21:39:49 with PID 009880

ff2(a),(e),ECI

Figure 8-52. Time trace of heat addition and heat removal response for gradual feedwater flow reduction at beginning-of-cycle reactivity

}}



Run ID: Run on Jun/01/2016 at 21:39:49 with PID 009880

}}^{2(a),(e),ECI}

Figure 8-53. Time trace of primary coolant flow response from 5000 seconds to end of the analysis for a gradual feedwater flow reduction at beginning-of-cycle reactivity

}}

The results show the NPM is highly stable for a gradual shutdown. Sensitivity with EOC reactivity shows no discernable difference except that oscillations seen in Figure 8-53 are less. }}^{2(a),(e),ECI}

8.2.9 Stability During Non-Nuclear Heatup (Before Criticality)

}}

}}^{2(a),(c),ECI}

{{

}}^{2(a),(c),ECI}

{{

}}^{2(a),(c),ECI}

Figure 8-54. Time trace of equipment heat rates during the heatup phase

{{

}}^{2(a),(c),ECI}

Figure 8-55. Time trace of system pressurization during the heatup phase

{{

}}^{2(a),(c),ECI}

Figure 8-56. Time trace of coolant and saturation temperatures during the heatup phase

{{

}}^{2(a),(c)-EOL}

Figure 8-57. Time trace of primary coolant flow calculated with artificial perturbations during the heatup phase

{{

}}^{2(a),(c),ECI}

Figure 8-58. Zoom of core flow showing the time trace of coolant flow damped oscillations in response to an artificial perturbation

{{

}}^{2(a),(c),ECI}

9.0 Demonstration of Module Protection System to Preclude Instability

In certain circumstances, the NPM relies on actuation of the MPS to preclude onset of unstable conditions during an operational event. As demonstrated in this section, the MPS actuation occurs in time to prevent the onset of oscillations.

Of the events to be considered, those relying on a trip related to loss of subcooling in the riser are the only events that are important in stability protection. If left unmitigated, the loss of subcooling could lead to undamped flow instabilities.

9.1 Decrease in Heat Removal by the Secondary System

Stability following reduction of feedwater flow for a condition in which the moderator reactivity coefficient is set to zero is explored in this section as a follow-on to Section 8.2.2. In the earlier section, core power responds quickly enough to changes in the loss of heat removal so that saturated conditions in the riser do not occur as shown in Figure 8-37. This section provides analysis results that show the effects of having a zero moderator reactivity coefficient, such that core power only responds to changes in fuel temperature and not to changes in coolant temperature.

Results for the event are provided below. ~~ff~~The event starts at 10 seconds with a 50-percent reduction in feedwater flow while the feedwater and steam pressure remain at their initial values. Figure 9-1 shows the coolant temperature through 120 seconds, which includes indication of the time of MPS trip (about 90 seconds after the change in feedwater flow). This trip occurs when the riser temperature in the vicinity of the hot leg temperature sensors is within 5 degrees-F of the saturation temperature at the pressurizer pressure, which is assumed constant in the analysis. The local saturation temperature in the riser is slightly higher due to static head, but this small effect is not credited.

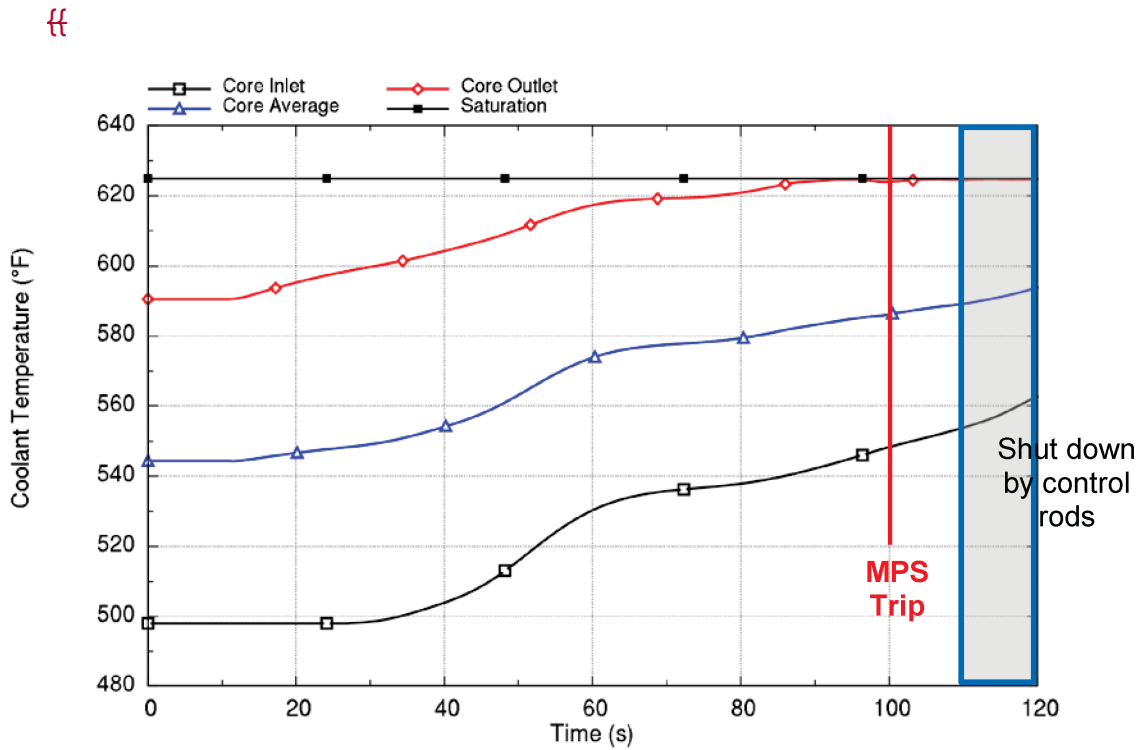
The control rods physically insert into the core within 10 seconds after the trip consistent with the discussion in Section 3.7. This delay time is related to physical lag of the temperature sensor instrumentation, delays in the MPS electronics, and in de-energizing the control rod couplings. Figure 9-1 shows the time of shutdown by the control rods. However, the effect of the shutdown is not included in the analysis; it is permitted to continue for approximately another 10 seconds to demonstrate that there are no sudden or drastic changes in the behavior of the NPM once the riser reaches saturation temperature, which can be seen by inspecting the core flow in Figure 9-2.

Figure 9-3 shows the power response. Comparing this figure with Figure 8-32, the effect of moderator feedback can be observed, where the BOC conditions in the reference figure show a core power of 110 MW at 100 seconds compared with more than 140 MW in this figure. Core power is reduced in Figure 9-3 as a consequence of fuel temperature increase, not the moderator temperature increase, given the imposed zero moderator reactivity feedback.

The void fraction exiting the core and at the top of the riser is shown Figure 9-4. Early voiding that occurs at the core exit is related to subcooled boiling in the core, which does not adversely impact the results before the riser actually reaches saturated conditions because the voids generated by subcooled boiling quickly condense. Note, PIM uses a one-dimensional core model that does not model the subcooled boiling in the high-power assemblies. Such localized boiling is judged not to affect results.

Figure 9-5 shows the CHF response for the event. There is a reduction in the CHF during the event progression, but the overall CHF shows significant margin for protecting the fuel, even well after the time when shutdown by control rod insertion would occur.

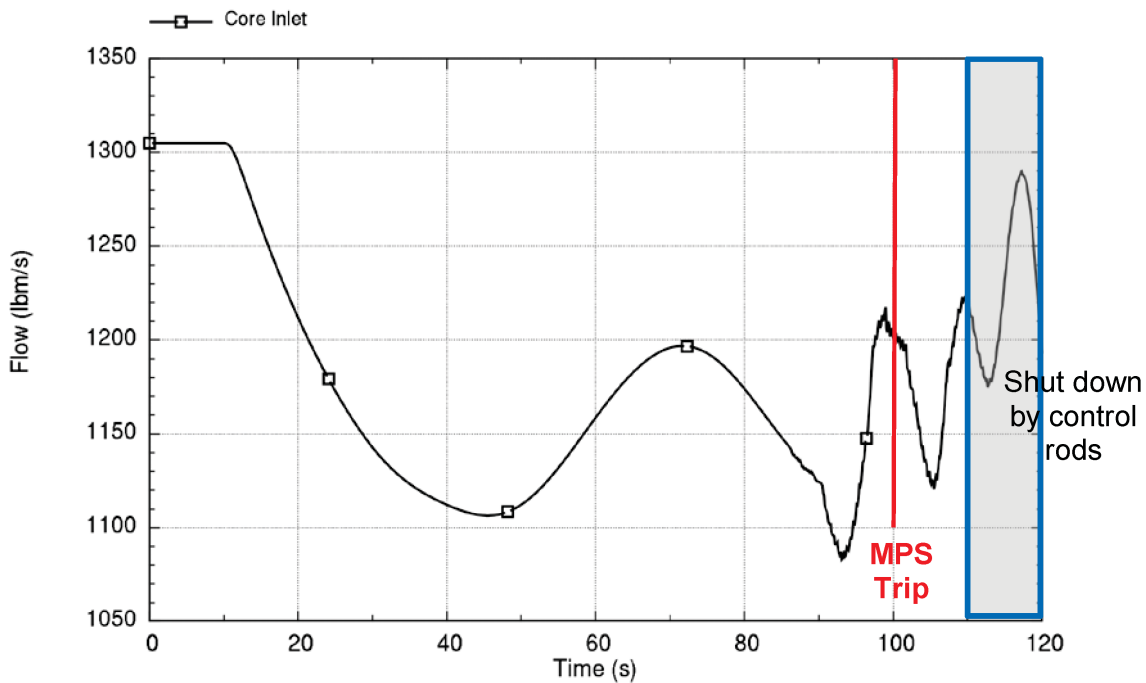
~~ff~~^{2(a),(e),ECI}



ff 2(a),(e), ECI

Figure 9-1. Time trace of coolant temperature response to a 50-percent decrease in feedwater flow at rated power and zero moderator reactivity feedback

ff

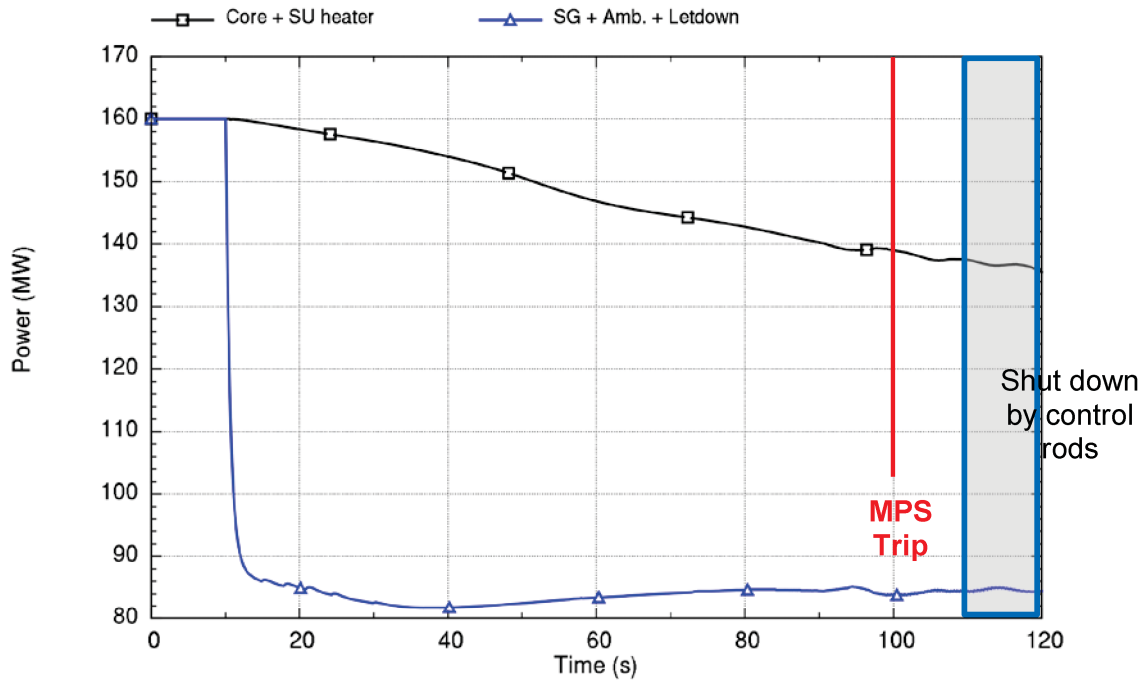


Run ID: Run on Jun/01/2016 at 21:34:32 with PID 007756

ff2(a),(e),ECI

Figure 9-2. Time trace of primary coolant flow response to a 50-percent decrease in feedwater flow at rated power and zero moderator reactivity feedback

ff

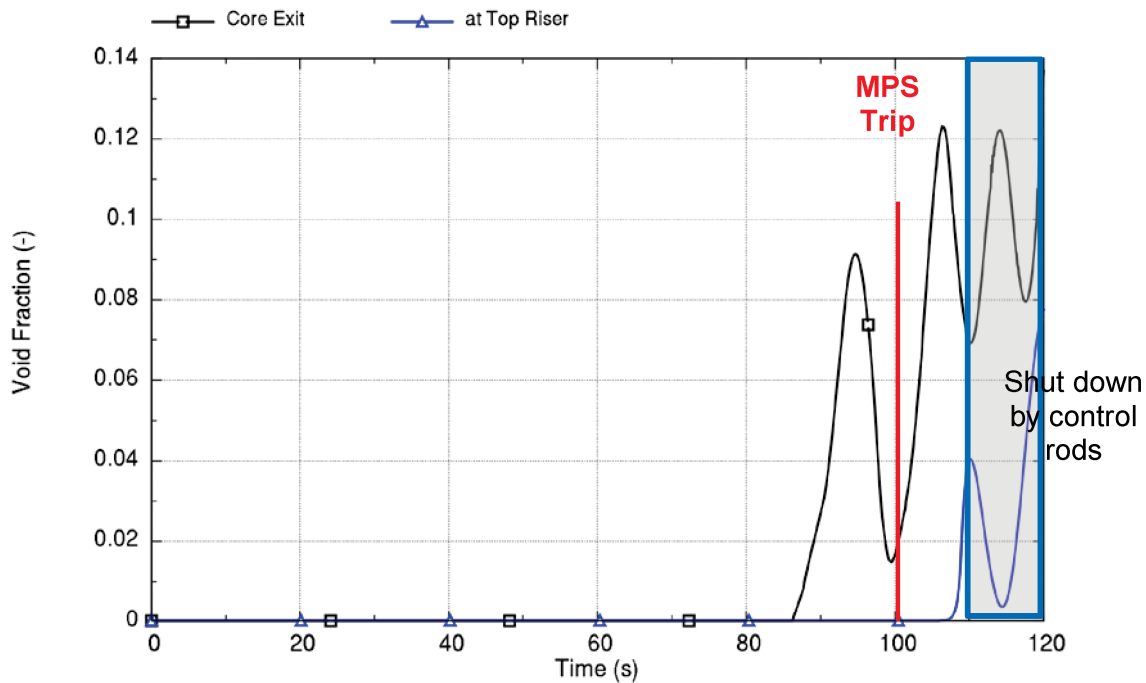


Run ID: Run on Jun/01/2016 at 21:34:32 with PID 007756

ff 2(a),(e),ECI

Figure 9-3. Time trace of heat addition and heat removal response to a 50-percent decrease in feedwater flow at rated power and zero moderator reactivity feedback

ff

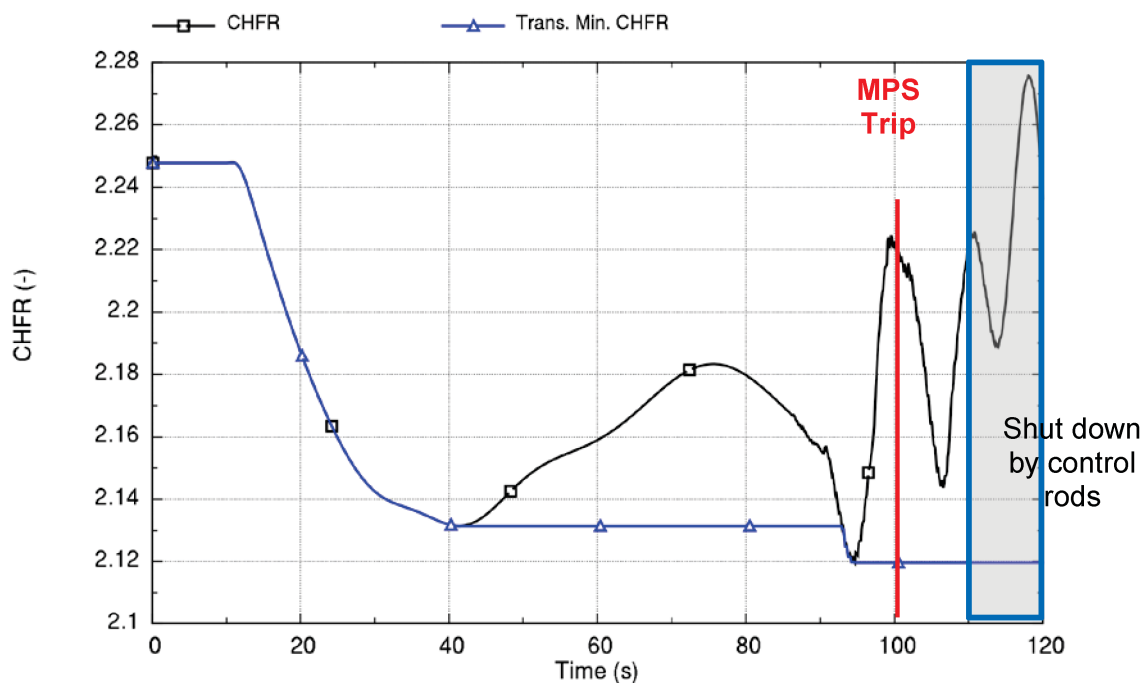


Run ID: Run on Jun/01/2016 at 21:34:32 with PID 007756

ff2(a),(e),ECI

Figure 9-4. Time trace of void fraction response to a 50-percent decrease in feedwater flow at rated power and zero moderator reactivity feedback

ff



Run ID: Run on Jun/01/2016 at 21:34:32 with PID 007756

ff2(a),(e),ECI

Figure 9-5. Time trace of CHF response to a 50-percent decrease in feedwater flow at rated power and zero moderator reactivity feedback

9.2 Decrease in Reactor Coolant Inventory

ff Decreasing reactor coolant inventory that results in decreasing pressure, but does not result in a level trip, is expected to produce no significant effect on stability as long as the primary coolant in the riser remains subcooled as described in Section 8.2.6. However, further depressurization beyond the trip setpoint that results in riser voiding can destabilize the system. This section provides analysis results that show the effects of depressurization and the ability of the MPS to mitigate the event, including consideration of the effects of sensor and hardware delays.

Results for the event are provided below for BOC core conditions. The event starts at 0 seconds with an approximate 14.5- psi/minute (1 bar/minute) depressurization. The depressurization is programmed to continue for 2000 seconds until the pressure is 1378 psia (95 bar) as shown in Figure 9-6. At this pressure, the riser is in saturated conditions and the depressurization is halted, which allows the system to show an unstable behavior. At this point, the system has already tripped and shut down on both riser subcooling and minimum system pressure. However, the effect of the shutdown is not included in the analysis; it is permitted to continue to demonstrate the extended duration before there are drastic changes in the behavior of the NPM. ff2(a),(e),ECI

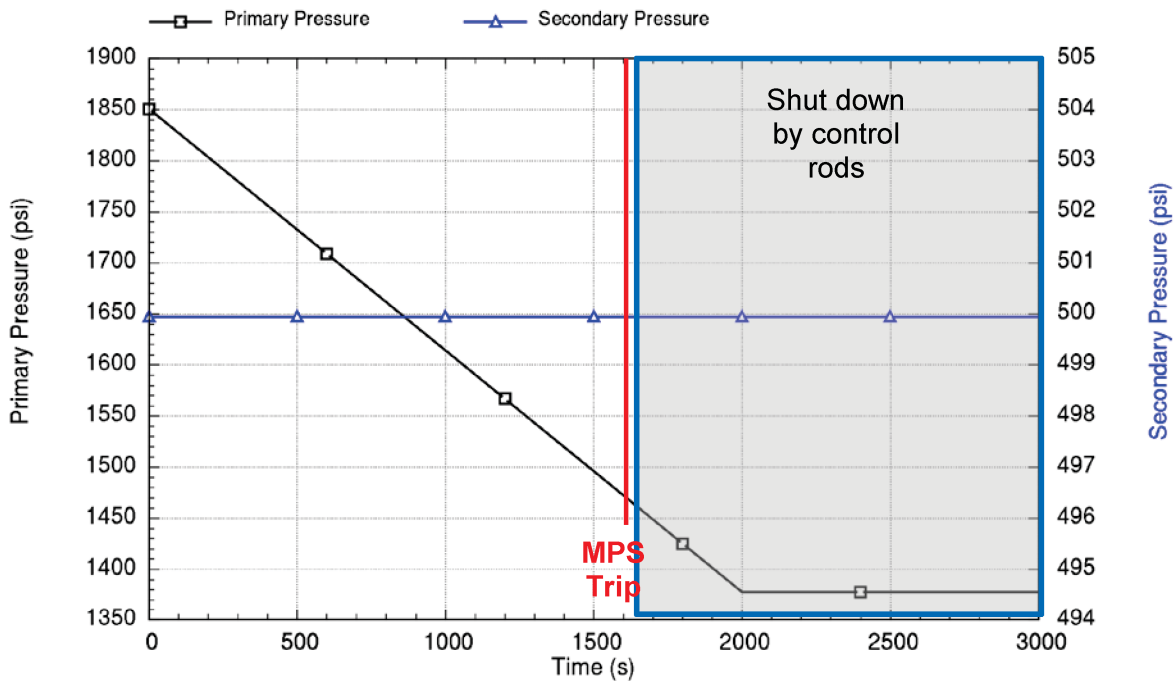
Figure 9-7 shows the coolant temperature through 3000 seconds, which includes indication of the time of MPS trip on loss of subcooling. This trip occurs at about 1608 seconds when the riser temperature in the vicinity of the hot leg temperature sensors is within 5 degrees-F of the saturation temperature at the pressurizer pressure. The trip on low-pressurizer pressure at 1600 psia would have occurred sooner. The control rods physically insert into the core within 10 seconds after the trip, consistent with discussion in the last section. The effect of the shutdown is not included in the analysis; it is permitted to continue to demonstrate the behavior of the NPM once the riser reaches saturation temperature, which can be seen by inspecting the core flow in Figure 9-8.

Figure 9-9 shows the power response. The figure demonstrates that limit-cycle oscillations in reactor power are established for this condition after the depressurization is stopped at 2000 seconds. The limit-cycle characteristics are discussed further below.

The void fraction exiting the core and at the top of the riser is shown in Figure 9-10. Early voiding that occurs at the core exit is related to subcooled boiling in the core as observed for the partial loss of feedwater event.

Figure 9-11 shows the CHF response for the event. There is an overall improvement the CHF during the event progression. This improvement is a result of a slight decrease in power, increase in core flow, and the overall dependence of CHF on pressure within the analyzed range. This improvement in CHF margin shows the fuel is not challenged from the perspective of CHF for the analyzed event. ~~2(a),(c),ECI~~

ff

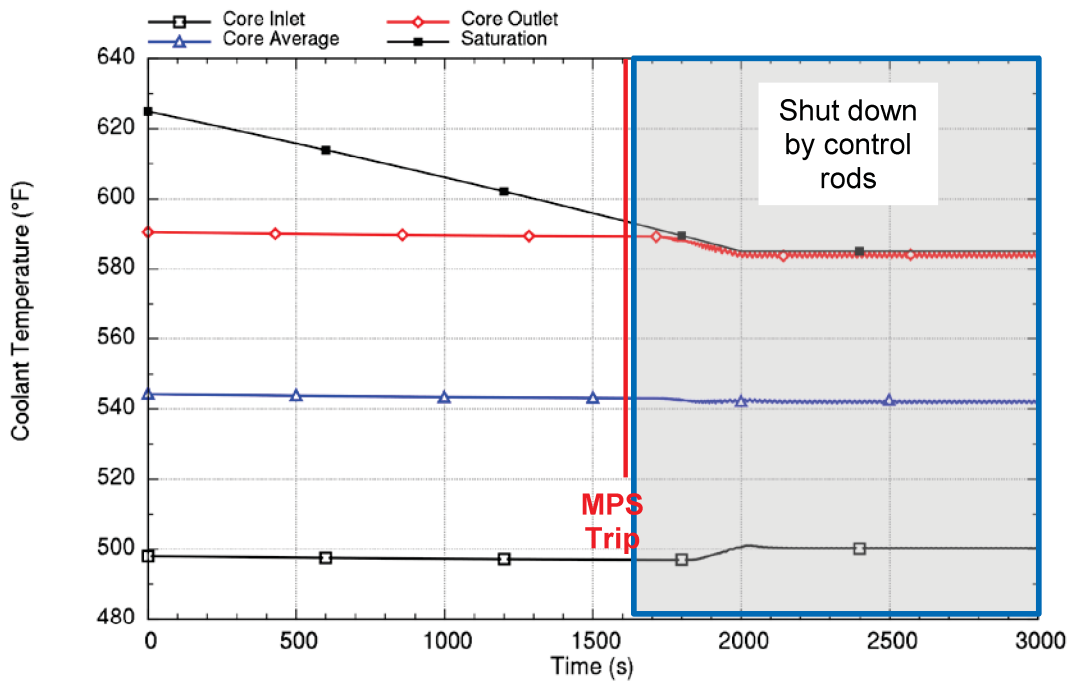


Run ID: Run on Jun/01/2016 at 21:39:04 with PID 009596

}}2(a),(e),ECI

Figure 9-6. Time trace of programmed system pressure at rated power

ff

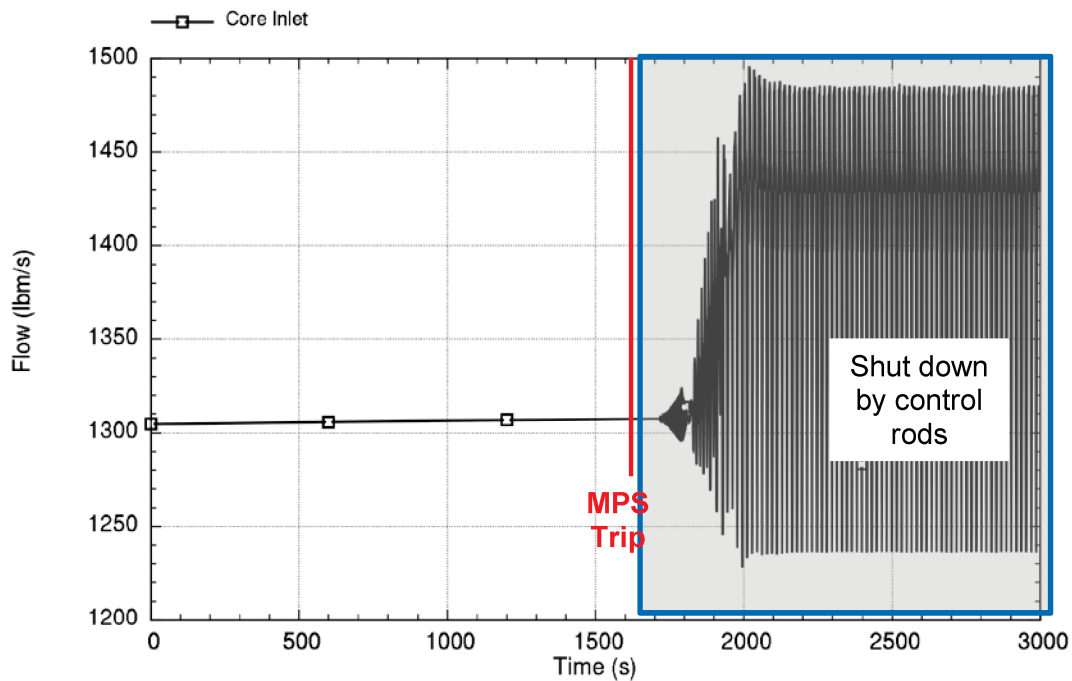


Run ID: Run on Jun/01/2016 at 21:39:04 with PID 005596

ff2(a),(e),ECI

Figure 9-7. Time trace of coolant temperature response to a depressurization at rated power and beginning-of-cycle reactivity feedback

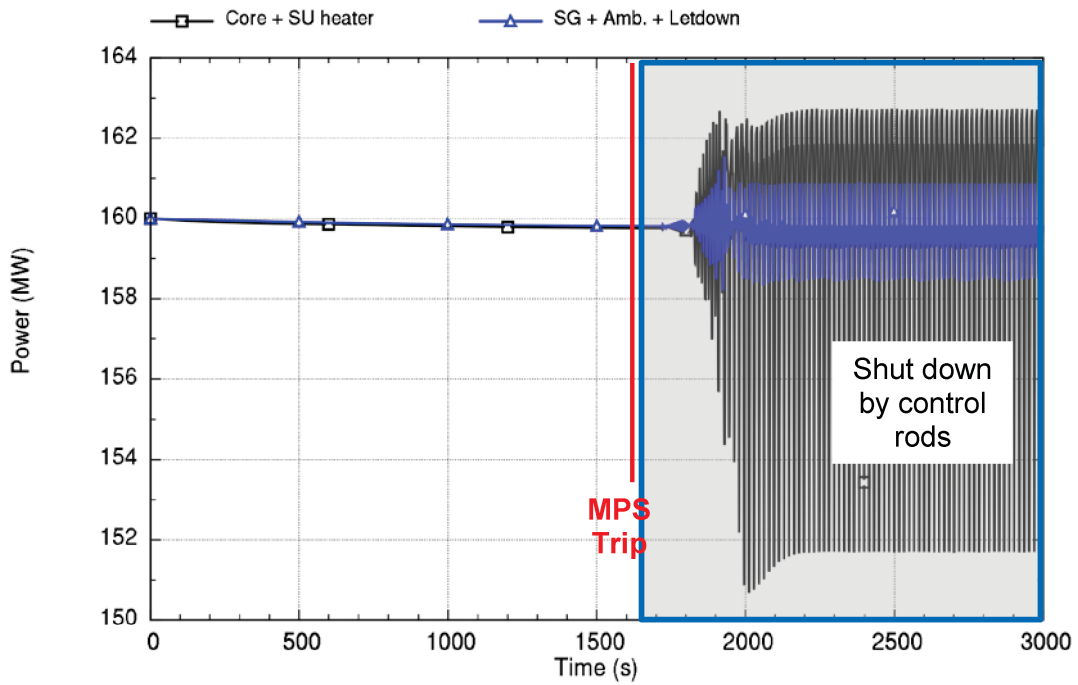
ff



ff2(a),(e),ECI

Figure 9-8. Time trace of primary coolant flow response to a depressurization at rated power and beginning-of-cycle reactivity feedback

ff

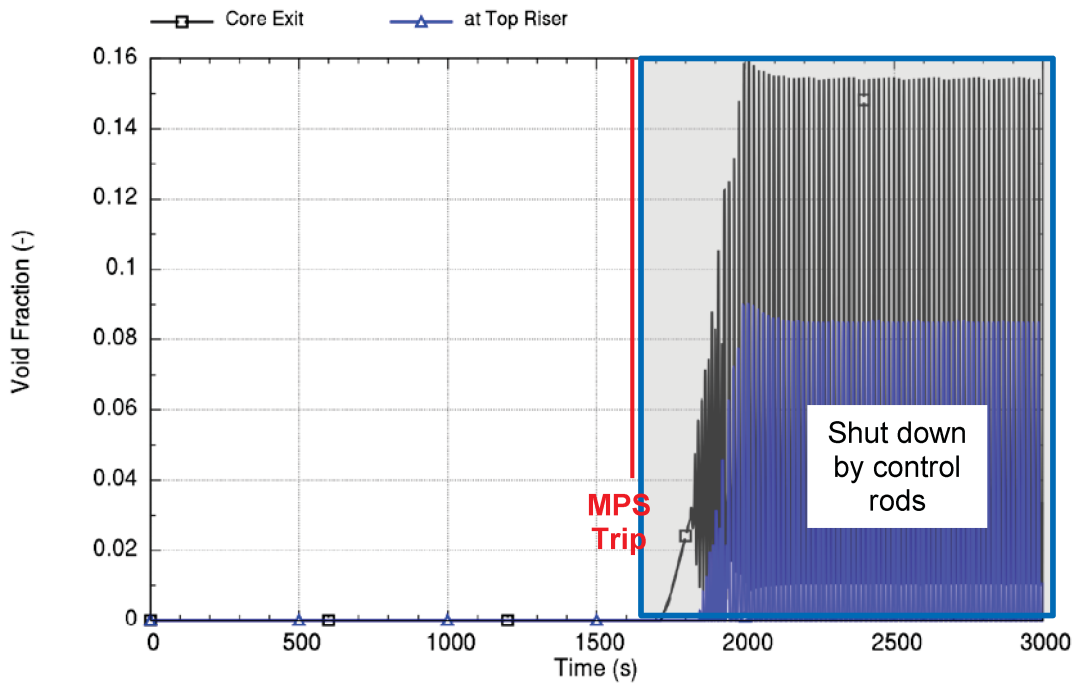


Run ID: Run on Jun/01/2016 at 21:39:04 with PID 009596

ff 2(a),(e),ECI

Figure 9-9. Time trace of heat addition and heat removal response to a depressurization at rated power and beginning-of-cycle reactivity feedback

ff

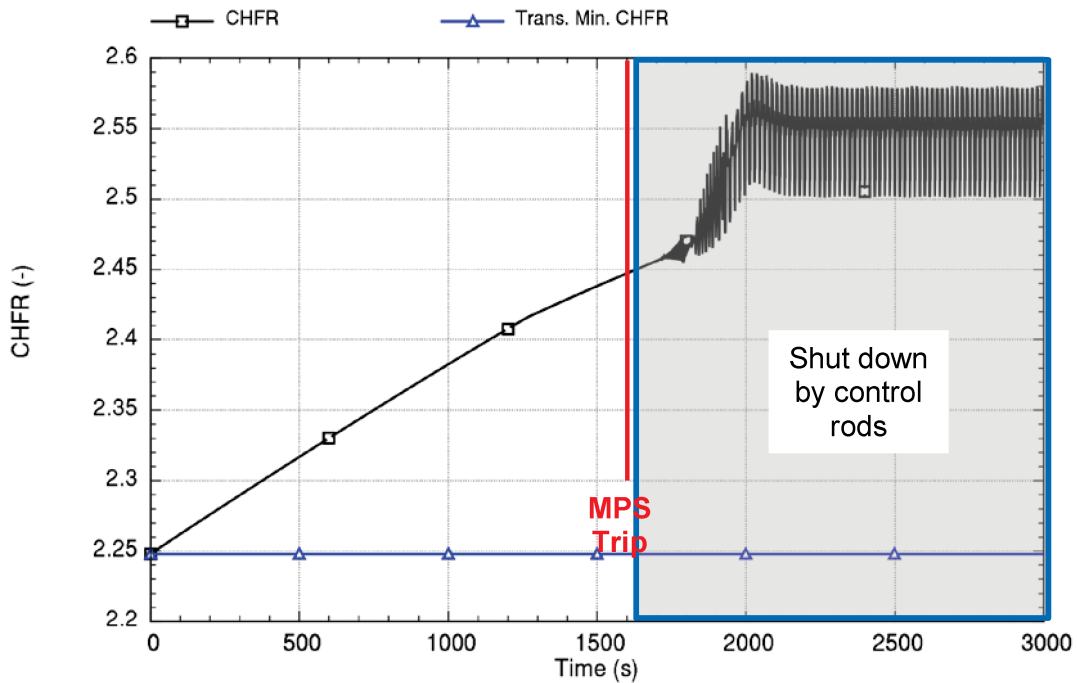


Run ID: Run on Jun/01/2016 at 21:39:04 with PID 005596

ff2(a),(e),ECI

Figure 9-10. Time trace of void fraction response to a depressurization at rated power and beginning-of-cycle reactivity feedback

ff



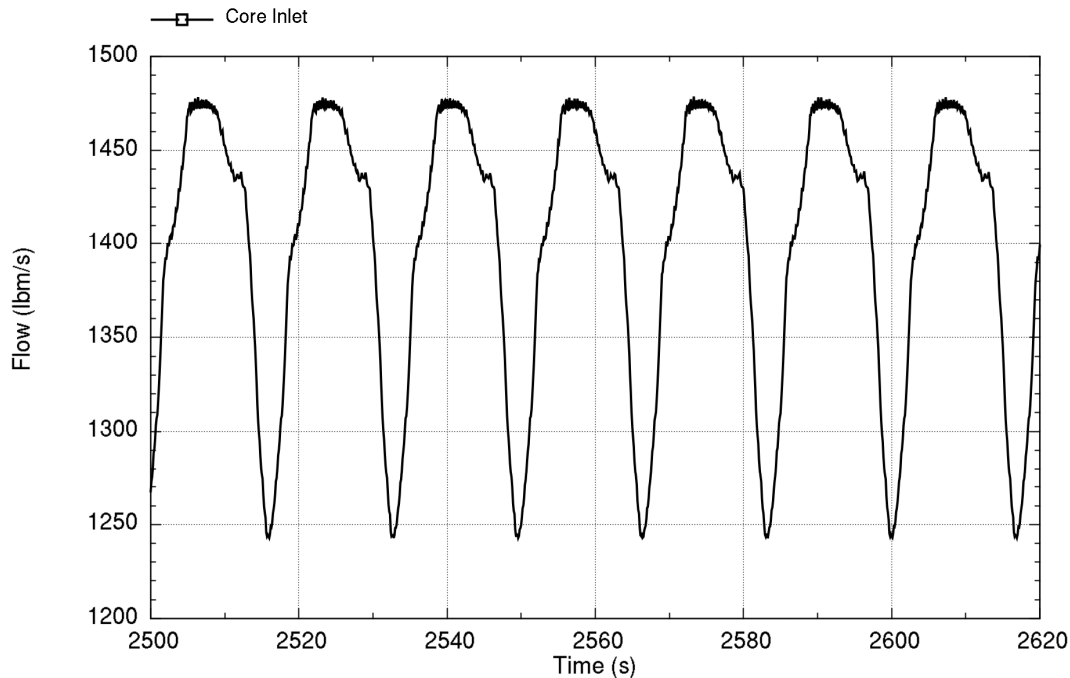
Run ID: Run on Jun/01/2016 at 21:39:04 with PID 005596

ff2(a),(e),ECI

Figure 9-11. Time trace of critical heat flux ratio response to a depressurization at rated power and beginning-of-cycle reactivity feedback

ff Limit-cycle oscillatory behavior is observable in the results shown above. The behavior arises from nonlinearities in the plant behavior that dampen the oscillation magnitude and prevent the continued oscillation growth. Figure 9-12 shows limit-cycle oscillations in primary system flow for a duration of 120 seconds. Oscillations with a period of about 17 seconds are evident in the figure. This period is related to the time for coolant to transit from the core to the top of the riser. ff2(a),(e),ECI

ff



Run ID: Run on Jun/01/2016 at 21:39:19 with PID 009872

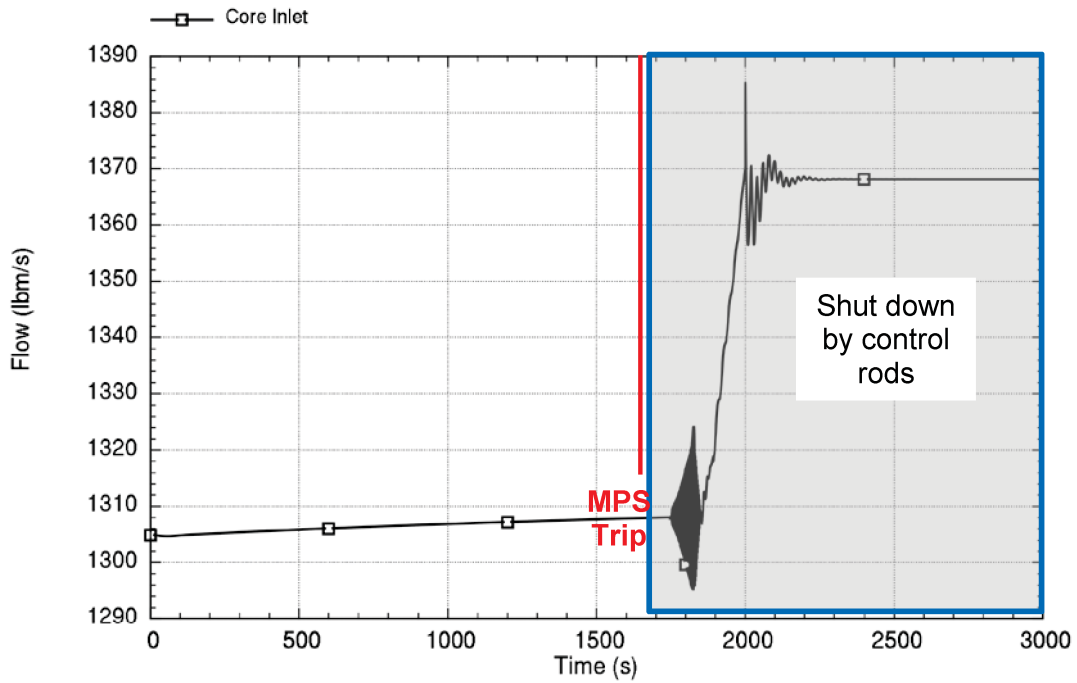
ff2(a),(c),ECI

Figure 9-12. Time trace of primary coolant flow limit-cycle response more than 120 seconds to a depressurization at rated power and beginning-of-cycle reactivity feedback

ff-Growth of the oscillation amplitude seen in Figure 9-12 is saturated and reaches a limit cycle due to nonlinear effects that limit further increase of the destabilizing phenomena. In this case, the full collapse of the riser voids seen in Figure 9-10 marks the maximum ability of the system to generate larger amplitudes as the range of the density head variation becomes saturated.

Analysis of conditions at EOC for the same depressurization scenario described above illustrates the importance of reactivity feedback on the strength of instability well after the expected shutdown time. Figure 9-13 and Figure 9-14 show the primary system flow and void fraction for this condition. The relatively strong negative moderator reactivity feedback allows the plant to reach a new steady state (oscillation-free) condition after a short transitory behavior. ff2(a),(c),ECI

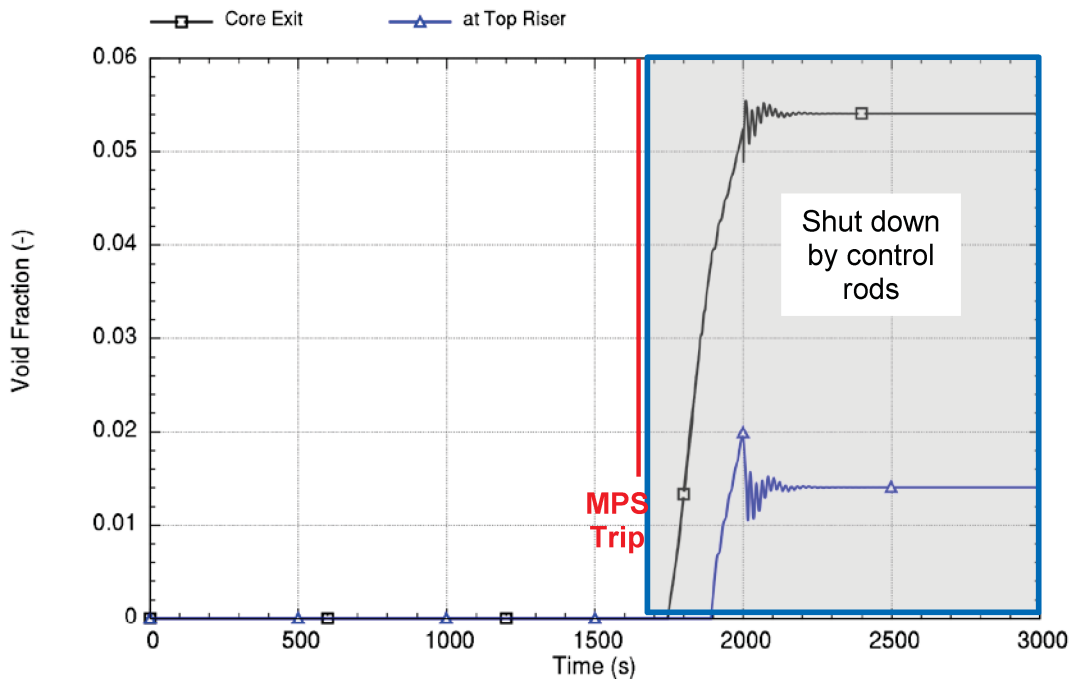
ff



ff2(a),(e),ECI

Figure 9-13. Time trace of primary coolant flow response to a depressurization at rated power and end-of-cycle reactivity feedback

ff



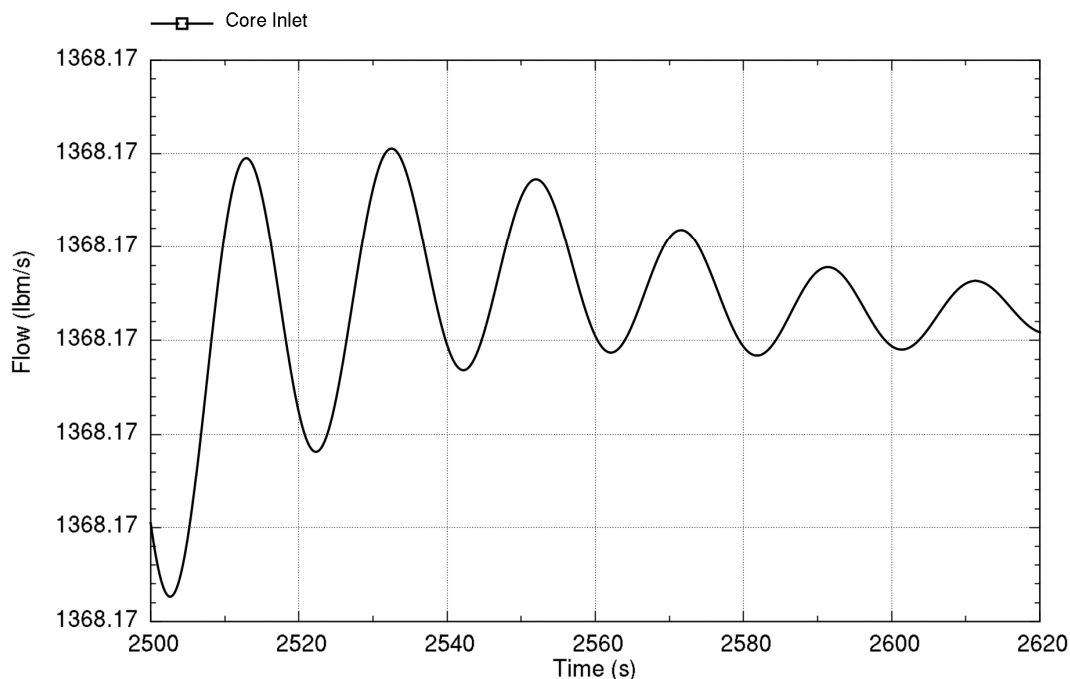
Run ID: Run on Jun/01/2016 at 21:39:34 with PID 009368

ff^{2(a),(e),ECI}

Figure 9-14. Time trace of void fraction response to a depressurization at rated power and end-of-cycle reactivity feedback

ff Figure 9-15 shows the primary coolant flow for the same 120-second window that is shown in Figure 9-12. Oscillations with a period of about 19 seconds are evident in the figure; however, the magnitude has no significance. ff^{2(a),(e),ECI}

ff



Run ID: Run on Jun/01/2016 at 21:39:34 with PID 009368

ff2(a),(e),ECI

Figure 9-15. Time trace of primary coolant flow response more than 120 seconds to a depressurization at rated power and end-of-cycle reactivity feedback

10.0 Stability Methodology

The physical basis of the stability analysis methodology was developed and presented in detail in the preceding sections. A phenomena identification and ranking table (PIRT) was created and used as basis for developing the stability analysis code that has been exercised over a wide range of operating conditions and transients. Post-analysis examination of the high-ranking phenomena was presented, and the general characteristics of the stability behavior were established. This physical basis substantiates for the stability analysis methodology.

The purpose of this section is to present two aspects of the stability methodology. The first aspect pertains to the selection of regional exclusion as the solution type and the rationale for this selection.

The second aspect pertains to the type and scope of the generic analysis that supports the definition of the region to be excluded, and the margins and MPS trips that enforce it. These elements constitute the stability analysis application methodology.

10.1 Revisiting High-Ranking Phenomena

{{

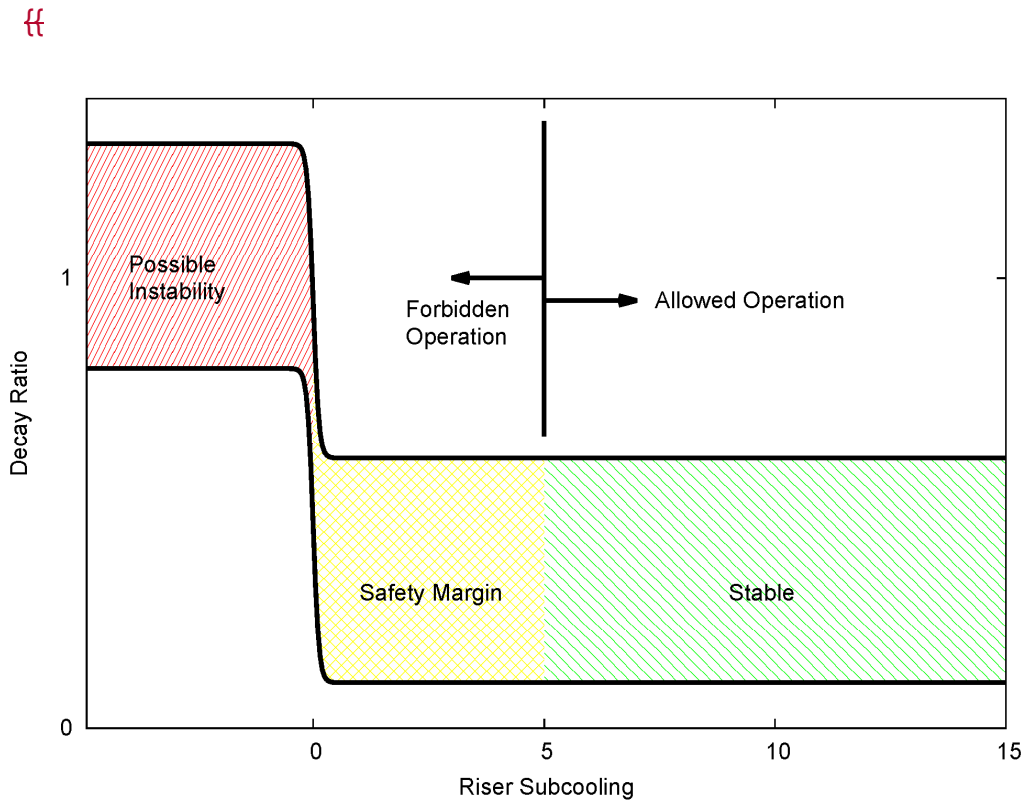
}}2(a),(c);ECI

 {{

 }}^{2(a),(c),ECI}

10.2 General Stability Characteristics

~~}}~~The characteristics of the stability behavior of the NPM were obtained based on the results of the PIM code analysis and supported by first principles and experimental data. The salient features of the stability characteristics are presented in the sketch provided as Figure 10-1. The sketch shows the qualitative dependence of decay ratio on riser (or equivalently core exit) subcooling. The decay ratio is generally small representative of a stable system for subcooled riser conditions, and experiences a significant step increase in decay ratio as the operating state transitions to two-phase flow in the riser upon loss of the subcooling margin. The high decay ratio state with no riser subcooling may exceed unity, indicating an unstable system, and so is precluded by the regional exclusion stability protection solution. ~~}}~~^{2(a),(c),ECI}



ff^{2(a),(c),ECI}

Figure 10-1 Illustration of decay ratio band as function of riser subcooling showing range of stability, possible instability, and safety margin

ff—The band of decay ratio curves as function of riser subcooling indicates variation due to other parameters. The main variation of decay ratio is due to the following parameters:

- Moderator density reactivity. For positive moderator density reactivity coefficient (equivalent to negative moderator temperature coefficient for single-phase moderator) the decay ratio is reduced, indicating a stabilizing effect. Small positive moderator density reactivity coefficient (equivalent to positive moderator temperature coefficient for single-phase moderator), which is possible at high boron concentration and low moderator temperature at low power operation, increases decay ratio. Decay ratio is likely to exceed unity and the system is unstable when vapor is present in the riser and moderator density reactivity is small as in BOC. For EOC conditions, voiding in the riser is not likely to result in instability. ff^{2(a),(c),ECI}

ff

- Core Power. The system is highly stable (i.e., decay ratio is less than 0.5) for high power operation. ff

ff^{2(a),(c)}

From the above discussion, two parameters are identified as controlling the stability of the reactor. The proposed stability analysis methodology considers these parameters as follows.

- Riser Subcooling. The loss of riser subcooling is identified as the condition for which instability is possible and likely. For this reason, riser subcooling is to be protected by a technical specification value with margin, where the margin is sufficiently large to cover instrumentation uncertainty and measurement delay. The riser subcooling margin is independent of the core design and burnup state and therefore is generically specified for the methodology and is not on a cycle-specific basis.
- Moderator Reactivity Coefficient. An analysis that utilizes the methodology described in this report is required to demonstrate that the decay ratio is at or below 0.8 for power at five percent of rated or above under the BOC conditions with subcooled riser, which places a limit on the MTC maximum positive value. A conservative positive MTC is used for the initial generic analysis, and therefore, a revision to the stability analysis would be needed only if this conservative value is exceeded in subsequent cycles.

ff^{2(a),(c),ECI}

10.3 Stability Protection Solution

There are two stability protection types, which emerged from a long history of licensing the operation of BWRs. These types are detect and suppress and regional exclusion. The main features of these two types are presented below with the rationale for adopting the regional exclusion type in this methodology.

- Detect and suppress stability solution. This is an automated solution in which in-core instrumentation signals are processed and oscillation detection algorithms are applied continuously to identify the onset of unstable oscillations. The system is functioning over a wide operational domain defined on a two-dimensional power-flow operating map. Reactor trip set points are based on statistical methods with assumed distributions of oscillation frequency and decay ratios, taking into account reactor trip delays. The system is sufficiently sensitive that it can respond to global and regional mode instabilities and suppress them before thermal limits are violated. The detect and suppress solution is used by most BWR utilities because it can efficiently protect the fuel automatically without reliance on operator action. The advantages for BWRs include the system's ability to detect regional out-of-phase

In order to utilize the methodology described in this report, the applicability of the regional exclusion stability protection solution by satisfying the condition that the conservative maximum (positive) MTC is within the value used for the generic analysis and the riser subcooling is within the technical specification value must be confirmed on a cycle-specific basis.

11.0 Summary and Conclusions

A methodology for the evaluation of the stability of the NPM has been presented. The stability phenomena are considered from the fundamental level and screened for applicability to NPM. The ranking of these phenomena is the guide for the computational models developed for the stability analysis and is assessed versus NIST-1 data and supported by first principles analysis of trends.

No assumptions are made with regard to stability trends being in any way similar to past experience, particularly with BWRs. Important differences between BWR and the NPM stability trends are identified, namely: ~~ff~~

- Negative moderator reactivity feedback is stabilizing in the case of the NPM, unlike BWRs. Note that a small positive moderator reactivity coefficient, which is destabilizing, is possible in principle for low exposure high boron and low-moderator temperature. ~~}}^{2(a),(e),ECI}~~

- ff • High core inlet flow subcooling is not destabilizing for the case of NPM, unlike for a BWR.
- High-power operation is more stable than low-power operation, unlike a BWR under natural circulation conditions.
- The period of flow and power oscillations in the NPM is one to two orders of magnitude higher than the oscillation period in a BWR, hence the selection of regional exclusion stability protection instead of the detect and suppress solution.

ff2(a),(e),ECI

The NPM primary coolant flow is found to be stable for the entire operational domain for the analyzed conditions. This finding is based on a wide range of exploratory calculations with varied operating conditions and assumptions. Uncertainty analysis does not identify the possibility of destabilization compared with the best-estimate hydraulic characterization.

Instabilities can be excited only when operating outside the design range in which riser voiding becomes possible. These instabilities are prevented by the reactor protection system being triggered by trip setpoints on reactor pressure or core exit subcooling violations. Simulating transients with growing oscillations destabilized by riser voiding do not challenge SAFDLs in the example cases. For EOC, the negative moderator coefficient suppresses the oscillation growth; while for BOC, the oscillations reach a large amplitude limit cycles without significant loss of CHF margin. However, as benign as these oscillations may be, the stability analysis methodology conservatively prevents their occurrence.

The proposed stability protection solution for the NPM belongs in the class of regional exclusion. The analytical methods support the identification of the unstable operating region as the one in which riser voiding is possible regardless of the cause of the loss of riser subcooling margin (e.g., high power, low pressure, or degraded SG heat sink). The MPS trip enforces the exclusion region. The licensing basis of the identification of the exclusion region is generic and applicable to the final design, and confirmation analysis is necessary in the case of design updates as explained in Section 10.0 above.



RAIO-0918-61722

Enclosure 3:

Affidavit of Zackary W. Rad, AF-0918-61723

NuScale Power, LLC
AFFIDAVIT of Zackary W. Rad

I, Zackary W. Rad, state as follows:

1. I am the Director, Regulatory Affairs of NuScale Power, LLC (NuScale), and as such, I have been specifically delegated the function of reviewing the information described in this Affidavit that NuScale seeks to have withheld from public disclosure, and am authorized to apply for its withholding on behalf of NuScale.
2. I am knowledgeable of the criteria and procedures used by NuScale in designating information as a trade secret, privileged, or as confidential commercial or financial information. This request to withhold information from public disclosure is driven by one or more of the following:
 - a. The information requested to be withheld reveals distinguishing aspects of a process (or component, structure, tool, method, etc.) whose use by NuScale competitors, without a license from NuScale, would constitute a competitive economic disadvantage to NuScale.
 - b. The information requested to be withheld consists of supporting data, including test data, relative to a process (or component, structure, tool, method, etc.), and the application of the data secures a competitive economic advantage, as described more fully in paragraph 3 of this Affidavit.
 - c. Use by a competitor of the information requested to be withheld would reduce the competitor's expenditure of resources, or improve its competitive position, in the design, manufacture, shipment, installation, assurance of quality, or licensing of a similar product.
 - d. The information requested to be withheld reveals cost or price information, production capabilities, budget levels, or commercial strategies of NuScale.
 - e. The information requested to be withheld consists of patentable ideas.
3. Public disclosure of the information sought to be withheld is likely to cause substantial harm to NuScale's competitive position and foreclose or reduce the availability of profit-making opportunities. The accompanying Request for Additional Information response reveals distinguishing aspects about the methodology by which NuScale develops its stability analysis of the NuScale power module.

NuScale has performed significant research and evaluation to develop a basis for this methodology and has invested significant resources, including the expenditure of a considerable sum of money.

The precise financial value of the information is difficult to quantify, but it is a key element of the design basis for a NuScale plant and, therefore, has substantial value to NuScale.

If the information were disclosed to the public, NuScale's competitors would have access to the information without purchasing the right to use it or having been required to undertake a similar expenditure of resources. Such disclosure would constitute a misappropriation of NuScale's intellectual property, and would deprive NuScale of the opportunity to exercise its competitive advantage to seek an adequate return on its investment.

4. The information sought to be withheld is in the enclosed response to NRC Request for Additional Information No. 437, eRAI9465. The enclosure contains the designation "Proprietary" at the top of each page containing proprietary information. The information considered by NuScale to be proprietary is identified within double braces, "{{ }}" in the document.
5. The basis for proposing that the information be withheld is that NuScale treats the information as a trade secret, privileged, or as confidential commercial or financial information. NuScale relies upon the exemption from disclosure set forth in the Freedom of Information Act ("FOIA"), 5 USC § 552(b)(4), as well as exemptions applicable to the NRC under 10 CFR §§ 2.390(a)(4) and 9.17(a)(4).
6. Pursuant to the provisions set forth in 10 CFR § 2.390(b)(4), the following is provided for consideration by the Commission in determining whether the information sought to be withheld from public disclosure should be withheld:
 - a. The information sought to be withheld is owned and has been held in confidence by NuScale.
 - b. The information is of a sort customarily held in confidence by NuScale and, to the best of my knowledge and belief, consistently has been held in confidence by NuScale. The procedure for approval of external release of such information typically requires review by the staff manager, project manager, chief technology officer or other equivalent authority, or the manager of the cognizant marketing function (or his delegate), for technical content, competitive effect, and determination of the accuracy of the proprietary designation. Disclosures outside NuScale are limited to regulatory bodies, customers and potential customers and their agents, suppliers, licensees, and others with a legitimate need for the information, and then only in accordance with appropriate regulatory provisions or contractual agreements to maintain confidentiality.
 - c. The information is being transmitted to and received by the NRC in confidence.
 - d. No public disclosure of the information has been made, and it is not available in public sources. All disclosures to third parties, including any required transmittals to NRC, have been made, or must be made, pursuant to regulatory provisions or contractual agreements that provide for maintenance of the information in confidence.
 - e. Public disclosure of the information is likely to cause substantial harm to the competitive position of NuScale, taking into account the value of the information to NuScale, the amount of effort and money expended by NuScale in developing the information, and the difficulty others would have in acquiring or duplicating the information. The information sought to be withheld is part of NuScale's technology that provides NuScale with a competitive advantage over other firms in the industry. NuScale has invested significant human and financial capital in developing this technology and NuScale believes it would be difficult for others to duplicate the technology without access to the information sought to be withheld.

I declare under penalty of perjury that the foregoing is true and correct. Executed on September 10, 2018.



Zackary W. Rad